Contact Mechanics Modelling of Articular Cartilage and Applications

Sainath Shrikant Pawaskar

Submitted in accordance with the requirements for the degree of

Master of Science (Eng) by Research

The University of Leeds

School of Mechanical Engineering

Institute of Biological and Medical Engineering

August 2006

The candidate confirms that the work submitted is his own and that appropriate credit has been given where reference has been made to the work of others.

Acknowledgements

I thank God for guiding me through this journey which looked impossible at the beginning. It was very kind of Prof. Zhongmin Jin to get me started quickly and to understand my earnest need to deliver in this very short time. I am immensely thankful to him for being patient with me and spending his valuable time with me almost on daily basis.

I am grateful to Dr. Salvatore Federico of University of Calgary, Canada for guiding giving valuable tips in ABAQUS and having some fruitful discussions. I also thank Mr. Ahmet Cagatay Cilingir and Dr. Itoro Udofia, both from the University of Leeds, U.K., Dr. Sally Clift of University of Bath, U.K. and Prof. Xian Chen of Kyushu University, Japan for providing help from time to time.

A person is guided along his way by many people and it is impossible to name all of them. I take this opportunity to thank Mr. Pramod Gudishetty, Mr. Vicky Lagad, Mr. Rameshkumar Muthusamy, Mr. Sanjit Singh, Mr. Stanley George, Mr. Ajay Narayan, Mr. Varadarajan Bala, Mrs. Rathna Sundaralingam, Mr. Krish Ellath, Mr. Vijay Agarwal, Dr. Graham Blyth, Mr. Edward Allwood, Mrs. Margaret Gibson, Dr. Alan Real, Dr. Feng Liu, Dr. Fengcai Wang, Mr Maheshwaran Kolandavel, Mrs. Debra Baldwin, Ms Karen Jones, Ms. Victoria Hutt, Mr. Don Stuckey and many others for their timely help and encouraging words. I would like to thank my room-mates Mr. Nandan Kumar and Mr. Atul Mohan for the adjustments they had to make in order to accommodate my rigorous schedule.

I dedicate this work to my to my Parents, elder brother Ajit, my mentor Mr. Joseph M. Fernandes and friends Prasad, Deepali and Shanta, without whom I would not have been where I am today.

Today, I remember my father who passed away on 9th of October, 2004 with profound admiration and respect for all the hardships he went through to ensure my growth in spite of limited resources at his disposal.

Abstract

Osteoarthritis (OA) is a degenerative disease of articular cartilage. The normal cartilage is known to be an excellent bearing material with remarkable lubricating properties and very low frictional co-efficient and wear and generally survives the lifetime of a person. The contact mechanics of the articular cartilage was investigated in this study. The contact mechanics of the cartilage surface against both rigid metallic and cartilage surfaces was investigated using finite element method. Axisymmetric and two-dimensional plane stain models were developed to examine consolidation and sliding respectively.

A new contact detection algorithm was developed to be used with ABAQUS (ABAQUS., 2005) which was more generic in nature. Two versions were developed; one for the indenter-cartilage models and the other for the cartilage-cartilage models. The first algorithm and the corresponding model were validated against the previous study (Warner, 2000) for the indentation of the articular cartilage using a rigid spherical indenter. The second algorithm and the model were validated against the study by Federico and colleagues (Federico *et al.*, 2004) for the cartilage-cartilage configuration. The results presented in these studies could be reproduced with high degree of accuracy. The first algorithm was also applied to derive the mechanical properties of the cartilage from the experimental indentation measurements as well as to study its behaviour.

All the sliding models showed the interstitial fluid pressurization persisted over a long time period. This fluid load support of the cartilage had been shown to contribute towards lowering the frictional co-efficient (Forster *et al.*, 1995; Krishnan *et al.*, 2005).

The model of a rigid plate sliding over the cartilage covering it entirely during the course of sliding showed similar results as consolidation. The fluid exudation suggested in the weeping lubrication (McCutchen, 1959; McCutchen, 1962) mechanism was also observed in this model.

In the model of a rigid cylindrical indenter sliding over cartilage the fluid pressurization was found to decrease initially before attaining the steady value. The stress shielding phenomenon of the cartilage was also observed as in other models. The self generating lubrication (Mow and Lai, 1980) phenomena and boosted lubrication (Maroudas, 1967; Walker *et al.*, 1968) were observed in this model.

Contents

Figures

Tables

Abbreviations

BSAL	-	Biphasic Surface Amorphous Layer
ECM	-	Extra Cellular Matrix
FE	-	Finite Element
FEM	-	Finite Element Model (Method)
OA	-	Osteoarthritis
STZ	-	Superficial Tangential Zone
SPG	-	Stereophotogrammetric
VRDP	-	Void ratio dependent permeability

Chapter 1 Introduction and Literature Review

1.1 Introduction

There has been an immense interest in the study of articular cartilage mainly because of the important role it plays in Osteoarthritis (OA). Articular cartilage provides a well lubricated load bearing surface with a very low co-efficient of friction and can withstand and transfer very high loads; as high as 7 - 10 times body weight, under normal physiological conditions (Crowninshield *et al.*, 1978; Hodge *et al.*, 1986; Mow and Huiskes, 2005). The cartilage experiences a wide variety of loads from static, impact, cyclic to long duration loads and the relative motion of the cartilages in a joint can be very complex. The cartilage experiences normal wear and tear of the tissue with age but can survive for almost seven decades with trouble-free functioning.

OA is attributed to the degradation and ultimately complete breakdown of this cartilage (Carter *et al.*, 2004; Mow and Huiskes, 2005), thus exposing the underlying subchondral bone. OA is accompanied by severe pain and needs to be alleviated either by therapeutic or operational means. It is believed that abnormal use, aging and injury are the main causes of OA (Yang, 2003). The degradation of articular cartilage manifests itself in the variations of its mechanical and biological properties (Carter *et al.*, 2004). This in turn makes the cartilage susceptible to structural failures, which degrades it further.

Researchers from different fields such as Medicine, Engineering, Chemistry, Physics, Biology, Computer Science, Materials Science, etc have been studying articular cartilage at nano – micro – and macro – levels. Many of these studies are centred around investigating mechanical response and properties of the cartilage and their effects on the biochemical properties of the cartilage, and vice versa. Experiments are carried out to quantify mechanical properties (McCutchen, 1962; Mow *et al.*, 1989; Kwan *et al.*, 1990; Macirowski *et al.*, 1994) and/or to study the behaviour of the cartilage under different experimental and physiological conditions (McCutchen, 1959; McCutchen, 1962; Brown and Shaw, 1983; Setton *et al.*, 1993; Warner, 2000; Warner *et al.*, 2001a). Similarly, mathematical models have been postulated to give firm theoretical foundations to the understanding of the mechanical behaviour of the cartilage (Mow *et al.*, 1980; Lai *et al.*, 1991; Ateshian *et al.*, 1994a; Huyghe and Janssen, 1997). Finite Element Modelling is one such tool commonly used by the researchers (Roth and Mow, 1977; Spilker *et al.*, 1992a; van

der Voet, 1992; Federico *et al.*, 2004; Chen *et al.*, 2006) due to its availability, flexible pre- and post-processing and advantages such as ease in implementing complex geometry, material properties and creating configurations which would have been otherwise practically impossible or difficult to formulate as experiments. The present study is such an endeavour in understanding the mechanical response of the cartilage in consolidation and sliding.

1.2 Literature Review

1.2.1 Synovial joint – Its anatomy and physiology

The motion of the human or animal body is primarily because of the joints, though, not all the joints are capable of rendering motion. Structurally, the joints are classified as (Tortora and Grabowski, 2004):

1) Fibrous joints characterized by fibrous connective tissue and lack of synovial cavity.
2) Cartilaginous joints characterized by bones being held together by cartilage and lack of synovial cavity.
3) Synovial joints characterized by synovial cavity, connective tissue and articular cartilage as bearing material.

Diarthrodial joints are the ones which permit free movements of the bones and all such joints are synovial joints (Tortora and Grabowski, 2004). The examples of such joints are knee, hip, shoulder, etc. which exhibit different complex movements of the connecting bones.

All synovial joints are characterized by fibrous capsule lined by highly vascularized membrane called synovium as illustrated in Figure 1-1. Synovium secretes synovial fluid which provides nutrients to the tissues as well as carries waste of cellular activities and acts as a joint lubricant (Mow and Huiskes, 2005). The bones forming the joint are lined with hyaline articular cartilage which is compliant, highly hydrated, aneural and avascular (Tortora and Grabowski, 2004; Mow and Huiskes, 2005).

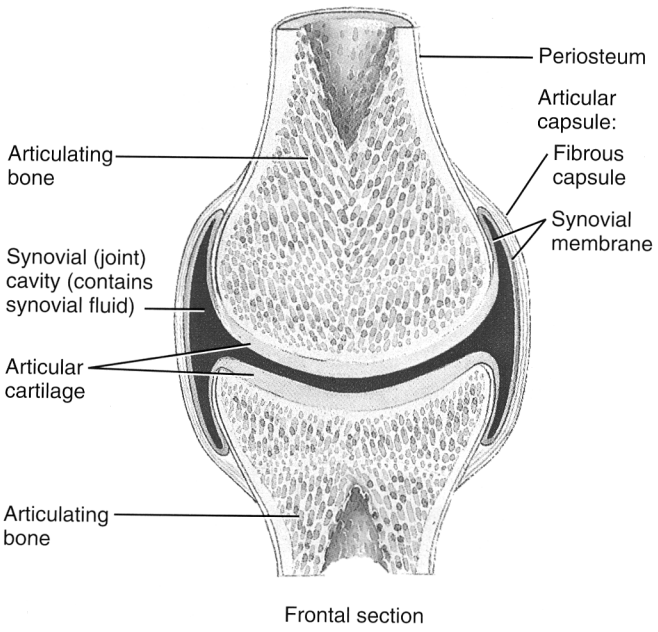

Figure 1-1 Structure of synovial joint in knee (Tortora and Grabowski, 2004)

The anatomy of all the synovial joints in the body is the same, however, the articulating surfaces vary in shape and based on the type of motion there are six different sub-types of synovial joints, viz. planar, hinge, pivot, condyloid, saddle and, ball and socket joint (Tortora and Grabowski, 2004). The hip and shoulder joints are typical ball and socket joints whereas the knee joint is a highly complex hinge joint comprising three different joints; one patello-femoral and two femero-tibial joints (Tortora and Grabowski, 2004; Mow and Huiskes, 2005).

1.2.2 Articular catilage

Cartilage is composed of a single cell type called chondrocyte and an extracellular matrix (ECM). The biochemical and molecular structure of the matrix divides the cartilages into three types; hyaline, elastic and fibrocartilage (Mow and Huiskes, 2005).

Articular cartilage is a hyaline cartilage with bluish white tinge and is glistening glassy smooth (Mow and Huiskes, 2005). It is highly hydrated with around 60 – 85% interstitial water containing dissolved electrolytes (Macirowski *et al.*, 1994; Olsen and Oloyede, 2002; Mow and Huiskes, 2005). ECM of the articular cartilage consists of type II collagen (10 – 20% wet weight), proteoglycans (5 – 10% wet weight), the chondrocytes and other components like link protein, hyaluronan, etc. It covers the part of the bone which articulates with other bones (Tortora and Grabowski, 2004; Mow and Huiskes, 2005). Thickness of the cartilage varies from 0.1 – 0.5 mm (rabbit knee joints) to 1.0 – 6.0 mm (human knee joints) (Simon, 1970;

Ateshian *et al.*, 1991; Mow and Huiskes, 2005) and this variation depends on the species, joints and location within joints (Simon, 1970; Ateshian *et al.*, 1991; Ateshian *et al.*, 1994b; Mow and Huiskes, 2005).

1.2.2.1 Structure

The ECM of articular cartilage consists of dense network of collagen fibres embedded in proteoglycan gel with high degree of fibrillar cross-linking and is often described as a fibre-reinforced structure in engineering terminology. This structure is not only highly inhomogeneous and varies along the depth of the cartilage, but is also non-linear, anisotropic and exhibits time-dependent behaviour (Elmore *et al.*, 1963; Lai and Mow, 1980; Mow *et al.*, 1980; Clift, 1992; Mow and Huiskes, 2005). Chondrocyte size and shape, and water content also varies with the depth and under electron microscopy, articular cartilage is visible as layered structure (Mow *et al.*, 1984; Clift, 1992; Mow and Huiskes, 2005). Articular cartilage contains approximately 2% chondrocytes and hence shows little metabolic activity (Clift, 1992).

The proteoglycans are negatively charged and are hydrophilic. The repulsion of proteoglycans and their affinity for water molecules make the cartilage swell which induces tensile stress in the collagen network enabling it to withstand high compressive stresses experienced by the joints (Maroudas, 1968; Mow and Huiskes, 2005).

Articular cartilage can be primarily divided into 4 zones as shown in Figure 1-2 (Clift, 1992; Mow and Huiskes, 2005):

1) Superficial Tangential Zone (STZ)

2) Mid Zone

3) Deep Zone

4) Calcified Zone

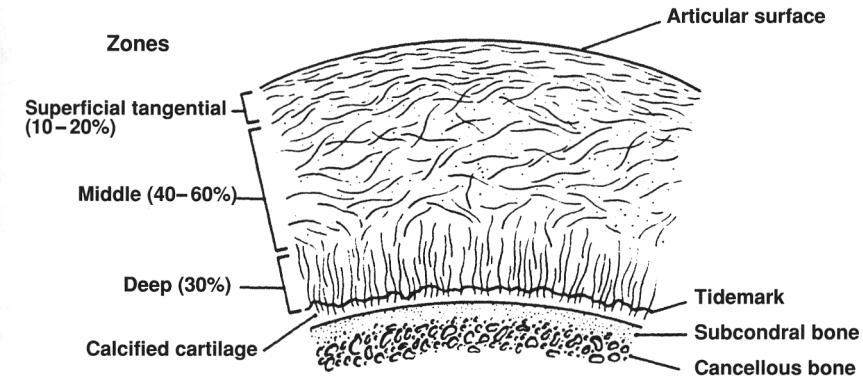

Figure 1-2 Layered structure of Articular Cartilage (Mow and Huiskes, 2005)

The STZ is typically 10 – 20% of the total thickness of the cartilage and contains around 75 – 80% of water. The dry weight of the collagen is around 85%. Water and collagen content are the highest in this zone whereas aggrecan (aggregating proteoglycans) content is the lowest. Collagen fibrils, which are around 5 – 20 nm in diameter (Mow *et al.*, 1974), are densely packed and are arranged parallel to the surface and can withstand very high tensile stresses. Very high tensile and compressive stresses are experienced in this zone.

Mid zone is 40 – 60% of the total thickness. Water and collagen content decrease in this zone compared to that in STZ but aggrecan content increases. Collagen fibrils in this zone have larger diameter of around 30 -5000 nm (Mow *et al.*, 1974) and are randomly oriented.

Deep zone is around 30% of the total thickness. In this zone water content decreases further and though collagen content remains constant they are bundled together and are perpendicular to the surface. These bundles anchor the soft cartilage onto the subchondral bone.

Calcified zone is where cartilage has become stiffer and is differentiated from the bulk of soft cartilage by tide-mark.

Recently, it has been hypothized that there may be two more acellular and non-collagenous layers covering the STZ (Orford and Gardner, 1985; Levanon and Stein, 1991; Forster and Fisher, 1999) viz. surface lamina of proteoglycans and boundary layer of phospholipids and glycoproteins (Figure 1-3). A single biphasic surface amorphous layer (BSAL) above STZ, without any individual consideration to surface lamina and boundary layer, has also been extensively studied by Graindorge and colleagues (Graindorge *et al.*, 2003; Graindorge *et al.*, 2004; Graindorge *et al.*, 2005).

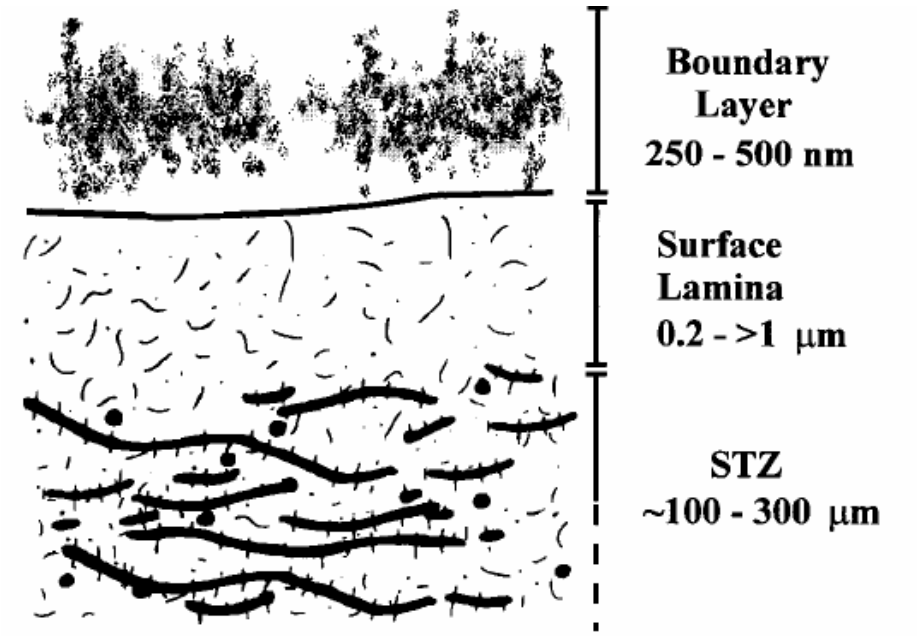

Figure 1-3 Cartilage structure showing surface lamina and boundary layer (Orford and Gardner, 1985; Forster and Fisher, 1999)

1.2.2.2 Osteoarthritis

Articular cartilage is highly hydrated hyaline cartilage and offers a very good bearing surface against the physiological loads and stresses it experiences. It has an efficient lubrication mechanism providing a very low co-efficient of friction, values ranging from 0.001 to 0.03 (Mow and Lai, 1980; Macirowski *et al.*, 1994; Persson, 2000) and undergoing little wear. Under normal physiological conditions it survives the lifetime of a human being in spite of experiencing very high loads, as high as 7 - 9 times body weight during stair climbing or stumbling (Crowninshield *et al.*, 1978; Hodge *et al.*, 1986; El'Sheikh *et al.*, 2003; Mow and Huiskes, 2005), and wide variety of motions, speeds ranging from 0.06 m/s to 0.6 m/s (Mow and Huiskes, 2005). Articular surface contact pressures of 18 MPa and higher have been reported in the literature (Hodge *et al.*, 1986).

Age, injury, improper use or loading, trauma, congenital and other joint diseases may lead to the breakdown of the cartilage. It may also lose its functionality due to the immune system malfunction and internal crystal depositions (Tortora and Grabowski, 2004). The complete breakdown of the cartilage will expose the underlying subchondral bone and cause immense pain.

Arthritis is a joint disorder which is characterized by swelling and pain. It can be broadly classified into three categories as follows (Tortora and Grabowski, 2004):

1) Rheumatoid Arthritis which is caused by the immune system attacking its own tissues and characterized by joint swelling, pain, redness and inflammation of synovial membrane.

2) Osteoarthritis is characterized by the degeneration and deterioration of the articular cartilage and its main causes may be ageing, injury, improper use (Yang, 2003), wear and tear, trauma or congenital or acquired disease.

3) Gouty Arthritis is characterized by the deposition of sodium urate crystals in the cartilage causing irritation, swelling, pain and ultimately complete erosion of the cartilage.

Of all the three, osteoarthritis or OA, as it is commonly known, is mostly induced by the mechanical factors, though, its exact etiology is still unknown. It shows degradation of cartilage structure and its mechanical properties and therefore, from mechanical engineering perspective, articular cartilage has been studied over many years directly or indirectly with respect to OA (Brown and DiGioia, 1984; Mow *et al.*, 1992; Ateshian and Wang, 1995; Ateshian and Wang, 1997; Donzelli and Spilker, 1998; Appleyard *et al.*, 1999; Guilak *et al.*, 1999; Setton *et al.*, 1999; Adeeb *et al.*, 2004; Federico *et al.*, 2004; Wilson *et al.*, 2004; Mow and Huiskes, 2005).

OA treatments fall broadly into two categories: medical care and surgical care (Lozada and Steigelfest, 2006). Medical care includes all the non-pharmacologic remedies like joint stress reduction and physiotherapy, and pharmacologic remedies. Surgical care includes arthroscopy, osteotomy, hemiarthroplasty and arthroplasty.

Of all these treatments only hemiarthroplasty will be discussed briefly because of its relevance to current work. As the name suggests it is a surgical treatment for OA where only one part of the joint is replaced by metallic implant. This implant rests against the natural articular cartilage of the adjoining bone in the joint. Hip hemiarthroplasty is normally employed for femoral neck fractures and is characterized by shorter surgical times and lower costs as compared to total hip replacement surgery (van der Meulen *et al.*, 2002). Though it is a very conservative approach, acetabular cartilage erosion (Dalldorf *et al.*, 1995) acetabular protrusion (Soreide *et al.*, 1982) have been reported. Hemiarthroplasty has been also used on other joints like shoulder (Neer, 1955) and knee (Macintosh, 1958). In hemiarthroplasty, the articulation is between metallic implant and natural articular cartilage and this may induce cartilage erosion which may also depend upon the location of the metal implant (van der Meulen *et al.*, 2002). The progressive degenerative losses of the cartilage leading to its complete loss were observed by Cruess and colleagues (Cruess *et al.*, 1984) in canine hip hemiarthroplasty.

1.2.2.3 Mechanical charactersization and Testing

Testing is an integral part of any study. Articular cartilage has been studied either to explain its observed behaviour or to quantify its mechanical properties. Cartilage testing can be either *in vivo* or *in vitro* or *in situ*. Apart from the instantaneous and equilibrium responses of the cartilage to the compressive loading, its transient response is also important in understanding the cartilage functionality.

A] Transient behaviour of cartilage

One of the important observations normally made in cartilage study is its transient or time-dependent behaviour. When the compressive deformation/load is applied to the cartilage, initially most of the load is carried by fluid phase due to the interstitial drag forces (Mow *et al.*, 1980; Mow and Huiskes, 2005). As the fluid redistribution takes place more and more load is supported by solid matrix and at equilibrium the load is entirely carried by solid matrix and the fluid flow ceases.

This time-dependent behaviour can be studied by observing two very basic responses of the cartilage when subjected to compressive loading: stress-relaxation and creep-deformation.

Stress-relaxation

Stress-relaxation is the stress-attenuation within the tissue in response to an applied deformation. This reduction in stress distribution is time-dependent. When ramp displacement is applied to the cartilage surface, the stresses in the cartilage increase till they reach maximum at the end of the ramp displacement. From this point onwards compressive strain is held constant and the stresses in the cartilage at this point are mostly carried by fluid phase. The stresses are then carried away from the area of compaction (Mow *et al.*, 1980; Mow and Huiskes, 2005) mainly due to fluid redistribution. The equilibrium stress will be eventually reached. Fluid exudation will occur at the surface during ramp phase which will stop during relaxation phase.

Creep-deformation

Creep response of the tissue is the time-dependent deformation under a constant load. In this case load is suddenly applied to the cartilage and is maintained thereafter. Fluid exudation is made possible by imposing free-draining condition on the cartilage surface. As the fluid flows out of the cartilage creep deformation occurs

till an equilibrium is reached (Mow *et al.*, 1980; Mow and Huiskes, 2005). At equilibrium the applied stress is entirely balanced by the solid matrix stresses (Warner, 2000).

It is to be noted that in both the stress-relaxation and creep-deformation, as the compaction occurs, the volume of the interstitial voids reduces thus reducing its permeability and therefore permeability is strain dependent.

B] Testing

Three different experimental testing configurations have been primarily used by different researchers: unconfined compression, confined compression and indentation.

Unconfined Compression

In unconfined compression, the circular plug of the articular cartilage or cartilage with intact bone is compressed between two impermeable platens making frictionless contact with the specimen. The radial displacement of the specimen and radial fluid exudation are not constrained.

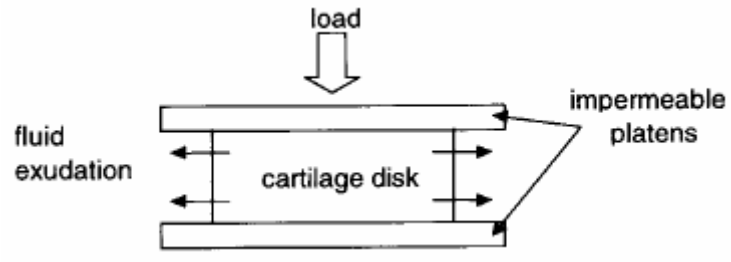

Figure 1-4 Unconfined compression (Warner *et al.*, 2001a)

It should be noted that there always exists friction at platen-specimen interface and initial contact conditions are unknown (Warner *et al.*, 2001a).

Confined Compression

In confined compression, a cylindrical plug of cartilage is compressed by porous-permeable indenter inside impermeable cylindrical sleeve. This prevents radial displacement of the cartilage and radial fluid exudation.

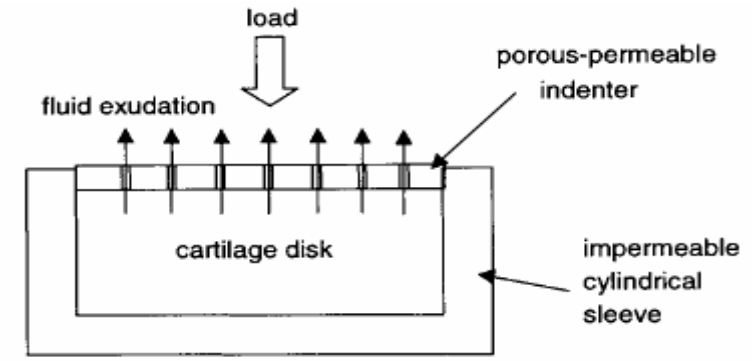

Figure 1-5 Confined compression (Warner *et al.*, 2001a)

Mow and his colleagues (Mow *et al.*, 1980) concluded that it was impossible to cut a cylindrical specimen with exactly smooth sidewalls and an accurate diameter. Thus, during compression the cartilage plug will expand laterally and fill the space in the cylindrical sleeve before true confined compression begins.

Indentation

In indentation tests, cylindrical plane-ended or hemispherically-ended indenter, which is either porous or non-porous, is used to compress articular cartilage. This method is widely used as it is easily reproducible, does not require complex specimen preparation and can be performed *in situ* when cartilage is still attached to the bone (Warner *et al.*, 2001a).

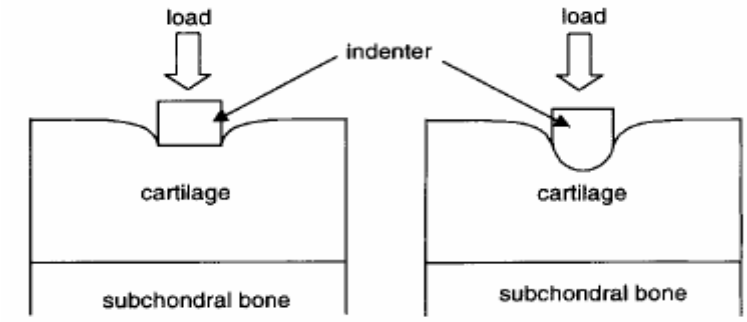

Figure 1-6 Indentation with plane ended cylindrical indenter and hemi spherically ended indenters (Warner *et al.*, 2001a)

1.2.2.4 Theoretical formulation and finite element modelling

A] Theoretical formulation

Though the articular cartilage is multiphasic, non-linear and anisotropic, the earliest studies on the cartilage assumed it to be single phase, elastic, linear, isotropic and homogeneous (Hirsch and Frey, 1944; Elmore *et al.*, 1963; Sokoloff, 1966;

Kempson *et al.*, 1971). Analytical models along with the indentation creep experiments were used to derive the useful mechanical properties of the cartilage. These models had limitations as they could only be used for the instantaneous and long-term equilibrium responses, but could not predict the transient behaviour (Hayes *et al.*, 1972).

Hayes and Mockros (Hayes and Mockros, 1971) presented the constitutive relationship for cartilage shear and bulk creep using a generalized Kelvin solid of dashpots and springs representing viscoelastic body. Hayes and colleagues (Hayes *et al.*, 1972) also suggested modelling the cartilage as viscoelastic rather than elastic in order to investigate time-dependent effects. Parsons and Black applied viscoelastic theory to the indentation creep using plane-ended ram and took into account the instantaneous response of the cartilage (Parsons and Black, 1977). These models, however, were not capable of explaining the role of interstitial fluid flow in load bearing capabilities of the cartilage

Higginson and colleagues (Higginson *et al.*, 1976) considered the effect of interstitial fluid flow and concluded that under cyclic loading the short-term creep deformation response was purely elastic. Johnson and colleagues observed that under uniaxial compression with sinusoidal compressive stress in the frequency range of 0.8 – 2.5 Hz superimposed upon static compressive stress, the cartilage response was purely elastic and was unaffected by interstitial fluid flow (Johnson *et al.*, 1977). However, Elmore and colleagues (Elmore *et al.*, 1963) had earlier shown that the creep response of the cartilage in indentation was mainly due to the exudation of the interstitial fluid.

Mow and colleagues (Mow *et al.*, 1980), proposed biphasic theory based on mixture theory to explain cartilage deformational behaviour where cartilage is considered to be made up of two immiscible phases: a fluid phase and a solid phase. The fluid phase representing the interstitial fluid is incompressible and inviscid, and solid phase representing collagen fibres, proteoglycans and other components is porous, permeable and incompressible. The compressive-deformational characteristics of the cartilage are due to the fluid flow and exudation through the porous, permeable solid. The rate of volumetric discharge Q across area A is related to permeability co-efficient *k* by Darcy's law (Mow and Huiskes, 2005):

$$Q = kA\Delta P/h \qquad \textbf{1-1}$$

where,

ΔP – Pressure gradient

h – Specimen thickness

The value of k ranges from 10^{-15} to 10^{-16} m^4/N-s. and is inversely related to diffusive drag co-efficient K by the following equation:

$$K = (\phi^f)^2 / k \qquad \textbf{1-2}$$

where,

Φ^f – Tissue porosity which is the ratio of the fluid volume to total tissue volume and its value is approximately 0.75.

From this discussion it is clear that the value of K will be very high and are in the range 10^{14} to 10^{15} N-s/m^4 (Mow and Huiskes, 2005). The flow of fluid in the tissue is thus accompanied by large drag forces.

When infinitesimal strain and constant permeability are assumed, this theory assumes the form of linear biphasic theory which can explain compressive creep and stress-relaxation responses of the cartilage or other hydrated soft tissues observed in experiments (Mow *et al.*, 1980; Armstrong and Mow, 1982; Mow *et al.*, 1984; Best *et al.*, 1994; Soltz and Ateshian, 1998).

It is well-known that the cartilage compaction is non-linear and it is not only due to the strains applied to the surface but also due to the drag forces of the interstitial fluid as it flows through ECM. As compaction increases the volume of the voids decreases which is accompanied by the increase in the drag forces and the decrease in permeability (Lai and Mow, 1980; Warner, 2000). The terms “apparent permeability” and “intrinsic permeability” have been used to define this phenomenon. Apparent permeability is the one which is due to both the applied strain and drag forces whereas intrinsic permeability is the one which is only due to the applied strain (Lai and Mow, 1980; Holmes, 1985; Warner, 2000). Strain-dependent permeability was thus accounted for in the biphasic model (Lai and Mow, 1980; Lai *et al.*, 1981; Mow *et al.*, 1984; Holmes, 1985; Holmes *et al.*, 1985)

Infinitesimal strain assumed in linear biphasic theory does not hold true for the cartilage in the actual joints as they experience high stresses and large strains (Kwan *et al.*, 1990), sometimes more than 20% (Mow and Huiskes, 2005). Hence the model was further improved upon by including non-linear finite-deformation to get more realistic and physiologically relevant results (Mow *et al.*, 1984; Holmes *et al.*, 1985; Holmes, 1986; Holmes and Mow, 1990; Kwan *et al.*, 1990). The compressive stiffening effect was observed using finite deformation theory at high stresses (> 0.2 MPa) and high strains (> 20%).

Material anisotropy (Cohen *et al.*, 1998) and structural non-homogeneity (Li *et al.*, 1999; Li *et al.*, 2002) were also accounted for subsequently.

The biphasic theory can explain only the flow-dependent drag-induced viscoelasticity of the cartilage. Flow-independent viscoelasticity of the solid matrix was studied by Hayes and Bodine (Hayes and Bodine, 1978) and was incorporated in the biphasic theory by Mak (Mak, 1986). Uniaxial creep compression experiments were conducted by Setton and colleagues (Setton *et al.*, 1993) using this biphasic poroviscoelastic theory and was shown that the flow-independent viscoelasticity plays a significant role with the increase in the permeability of the cartilage as could be seen in the damaged cartilage.

Lai and colleagues (Lai *et al.*, 1991) proposed triphasic theory where the dissolved cations and anions were considered to be the third phase. This theory, apart from biphasic effects, described the swelling of the cartilage due to Donnan osmotic pressure. The pressure gradient due to the difference in the negatively charged ionic concentrations in the interstitial fluid and external environment was found to give rise to osmotic pressure (Wilson *et al.*, 2005) which could support 13 – 22 % load at equilibrium in unconfined compression (Sun *et al.*, 2004). This osmotic pressure under unloaded physiological conditions could be as high as 0.2 MPa (Mizrahi *et al.*, 1986; Olsen and Oloyede, 2002). Negatively charged glycosaminoglycan (GAG) of proteoglycans were found to be responsible for this phenomenon (Maroudas, 1968; Oloyede and Broom, 1991).

Huyghe and Janssen (Huyghe and Janssen, 1997) represented cartilage as quadriphasic with separate cation and anion phases apart from fluid and solid phases. Both experimental and numerical validations of this theory for intervertebral disc were done by Frijns and colleagues (Frijns *et al.*, 1997).

Loret and Simoes modelled articular cartilage with one solid phase and two fluid phases (Loret and Simoes, 2004). In their model the solid phase represents collagen fibres and one fluid phase represents intrafibrillar water stored between collagen fibrils along with dissolved NaCl while the other represents extrafibrillar water, proteoglycans and anions and cations of NaCl.

The tension modulus at the cartilage surface was found to be higher than the compressive modulus (Park *et al.*, 2003). High interstitial fluid pressures induced at the surface were due to this tension-compression non-linearity at the surface and this high pressure was found to support more than 90% of the load for a long duration (Ateshian and Wang, 1995; Soltz and Ateshian, 1998). Low friction and wear observed in cartilage was also found to be due to this interstitial fluid pressurization (Ateshian, 1997; Ateshian *et al.*, 2003).

B] Finite element modelling

To study any complex system, it is necessary to break it down into simple manageable sub-systems and study them individually. The understanding of these sub-systems helps us deal with the complex system in a much more simplistic and easier way.

Molecules, atoms and subatomic particles form the matter, however, many of the observed behaviour of the matter can be explained without going down to the molecular level (Batra, 2006). This constitutes the basis of continuum theory. It can be further said that many of the engineering problems involving continuum mechanics, may not require "exact closed-form" solutions in order to understand them (Owen and Hinton, 1980) and approximate solutions are often sought.

Finite element (FE) method is a numerical technique where the entire continuum is subdivided into number of elements effectively reducing the degrees of freedom to the manageable number (Warner, 2000). Each element has nodes at their vertices and sometimes on the edges as well as within the element (Owen and Hinton, 1980; ABAQUS., 2005). One element is connected to the next at these nodes thus forming a mesh of elements representing the original continuum. The variables of interest like displacement, stresses, etc are usually obtained at nodal points by solving set of equations constructed by taking into consideration the individual elemental properties

As is evident from this process of discretization i.e. breaking down the continuum into finite number of elements, the solution obtained by FE method is not exact but approximate. As the number of element increases the solution will improve due to the increase in the number of degrees of freedom but at the cost of added computations. Approximations mentioned before are not only in the geometry but also in material properties, loading conditions, boundary, interface and initial conditions (Warner, 2000). These approximations will add inaccuracies to the model and thus validation becomes an important step towards using the model.

Finite Element Method (FEM) was first used by aeronautical engineers for stress evaluation (Owen and Hinton, 1980) in 1950s, however, it was first used in orthopaedic biomechanics literature only in 1972 by Brekelmans and colleagues (Huiskes and Chao, 1983) in their paper published in Acta Orthopaedica Scandinavica (Brekelmans *et al.*, 1972) for mechanical analysis of skeletal parts. Since then FEM has come a long way in its application to orthopaedic biomechanics. It is particularly suited to biomechanics due to the complexities in geometry, loading and material of the systems to be evaluated (e.g. bones, articular cartilage, spine, etc.) (Huiskes and Chao, 1983).

The FEM was first used to model soft tissues (intervertebral disc) by Belytschko and colleagues (Belytschko *et al.*, 1974), however, it was not until 1977 that articular cartilage was first modelled by Roth and Mow (Roth and Mow, 1977) as a single phase linearly elastic homogeneous isotropic material. An increase in stress in pathogenic cartilage was observed as compared to normal cartilage when indentation was carried out with hemispherical indenter and the softening was introduced directly below the contact.

There have been other single phase models (Brown and DiGioia, 1984; Brown *et al.*, 1984; Carter *et al.*, 1987; Anderson *et al.*, 1990; Anderson *et al.*, 1991) where entire joint was modelled as linearly isotropic.

Mixture theory has been used to describe biphasic constitutive behaviour of the soft hydrated biological tissues (Mow *et al.*, 1980). Soils consolidation theory of Biot (Biot, 1941), on the other hand, can be applied to the porous media under compression (Goldsmith *et al.*, 1996) and when time-dependent behaviour of the porous material is to be studied. Articular cartilage is hydrated as well as porous-permeable. Thus, both these theories can be applied for FE analysis of articular cartilage. Application of soils consolidation theory to the uniaxial confined compression problem of the cartilage was made by Oloyede and Broom (Oloyede and Broom, 1991) and inferred that the soils consolidation theory could be applied for cartilage consolidation.

Two different formulations have been used in FE analysis: *u-v* and *u-p*. In *u-v* formulation governing equations use displacement and relative fluid velocity and was developed by Spilker and colleagues (Spilker *et al.*, 1988; Spilker *et al.*, 1992b; Spilker *et al.*, 1992a; Goldsmith *et al.*, 1996). On the other hand, *u-p* formulation uses displacement and pressure (Wayne *et al.*, 1991; van der Voet, 1992; Wayne, 1995; Warner, 2000).

Purely linear biphasic theory has been modelled for unconfined compression (Spilker *et al.*, 1990) and indentation (Spilker *et al.*, 1992a; Hale *et al.*, 1993; Suh and Spilker, 1994) under stress-relaxation. Indentation creep-deformation was modelled by Suh and Spilker (Suh and Spilker, 1994).

FE model of a plane ended cylindrical indenter and cartilage was examined under stress-relaxation by Spilker and colleagues (Spilker *et al.*, 1992a). The indenter was either porous or impermeable and the cartilage-indenter interface was either perfectly lubricated or perfectly adhesive. It was found that the peak reaction force was about 10% larger in case of solid indenter and adhesive interface when compared with porous indenter and lubricated interface respectively.

Some important observations regarding cartilage FE models were made during this study. Those relevant to the current study have been quoted below:

1) The subchondral bone can be modelled as rigid and impermeable as the bone is much stiffer as compared to cartilage, approximately by 3 orders of magnitude (E_{bone} ~ 20 GPa and $E_{cartilage}$ < 1 MPa) (Goldsmith *et al.*, 1996; Warner, 2000) and do not affect the predicted cartilage response.

2) In an axisymmetric indentation model, the cartilage can be assumed to represent large specimen if its width is greater or equal to the larger of four times cartilage thickness or four times indenter radius (see section 2.2.1).

3) Non-linear finite deformation theories need to be used to quantitatively interpret strains observed for "thin tissue at short ramp times" and for "high strain levels in thick tissues" as the tissue experiences significantly high level of local strains and stresses.

4) The fluid phase plays an important role in short-time and transient response of cartilage. Thus model needs to be biphasic (Warner, 2000).

It is to be also noted here that the choice of material properties to be used in FE models is also of prime importance as shown by Hale and colleagues (Hale *et al.*, 1993). In their linear biphasic model of indentation stress-relaxation tests to study osteochondral defects, they found out that the solution error is much more sensitive to aggregate modulus and Poisson's ratio than permeability.

The permeability of the cartilage decreases with the increasing strain (Lai and Mow, 1980). This strain-dependent permeability was modelled by Spilker and colleagues (Spilker *et al.*, 1988) in confined and unconfined compression and indentation stress-relaxation configurations. The accuracy of the FE results increased with the inclusion of non-linear permeability (Goldsmith *et al.*, 1996).

Other nonlinearities like finite deformation were also successfully modelled (Suh *et al.*, 1990; Suh *et al.*, 1991) to take into account large strains and high stresses observed in the cartilage.

Triphasic theory was also used for FE modelling (Sun *et al.*, 1999; Olsen and Oloyede, 2002; Sun *et al.*, 2004; Chen *et al.*, 2006) and quadriphasic theory was validated for soft tissues by Frijns and colleagues. (Frijns *et al.*, 1997)

Biphasic poroelastic models were studied by many researchers (van der Voet, 1992; van der Voet *et al.*, 1992; Goldsmith *et al.*, 1995; Warner, 2000; Warner *et al.*,

2001a; Federico *et al.*, 2004). The solid phase in these studies was modelled as porous-permeable and elastic. Soils consolidation was used in these models.

Apart from purely elastic, the solid phase has also been modelled as hyperelastic or rubber-like (Spilker *et al.*, 1992b; Liu *et al.*, 2004) and viscoelastic (Ehlers and Markert, 2001; Wilson *et al.*, 2004) respectively to account for the finite strains and transient behaviour observed in the cartilage. Collagen fibrils have also been modelled separately (Li and Herzog, 2004; Shirazi and Shirazi-Adl, 2005).

The cartilage model with viscoelastic solid matrix by Ehlers and Markert (Ehlers and Markert, 2001) showed that the viscoelastic effects decreased with the increase in the loading time and that the long term cartilage response was due to the fluid flow. Li and Herzog modelled collagen fibres as viscoelastic and found that it plays important role only in tensile testing whereas the flow-dependent viscoelasticity was significantly more dominant under unconfined compression (Li and Herzog, 2004).

In the poroelastic model developed by Goldsmith and colleagues (Goldsmith *et al.*, 1995) stress-relaxation was studied using a plane ended rigid cylindrical indenter. The magnitude of deformation of 10% was applied over a ramp time of 500s and maintained further for another 2000s. The results were compared to those of Spilker and colleagues (Spilker *et al.*, 1992a). The higher peak stresses and strains observed were hypothized to be due to two reasons: first, Spilker and colleagues used infinitesimal strains whereas this study used finite deformation formulation available in ABAQUS; second, former used 4 node elements whereas latter used 8 node elements with mid-side nodes. Another important observation made was the finite time taken for the maximum pore pressure to build up before decaying. This is the characteristic of the cartilage and not soils.

1.2.3 Biotribology

Tribology is the "science and technology of interacting surfaces in relative motion and of related subjects and practices" and term itself was coined very recently in the year 1966 (Czichos, 1978). It includes friction, wear, lubrication and other related fields (Czichos, 1978).

Tribology as applied to animal or human joints is known as biotribology. It covers both the natural and artificial joints among other biological systems. Animal or human joints show excellent lubrication mechanism and their co-efficient of friction is very low; typically in the range of 0.001 – 0.03 (Mow and Lai, 1980; Macirowski *et al.*, 1994; Persson, 2000), though different researchers quote different

ranges. The corresponding range of values for Alumina femoral head of 22.25 mm radius on UHMWPE (Ultra High Molecular Weight Polyethylene) socket is 0.023 – 0.034 (Saikko, 1992; Hall and Unsworth, 1997).

1.2.3.1 Friction, Wear and Lubrication

A] Friction

When two opposing surfaces slide against each other, there is always going to be some resistance to this motion either due to the asperities on both the contacting surfaces or due to the viscosity of the lubricating fluid present between these surfaces. This resistance to motion is termed friction.

The two contacting surfaces are touching each other only at microscopic asperities and sum of all these micro areas is the real area of contact between them which carries the applied normal load.

The cartilage friction was found to be mainly due to the solid phase sliding against the solid phase of the articulating surface (Ateshian, 1997; Ateshian *et al.*, 1998). Thus, the more the load carried by interstitial fluid the lesser would be the load carried by the solid phase due to lesser asperity contacts (Mow and Huiskes, 2005). The terms "equilibrium friction co-efficient" and "effective friction co-efficient" were used to describe this phenomenon. The equilibrium friction co-efficient is the value when the cartilage has consolidated and reached its equilibrium and hence the entire load will be carried by solid matrix. The creep equilibrium time of more than 45 minutes has been reported in literature for tests with hemispherical indenter (Forster and Fisher, 1996). The cartilage of 2 – 4 mm thickness takes around 4 – 16 hours to reach creep equilibrium where as the one with less than 1 mm thickness takes around 1 hour (Nordin and Frankel, 1989). Effective friction co-efficient is the one during initial and transient phase and will depend upon the load carried by the fluid phase at that instance.

If N is the total normal load and N^s and N^f are the fractions of normal load supported by solid and fluid phases respectively, then;

$$N = N^s + N^f \qquad \textbf{1-3}$$

$$\mu_{eff} = \mu_{eq} N^s/N \quad \textbf{1-4}$$

where

μ_{eff} – Effective friction co-efficient

μ_{eq} – Equilibrium friction-coefficient

As can be seen, the value of μ_{eff} will be much smaller when the interstitial fluid is pressurized even though the value of μ_{eq} is not small.

B] Wear

Wear is "the progressive loss of substance from the operating surface of a body occurring as a result of relative motion at the surface" (Czichos, 1978).

The mass of volume loss was found to be difficult to measure in hydrated tissues mainly because of swelling (Mow and Huiskes, 2005). The wear rate was measured by sliding cartilage plugs against polished stainless steel surface in saline bath and measuring the contents of hydroxyproline (collagen marker) and hexosamine (Proteoglycan marker) which were used as markers (Lipshitz *et al.*, 1975; Lipshitz and Glimcher, 1979; Mow and Huiskes, 2005). Wear rates were found to be extremely low. Initial wear was high which moved towards steady state conditions. It was also observed that the wear rate was dependent upon the applied load and the roughness of the stainless steel surface. Wear rates were found to be increasing with the applied load and the relative sliding speed of the opposing surfaces. Synovial fluid was found to reduce wear but the reasons for the same were not conclusive enough though many hypotheses were put forward like presence of lubricin (Swann and Radin, 1972), phospholipids (Hills, 1989) and hyaluronic acid (Bell *et al.*, 2002).

The remarkably low wear rates may be because of interstitial fluid pressurization and the rates may increase due to abrasion and adhesion if permeability increases as in case of OA due to reduced fluid load support (Mow and Huiskes, 2005). The joint is subjected to repetitive loads and motion and also the impact loads which can induce wear.

C] Lubrication

Lubrication is a mechanism to reduce friction and wear. If the two contacting surfaces moving relative to each other are separated by a film of fluid, relatively

little friction may be expected. This film can be easily sheared to bring about the relative motion without damaging the underlying contacting surfaces.

Many hypotheses have been proposed to explain the lubrication mechanism operating in the cartilage joint. The loading in the joint is very complex and occurs at different speeds and may remain so for different time durations. The spatial and temporal distribution of the loading is so varied that, though, some of these hypotheses may explain the lubrication mechanism under certain conditions they are not able to do so under all the possible scenarios.

Articular cartilage was found to be an excellent bearing material providing a well lubricated surface with a very low co-efficient of friction and minimal wear by virtue of its properties and synovial fluid (Mow and Huiskes, 2005). Synovial fluid, a clear or yellowish highly viscous non-Newtonian fluid secreted by synovium, was found to be a "dialysate of blood plasma without clotting factors, erythrocytes, or haemoglobin". However, it was found to contain hyaluronate, lubricating glycoprotein and wear-retarding phospholipids, exhibiting reduction in viscosity in degenerative joints (Mow and Huiskes, 2005).

Articular cartilage surface was found to be rough when compared to other engineering bearing surfaces. Arithmetic mean deviation (R_a) has been used to quantify the roughness of the surfaces. R_a is the average of microscopic surface areas above and below a reference line over a given length.

Under unloaded conditions, R_a for articular cartilage was found to vary from 1 to 6 μm where as for metal femoral head it was around 0.025 μm (Dowson, 1981) and for ceramic it was 0.005 μm (Jin *et al.*, 1997). As can be seen, microscopically, cartilage surface is very rough and still show remarkable lubricating properties.

Stribeck plotted the coefficient of friction as a function of lubricant viscosity, velocity and normal load for sliding and rolling surfaces (Czichos, 1978). Based on these parameters and the separation of two surfaces, three main lubrication regimes were identified as below:

I) Fluid film lubrication

Fluid film lubrication would be present where the bearing surfaces were separated by a lubricant film whose thickness was larger than the combined surface roughness of the two surfaces. The film thickness should be 2 – 3 times the surface roughness for effective fluid film lubrication. In this regime, the load would be entirely carried by the fluid film and the resistance to the motion would be due to the

internal fluid friction. In this regime, there would be minimal of wear as the two surfaces would not have come in physical contact.

The synovial joint would function in this regime only when the minimum fluid-film was maintained to completely separate the two articulating surfaces. This regime is further classified into following categories:

Hydrodynamic lubrication

Hydrodynamic lubrication would be possible only when the two articulating surfaces move at high-speeds relative to each other so that the lubricating fluid could be drawn into the converging wedge-shaped gap. The lubricating fluid pulled into the gap would then lift the surfaces due to high pressure generated, but to maintain this film the high-speed relative motion between the two surfaces would have to be continuous. The minimum film thickness for the knee joint could be 0.029 μm and for hip joint it could be 0.020 μm which was found to be too small (Mow and Huiskes, 2005). The hydrodynamic lubrication could be present in the glenuhumeral joint of the shoulder of the baseball pitcher which experiences high-speed motion and light loads during pitching (Mow and Huiskes, 2005). It might also possibly exist during swing phase of walking. However, with so many different low-speed motions at other joints combined with the effects of varying viscosity of synovial fluid, cartilage deformation and interstitial fluid flow, hydrodynamic lubrication could not be generalized as the only one existing at these joints (Mow and Huiskes, 2005).

Elastohydrodynamic lubrication

When the hydrodynamic pressure generated from the hydrodynamic action would be sufficiently high or when the elastic moduli of the bearing surfaces would be relatively low, elastic deformation of the bodies might take place. In this kind of lubrication, known as elastohydrodynamic lubrication, here would be no physical contact between the surfaces and hence wear is minimal.

With the consideration of the cartilage deformation, the load would spread over a larger surface area and would help in enhancing lubrication by increasing fluid-film thickness to around 1.25 μm for knee joint and 1.3 μm for hip joint (Dintenfass, 1963a; Dintenfass, 1963b; Mow and Huiskes, 2005). Dowson and Jin (Dowson and Jin, 1986) studied the effect of local deformation on surface asperities and found that this local loading can flatten or smooth out the surface asperities, thus

effectively increasing the film thickness by the factor of 19 relative to R_a. Linn also supported the existence of elastohydrodynamic lubrication (Linn, 1968).

Self-generating fluid-film

Under slow and moderate loading, self-generating fluid-film mechanism was observed by Mow and Lai (Mow and Lai, 1980; Mow and Huiskes, 2005). In their model thin articular cartilage attached to the bone was considered with "parabolically distributed normal load sliding over its surface at physiological speeds". Synovial fluid hydrodynamic pressure acting on the cartilage surface was modelled by this load distribution. Fluid exudation from the trailing and leading edges of the load and imbibition near the centre was observed, from which it was concluded that the fluid exuded from the leading edge could be providing the fluid supply required to maintain the fluid film. Similar studies were done by Kwan and colleagues (Kwan *et al.*, 1984). This was also observed experimentally by Mow and Lai (Mow and Lai, 1979).

This self-generating mechanism would diminish with the progression of OA resulting in the higher co-efficient of friction.

Squeeze-film lubrication

When two surfaces approach normal to each other, the lubricant would be trapped inside the gap as it cannot be squeezed out instantaneously due to its viscosity. This viscous resistance would give rise to time varying pressure field which could support high loads. This kind of lubrication mechanism would possibly exist in the joints in knee, hip and ankle (Mow and Huiskes, 2005). Squeeze-film time or the theoretical time required to reduce the fluid film thickness to a certain level before asperity contact occurs (Higginson and Unsworth, 1981), should be greater than physiological loading times for the joint to be in this lubrication regime (Mow and Huiskes, 2005). The replenishment of this film would take place during the motion of the joint as in the case of swing phase of walking when the load on the hip joint would decrease and velocity would increase.

II) Mixed lubrication

If, however, the fluid film thickness were to decrease for variety of reasons like decrease in viscosity or velocity, the asperities of two surfaces would begin to make contact. The load would be then carried by lubricant as well as contacting asperities and wear would be more. The resistance to motion would be due to the shear

resistance of the lubricant as well as due to the contacting asperities. This would be mixed lubrication regime.

In synovial joint, sometimes both fluid-film and boundary lubrication were found to exist. The part of the load would be carried by the fluid and part by the cartilage asperities under boundary lubrication regime (Linn, 1968). The coefficient of friction would depend on both the phenomenon. These can be subcategorized into:

Weeping lubrication or Hydrostatic lubrication

Weeping lubrication or hydrostatic lubrication was proposed by McCutchen (McCutchen, 1959) and experimentally proved by Lewis and McCutchen (Lewis and McCutchen, 1959; McCutchen, 1962). According to McCutchen and Lewis, as the contacting surfaces came in contact, the interstitial fluid exuded through the porous structure. This fluid was enough to maintain the surface layer of around 15 – 35 μm thick which could keep the surface well lubricated. Macirowski and his colleagues (Macirowski *et al.*, 1994) proposed that the weeping reduced friction and wear by reducing solid-to-solid contact and not by reducing co-efficient of friction at the contact points. Co-efficient of friction got reduced mainly because of load partitioning and effective lubrication of contact area.

Interstitial fluid pressurization

The frictional co-efficient was found to increase and attain an equilibrium value as the cartilage reaches its creep-deformation equilibrium (Mow *et al.*, 1992; Forster *et al.*, 1995; Forster and Fisher, 1996). In weeping lubrication mechanism discussed earlier the majority of the load was carried by interstitial fluid pressurization which helped to reduce the friction (McCutchen, 1962). Boundary friction model based on biphasic theory was proposed by Mow and Lai (Mow and Lai, 1980) and was experimentally verified by Forster and Fisher (Forster *et al.*, 1995). It was later verified theoretically by Ateshian (Ateshian, 1997). The co-efficient of friction was shown to be time-, velocity- and load-dependent and the interstitial fluid pressurization reduced the effective co-efficient of friction. Experimental support to this hypothesis was also provided. Forster and colleagues (Forster *et al.*, 1995; Forster and Fisher, 1996) conducted creep-deformation experiments to study the effect of loading time on friction and found interstitial fluid pressurization to be an important factor responsible for reducing effective co-efficient of friction. Soltz and Ateshian (Soltz and Ateshian, 1998) conducted both confined compression creep-deformation and stress-relaxation in order to measure

the interstitial fluid pressure and to prove that this pressure could be predicted using biphasic theory. It was found that under physiological conditions of loading for up to 3500 seconds, around 90% of the load was supported by the interstitial fluid pressurization which reached 100% under confined compression experiments.

The fluid load support was also studied by Park and colleagues (Park *et al.*, 2003) in unconfined compression stress-relaxation. It supported the hypothesis of 90% load support by interstitial fluid pressurization and further showed that this pressurization decreased with depth and was the maximum at the surface. This was attributed to tension-compression non-linearity at the surface.

Ateshian and colleagues (Ateshian *et al.*, 2003) found that the equilibrium co-efficient of friction decreased with the increase in applied load, compressive strain and concentration of salt solution in unconfined compression creep apart from time dependence of effective co-efficient of friction due to interstitial fluid pressurization.

Some (Bell *et al.*, 2006) prefer to call it biphasic lubrication as its theoretical foundation is biphasic theory of Mow and colleagues.

Biphasic surface amorphous layer (BSAL) was studied by Graindorge and colleagues (Graindorge *et al.*, 2004; Graindorge *et al.*, 2005). It was observed that the load supported by the fluid in this layer is greater than that supported by the fluid in the bulk of the cartilage as the solid content is lesser in the BSAL. It was also found that under cyclic loading, BSAL was more effective in maintaining the lubrication compared to static loading.

Boosted lubrication

In boosted lubrication proposed by Maroudas and, Walker and colleagues (Maroudas, 1967; Walker *et al.*, 1968), as two articulating surfaces came closer creating squeeze-film, water part of the synovial fluid entered the articular cartilage surface in the contact area. As this happened synovial fluid got filtered leaving behind hyaluronic acid – protein complex in the gap owing to its larger size (4000 A^o) compared to cartilage pore size (20 – 70 A^o) (Balazs *et al.*, 1967; Mow and Huiskes, 2005). This gel-like formation was believed to help in the lubrication process. Seller and colleagues (Seller *et al.*, 1971) observed hyaluronic acid – protein complex under scanning electron microscopy.

III) Boundary Lubrication

In the third lubrication regime, i.e. boundary lubrication, lubricant film thickness was found to further reduce to a monolayer or more and solid-lubricant-

solid interface was found to be created. Here the chemical properties of the lubricant and contact mechanics of the asperities played important role. The load was entirely carried by the deformation of the asperities and the wear increased. The resistance to motion was due to the contacting asperities, either because of their deformation or shearing of adhesive junction formed between them.

In synovial joint an adsorbed lubricant monolayer or several molecules thick layer was found to exist between two articulating surfaces (Linn, 1968; Mow and Huiskes, 2005). See (Charnley, 1959; Charnley, 1960). This form of lubrication was more because of chemical properties of the synovial fluid rather than its physical properties (Linn, 1968; Radin *et al.*, 1970).

It was suggested that this monolayer could be either of hyaluronic acid (Bell *et al.*, 2002; Bell *et al.*, 2006) or lubricin (Swann and Radin, 1972; Swann *et al.*, 1979; Swann *et al.*, 1981a; Swann *et al.*, 1981b; Swann *et al.*, 1985; Rhee *et al.*, 2005) or surface-active phospholipid (Hills, 1989; Hills, 2000; Hills and Crawford, 2003). It was also suggested that this layer could be of several molecules thick "structured water" layer absorbed into the surface of the cartilage (Davis *et al.*, 1979).

1.2.3.2 Measurement of co-efficient of friction

To measure the co-efficient of friction either sliding experiments or specially designed pendulum devices called arthrotripsometers are used. In the pendulum devices joint acts as a fulcrum and one joint surface rocks over the other (Mow and Huiskes, 2005). Sliding experiments have been carried out using metal indenter/metal platen on cartilage, cartilage on cartilage and cartilage on metal counterface (Forster *et al.*, 1995; Forster and Fisher, 1996; Wang and Ateshian, 1997; Forster and Fisher, 1999; Chen *et al.*, 2005) and cartilage on glass configurations (McCutchen, 1962). Most of these studies are usually made using custom made experimental arrangements. Forster and colleagues (Forster *et al.*, 1995; Forster and Fisher, 1996) used the sliding machine used by Caravia and colleagues (Caravia *et al.*, 1993) where as Wang and Ateshian used mechanical spectrometer for their friction tests.

In the sliding experiments performed by Forster and colleagues (Forster *et al.*, 1995), stationary load of 30 N was applied for 5 s, 2 min, 5 min and 45 min before the friction reading was recorded by sliding it over metal counterface. The sliding speed of 4 mm/s was maintained to reduce the effects of elastohydrodynamic lubrication. This experiment was performed with synovial fluid and Ringer's solution as lubricants and without any lubricant. It was observed that the film thickness at the time of measurement was 0.1 μm and the co-efficient of friction for 5 s loading period was 0.005 – 0.015, making it mixed regime lubrication. The co-

efficient of friction was found to be increasing with the loading time and was mainly due to diminishing fluid load support mechanism. The difference between the effect of the synovial fluid and Ringer's solution was found be diminishing after 2 minutes of stationary loading. Thus it was concluded that boundary lubrication may be the inherent property of the cartilage surface.

In the later studies by the same authors (Forster and Fisher, 1996; Forster and Fisher, 1999), the synovial fluid was found to have significant effect in reducing frictional co-efficient for cartilage-cartilage contacts. The increase in the friction during reciprocating motion was found to be because of reduction in load carried by the fluid phase and not due to wear (Forster and Fisher, 1999). Two acellular, non-collagenous surface layers; viz. boundary layer and surface lamina, were identified under Environmental Scanning Electron Microscopy and Transmission Electron Microscopy. Boundary layer of phospholipids/glycoprotein was believed to be providing boundary lubrication and surface lamina of proteoglycan was believed to be preventing fibrillation of underlying collagen fibres.

Normal stress effect due to shear was studied by Wang and Ateshian (Wang and Ateshian, 1997). Compressive strain of 3 – 5% was applied to the cartilage of 2 mm thickness and 2.5 mm radius in unconfined stress-relaxation experiments. Frictional torque was applied by rotating the bottom plate. The decrease in the equilibrium friction co-efficient was observed with increasing sliding speed except for very low speeds. At the same time, an increase in the normal stress was observed which was more than typically observed in static loading. Intrinsic cartilage properties were hypothized to be playing role in the increase in the stiffness rather than exclusive contribution from boundary lubrication as the same behaviour was observed when experiments were performed without the surface zone and without saline bath. It was, however, not observed with rubber specimen.

The decrease in the equilibrium friction co-efficient was also observed with increasing compressive strain due to non-proportional increase in normal and shear stresses.

1.2.4 Contact mechanics of articular cartilage

A] Theoretical modelling

Contact mechanics between the articulating surfaces in the joint has been of immense interest because of the extraordinarily low friction and wear of the surfaces and their capabilities to transfer high loads. It is also due to the pathological observations in cartilage like surface fissures, vertical surface cracking and

horizontal splitting at tidemark which may be linked to the way in which two articulating surfaces interact with each other.

An analytical joint contact model using a layered elastic sphere and a layered elastic cavity was proposed by Eberhardt and colleagues (Eberhardt *et al.*, 1990) to observe "crack initiation and propagation" due to mechanical loading. The model was improved (Eberhardt *et al.*, 1991a) by having "two identical elastic spheres with identical elastic layers". The model was further enhanced with two elastic layers on each sphere instead of one (Eberhardt *et al.*, 1991b), the middle layer representing either the calcified cartilage zone or subchondral plate.

Frictionless rolling contact model of cylindrical biphasic cartilage layers was proposed by Ateshian and Wang (Ateshian and Wang, 1995). Interstitial fluid pressurization during rolling was found to depend on four dimensionless parameters, R_h, $W/2\mu b$, R/b (joint congruency) *and* v, where:

$$R_h = Vb / H_A k \qquad \textbf{1-5}$$

where

V - surface velocity

b - cartilage thickness

H_A - aggregate modulus

k – permeability

W - applied load per unit cylinder length

μ - shear modulus

R - radius of cylindrical surfaces.

The increase in R_h was accompanied by the increase in the interstitial fluid pressurization and for physiologically relevant value of 10^4 the fluid load support was as high as 90%. The increase in rolling/sliding velocity will increase the value of R_h. Thus the higher the surface speed the more load will be supported by interstitial fluid pressurization and lesser will be the friction. Increase in joint congruency and the applied load was also found to increase the fluid load support. In case of pathological cartilages the value of R_h was found to decrease. Fluid pressurization was thus found to depend upon joint congruence, load, surface velocity, cartilage thickness and material properties.

Fluid exudation was also observed at the leading edge of the contact where as it was imbibed back into the tissue at the trailing edge for a smaller values of R_h. At higher values of R_h fluid exudation was observed both at the leading and trailing edge of the contact and imbibition was observed only at some distance from the trailing edge.

A transversely isotropic linear biphasic model was developed by Donzelli and colleagues (Donzelli *et al.*, 1999) to predict the high stress sites corresponding to cartilage failure in impact loading. The peak stress pattern was shown to be dependent upon the curvature of the contacting surfaces. The contact stresses were found to increase with the increase in the curvature which is not seen in isotropic models. The model could successfully predict the sites of peak stresses both at the surface and the cartilage-bone interface but showed lesser fluid load support. The specifics of contact detection were not discussed but the contact boundary conditions were taken from Hou and colleagues' work (Hou *et al.*, 1989).

B] Experimental and clinical studies

Mow and Lai used optical sliding contact analytical rheometer to observe the self-generating lubrication mechanism at the cartilage surface. (Mow and Lai, 1979). They observed the fluid exudation from the trailing and leading edges of the contact and fluid imbibition in the contact zone. The fluid exudation from the leading edge was hypothized as providing necessary fluid for lubrication.

Brown and Shaw studied *in vitro* contact stress distribution in the natural human hip (Brown and Shaw, 1983). They found that the full contact stress distribution was highly complex and non-uniform with peak stress as high as 8.8 MPa and mean stress of around 2.92 MPa for an applied load of 2700N which is approximately 3 - 4 times body weight.

Hodge and colleagues measured *in vivo* contact pressures in human hip joint using pressure-instrumented endoprosthesis (Hodge *et al.*, 1986). They observed, for a load of 2.6 times body weight, peak contact stress of 6.8 MPa and mean stress of 2.14 MPa for single leg support phase of walking. The peak contact stress of 18 MPa was also observed in this study after 12 months of surgery as the patient got up from the sitting position and even higher after 15 months. Morrell and colleagues confirmed this in their recent study and also observed that lower the height of the chair higher is this stress with peak value of 18 MPa for rising from a chair of height of 80% of knee height (Morrell *et al.*, 2005).

Ateshian and colleagues made *in situ* stereophotogrammetric (SPG) contact study to determine the contact areas of the diarthrodial joints (Ateshian *et al.*,

1994b). They compared their technique with other techniques like dye staining, silicone rubber casting and Fuji film contact measurement technique. The surface topography and kinematic data were both obtained from SPG contact method. The shape, size and location of the contact areas obtained using four techniques were compared. It was concluded that none of these methods could give exact time-dependent contact regions. Nevertheless, SPG technique gave more reliable results for both incongruent and congruent joints. The contact areas in incongruent joints were consistent in all four methods whereas in case of congruent joints only SPG and Fuji film techniques gave consistent results. The advantage of SPG was that it could be used in intact joints and was found to give quicker results making it possible to study moving contact areas.

Studies have been conducted on hip joints (Brown and Shaw, 1983; Hodge *et al.*, 1986), shoulder joints (Ateshian *et al.*, 1994b), ankle joints (Wan *et al.*, 2006) and knee joints (Herzog *et al.*, 1998; Li *et al.*, 2005; Walker *et al.*, 2006) mainly to determine contacts stresses and areas.

C] Finite element modelling

Linear biphasic mixed-penalty contact finite element model for soft hydrated tissues was developed by Donzelli and Spilker (Donzelli and Spilker, 1998). The importance of evolving contact detection was emphasized and implemented in the model. The potential surfaces which would be in contact were identified beforehand and for each point on one surface (contactor surface) a closest point was sought on the mating surface (target surface) using minimization function.

The model was validated using the plane strain Hertz contact problem and a integral transform solution of Kelkar and Ateshian (Kelkar and Ateshian, 1995). The non-linearities like finite deformation, material anisotropy and sliding speed were not considered in this model.

The effects of contact geometry on the pore pressure and strain distribution in the cartilage were studied by Warner and colleagues (Warner *et al.*, 2001a) using biphasic poroelastic finite element model. Porous/non-porous rigid cylindrical indenter of 5 mm radius, hemispherical rigid indenter of 5 mm radius and physiological relevant indenter configurations with effective radii of 20 mm and 100 mm for modelling knee and hip contacts respectively were used.

It was found that the porous cylindrical indenter produced lower pore pressure and higher compressive strain compared to those produced by non-porous indenter, which is obvious as no fluid flow was possible across non-porous indenter surface. Due to the reduction in the load carrying capacity of the fluid phase, the compressive

strain experienced by the solid phase increased for porous indenter compared to non-porous indenter.

The plane ended non-porous indenter produced discontinuity in loading conditions at the indenter edge and the peak pressure and compressive strain occurred near the edge of the indenter.

This problem was overcome by using hemispherical indenter. The peak pore pressure predicted here was at the articular surface under the centre of the indenter and was lower than that predicted using plane ended cylindrical indenter. The peak compressive strain was 56 percent lower compared with plane ended cylindrical indenter results and was under the indenter centre at $1/4^{th}$ the thickness below the articular surface.

When using physiological effective radii for the indenter, the pore pressure and compressive strain distribution patterns were similar to that found with 5 mm hemispherical indenter though the values reduced with the increase in the indenter radii.

Axisymmetric poroelastic model of cartilage-cartilage was presented by Federico and colleagues (Federico *et al.*, 2004) to study fluid boundary conditions in normal and OA cartilages. Sealed and open surface conditions were investigated. Strain-dependent permeability was also modelled. The sealed surface was found to be poor representation of the actual cartilage.

The load sharing between the solid and fluid phase was found to be affected by the boundary conditions on the surface. The model with non-linear permeability was found to adequately represent the cartilage in the joint. The early OA cartilage was found to show decrease in peak pore pressure by half and increase in contact area by 30%. This agreed well with experimental results on feline patello-femoral joints which showed 50% decrease in peak pore pressure and 22% increase in contact area (Herzog *et al.*, 1998). The results for the late OA were not compared.

Most of the frictional FE models discuss the role of interstitial fluid pressurization in frictional characteristic of the cartilage (Ming *et al.*, 1997; Jin *et al.*, 2000; Krishnan *et al.*, 2003) . The rolling and sliding contact problems have been studied theoretically and experimentally but there appears to be no finite element studies of metal indenter rolling/sliding over the cartilage. Sliding of cartilage over cartilage was studied by Chen and colleagues (Chen *et al.*, 2005) who self-coded the entire formulation and no commercially available package was used.

Many packages like NASTRAN (Chand *et al.*, 1976), ABAQUS (Goldsmith *et al.*, 1995; Wu *et al.*, 1998; Warner, 2000; Warner *et al.*, 2001a; Federico *et al.*, 2004), and LUSAS (Kerin *et al.*, 1998) have been used for finite element modelling

and analysis of contact mechanics of articular cartilage. Some prefer to self-code the entire solution technique to have better control over the agreement between theoretical and numerical solutions (Chen *et al.*, 2005).

Wu and colleagues (Wu *et al.*, 1998) and Goldsmith and colleagues (Goldsmith *et al.*, 1995) studied the suitability of using ABAQUS, an *u-p* formulation (Goldsmith *et al.*, 1996), for modelling biphasic tissues to study joint contact mechanics using soils consolidation procedure available. Earlier van der Voet and colleagues (van der Voet *et al.*, 1992) had shown that both *u-v* and *u-p* FE formulations give comparable and accurate results (Goldsmith *et al.*, 1996).

The solutions obtained using ABAQUS were compared to those obtained using other finite element models and analytical solutions by Wu and colleagues (Wu *et al.*, 1998). Three tests were compared: unconfined indentation test, contact test of spherical cartilage surface with rigid plate and an axisymmetric joint contact test. ABAQUS was found to be suitable to be used for such modelling.

1.3 Aims and Objectives

1.3.1 Aims

This study was aimed to develop methodology for FE modelling of joint contact mechanics.

1.3.2 Objectives

The objectives of this study were:

1) Developing and validating general contact detection algorithm for biphasic surfaces.
2) Developing and validating poroelastic indentation models.
3) Studying the effects of element types, mesh density and geometric non-linearity on the model mentioned before in 2)
4) Developing and validating physiologically relevant joint contact model.
5) Developing indentation model for deriving cartilage material properties.
6) Developing models with sliding indenter.
7) Studying the role of interstitial fluid pressurization in joint contact mechanics.

Chapter 2 Finite Element Modelling

Several biphasic poroelastic models were investigated to validate the modelling process itself and to study the applications. All the models were two-dimensional and were either axisymmetric or plane strain element models.

When using FEM, a clear demarcation must be made between the validity and the accuracy of the model. The validity of the model can be checked either with the experimental results or previously established FEM results or parametric studies; whereas accuracy can be confirmed, among other methods, with mesh sensitivity analysis (Huiskes and Chao, 1983).

The validation of the model must be made keeping in mind the objectives of analysis (Huiskes and Chao, 1983). In most of the models presented below the aim was not to get the absolute values of the parameters but to make the relative analysis and study the trends depicted by these parameters.

The models were created and analysed using ABAQUS 6.5-5, the latest available on Windows systems at the University.

The linear and radial dimensions, if shown in the figures, are always in mm.

2.1 Contact detection

In indentation FE models, whenever a spherical indenter is involved the contact between the indenter and the cartilage is developed incrementally unlike in plane ended cylindrical indenter where the initial contact region does not change. The free flow conditions will exist at all the nodes on the cartilage which are not in contact with the indenter whereas at the nodes which are closed by the indenter there will not be any flow. This requires that at every increment in the simulation, one should know which nodes are in contact and which are not, so that the interface condition can be applied correctly at each node.

Many techniques have been reported for contact detection. One such technique involved identifying the potential points in contact on both the indenter and the cartilage by measuring the vertical distances travelled by them with respect to the cartilage surface (Hale *et al.*, 1993). If the distances were equal the points were assumed to be in contact. In another technique, for every point on one surface a closest point on the interacting surface was found using minimization function. (Donzelli and Spilker, 1998).

Another methodology, applicable only to the elements with mid-side nodes, was developed by Warner (Warner, 2000). For each 8-node element on the surface, the contact stress at mid-side node was recorded. If this stress was above a given threshold, the entire element was assumed to be in contact and sealed conditions were applied to that element. This would stop the flow at a corner node even when it is not in contact if the contact stress at mid-side node was higher than the threshold value. The method developed by Warner had wider applicability; however, it could not be used for the models with 4-node elements which do not have mid-side nodes.

Therefore, a new method was developed in the present study for contact detection which made use of contact stresses as was done by Warner but changing the flow conditions only at the nodes rather than the entire element. This algorithm was more generic since it could be used for 4-node elements as well 8-node elements. It could be used in both the axisymmetric and other two dimensional models. It could be used for 3-dimensional elements as well but was not tested for the same.

2.1.1 New contact detection algorithm

Two subroutines provided by ABAQUS (ABAQUS., 2005) were used; URDFIL and FLOW. In contact mechanics problems, ABAQUS needed one master and one slave surface which were used to define the contact pair. It created internal surface elements for each contact pair.

URDFIL was used to read the result file and got invoked after every increment when new information was written to that file.

FLOW, on the other hand, was called at “each surface integration point of the element based surfaces for which surface-based or element-based non-uniform surface seepage flow was defined” (ABAQUS., 2005). These integration points were not the same as the integration points of the elements used to define the model geometry but were close to the actual surface nodes of the elements defining the surface. In case of 8-node element, there would be 3 surface integration points close to the 3 surface nodes of the element. Similarly for 4-node element there would be 2 surface integration points.

The new algorithm made use of a COMMON block (of FORTRAN) so that the information could be exchanged between the two user subroutines. There were two versions; first for indenter-cartilage configuration and second for cartilage-cartilage configuration. The algorithms are given in steps and illustrated in flowchart below.

A] Indenter-cartilage configuration

I) Algorithm in steps

1) URDFIL reads the result file after each increment.
2) Finds each element (not internally generated) used in defining the surface along with the nodes on the surface and stores in COMMON block.
3) Finds the pore pressure and co-ordinates of each of these surface nodes and stores them.
4) Records contact stress at each of these nodes and if the contact stress is greater than a given threshold (0.01 kPa for validation with Warner's study or zero in all the other cases), the node is assumed to be in contact otherwise it is assumed to be open and stores this information in COMMON block.
5) FLOW is called for each surface integration points of internally defined surface elements.
6) For the current surface integration point and element number, finds the closest surface node (stored previously in step 2) of that element.
7) Decides whether the integration point is in contact or not based on the status of the closest surface node (if the node is in contact, integration point is also assumed to be in contact).
8) Sealed conditions are applied if integration point is in contact by assigning zero seepage co-efficient and zero sink pore pressure or else free flow conditions are applied by assigning seepage co-efficient as 1 and sink pore pressure as zero.
9) Repeat steps 5 – 8 for each integration point till increment converges.
10) Increment converges and data is written to results file by ABAQUS
11) Repeat steps 1 – 10 till the end of simulation.

II) Algorithm in Flowchart

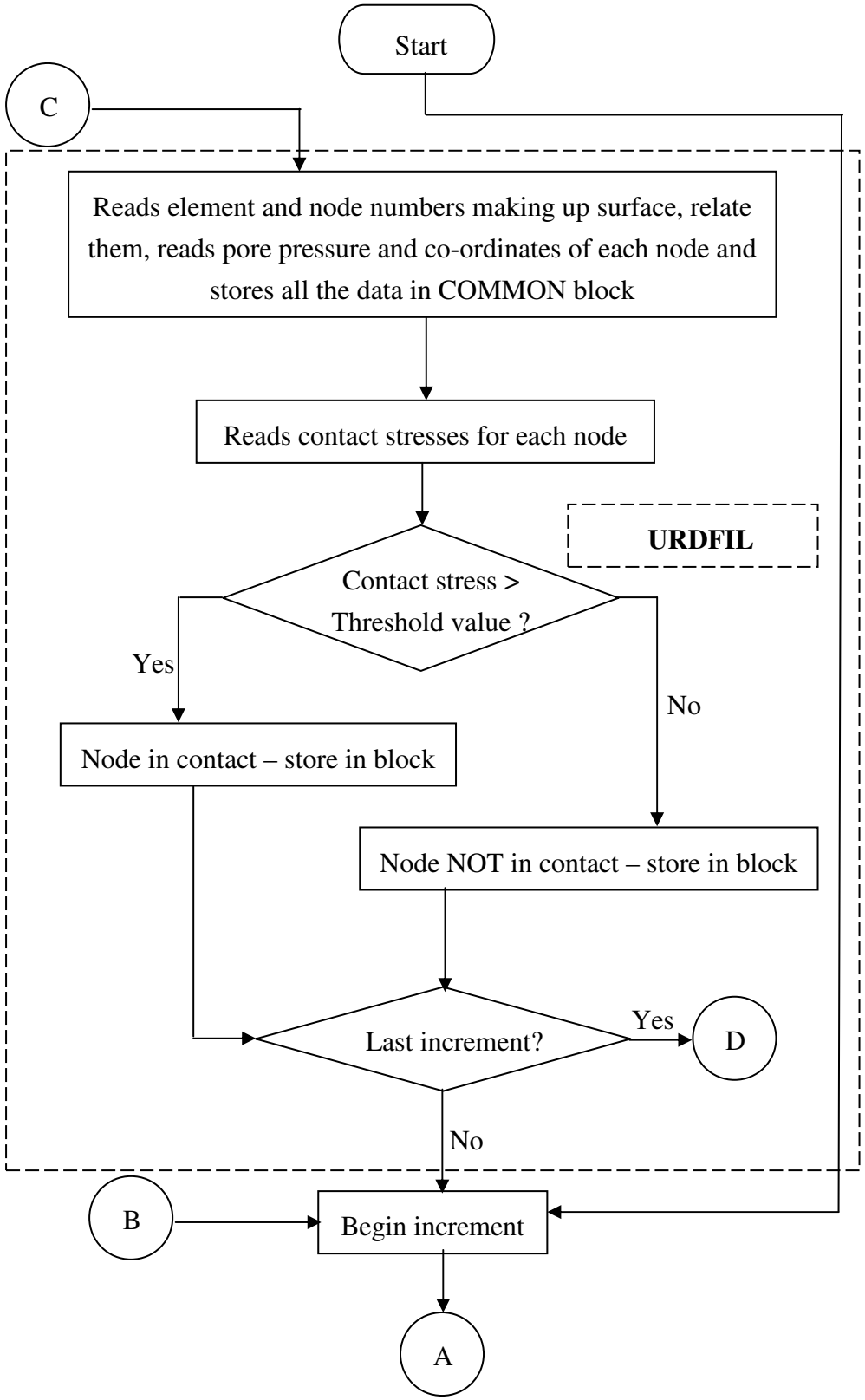

Figure 2-1 First part of the flowchart for contact detection algorithm

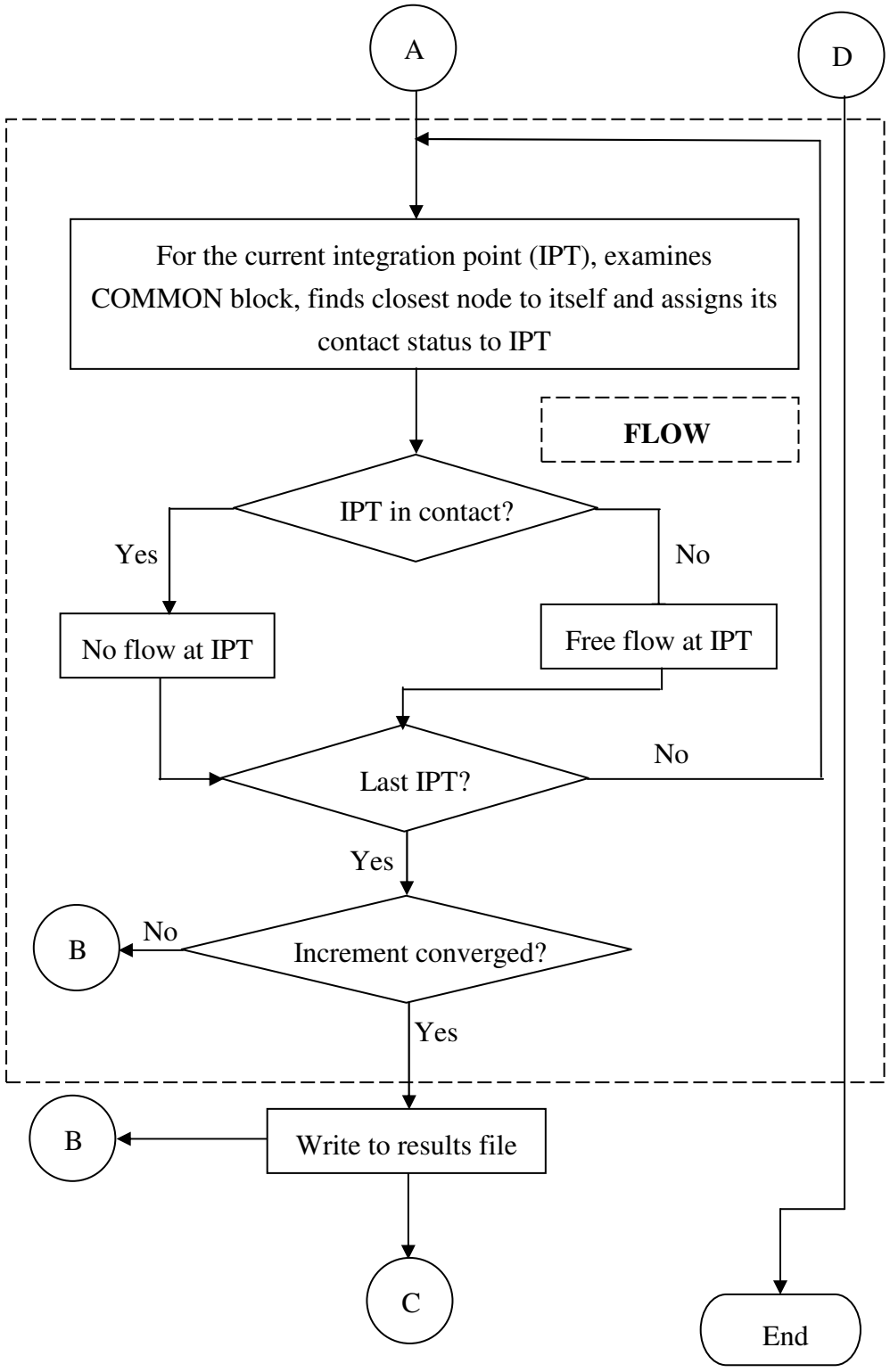

Figure 2-2 second part of the flowchart for contact detection algorithm

B] Cartilage-cartilage configuration

In case of cartilage-cartilage configuration, the biphasic jump condition (i.e. maintaining continuity of the normal component of the pore fluid velocity w_n) had to be implemented in the contact region as follows (Federico *et al.*, 2004; Federico *et al.*, 2005):

$$\left[\!\left[\phi^f \left(v^f - v^s\right)\right]\!\right] \cdot n = 0 \Rightarrow \left[\!\left[w_n\right]\!\right] = 0 \qquad \textbf{2-1}$$

where,

Φ^f – Fluid phase volume fraction

v^f – Velocity field in fluid phase

v^s – Velocity field in solid phase

n – is the outward normal to the surface

w_n – The pore fluid velocity component in the outward normal direction.

Accordingly, when the two surfaces are represented as (1) and (2), this jump condition was implemented in ABAQUS as follows (Federico *et al.*, 2004; Federico *et al.*, 2005) using the contact detection algorithm:

$$w_n^{(1)} = k_s\left(p^{(1)} - p^{(2)}\right) \text{ contact region} \qquad \textbf{2-2}$$

$$\begin{array}{ll} w_n^{(1)} = k_s p^{(1)} & \forall p^{(1)} \geq 0 \\ w_n^{(1)} = 0 & \forall p^{(1)} < 0 \end{array} \text{ free-draining area} \qquad \textbf{2-3}$$

where,

k_s – seepage co-efficient

p – pore pressure

The seepage co-efficient, k_s was used as a flag to either allow the fluid flow or stop the fluid flow. But it should be such that (Federico *et al.*, 2004; ABAQUS., 2005):

$$k_s >> \frac{k}{\gamma_\omega c} \qquad \textbf{2-4}$$

where,

k – permeability of the material

γ_ω – Specific weight of fluid = 9.81 kN/m^3

c - characteristic length of the underlying element

The seepage co-efficient should not exceed 10^5 times the term on right hand side in Eq. 2-4 so that pore pressure is zero on freely draining surfaces (ABAQUS., 2005). In the models developed in this study, this factor was chosen as 10^3 by specifying seepage co-efficient as 1 mm^3/Ns.

The cartilage-cartilage version of the algorithm was the same as the first one except some changes mentioned herein. In steps 2 – 4 the data was stored for both the surfaces instead of just one surface. An additional step was performed after that. For the nodes which were in contact on one surface the closest nodes on the second surface were found and were assumed to be in contact. Similar information was found for the nodes not in contact. This information was stored along with the slave surface information. The COMMON block now contained element and node numbers making up the slave surface along with pore pressures, co-ordinates, and contact information of those nodes. The similar information of the corresponding nodes on the master surface was also in the COMMON block. The information of the slave and master surfaces were related based upon the proximity of the corresponding nodes.

When FLOW would be called for the first surface, it would go through steps 5 – 7. At step 7, if the integration point was not in contact, free flow conditions would be applied by making seepage co-efficient as 1 and sink pore pressure as 0 (zero). If the integration point was in contact then it would have to satisfy jump condition mentioned in Eq. 2-1, Eq. 2-2 and Eq. 2-3. Thus, the sink pore pressure would be set as the pore pressure of the corresponding node on the other surface and the seepage co-efficient as 1. If the pore pressures on the corresponding nodes on two opposing surfaces were to be equal there would not be any flow, otherwise it would be proportional to the difference in these pore pressures. This was repeated for each and

every integration point on first surface. The similar steps were followed for each and every integration point on the second surface.

These steps were repeated and the information was written to the results file upon convergence and the entire procedure was repeated till the end of simulation.

2.2 Consolidation models and materials

These models were mainly to observe and validate articular cartilage modelling process, to validate new contact detection algorithm and to quantify the mechanical parameters of the cartilage used in experiments.

2.2.1 Cartilage indentation with a rigid spherical indenter

Cartilage of 3 mm thickness and 20 mm radius with a rigid spherical indenter of 5 mm radius was modelled. This configuration models infinite layer of the cartilage (Spilker *et al.*, 1992a) in order to remove indentation effects on the cartilage edges. In practice, rather than indenter radius it is the amount of cartilage deformation and contact area which will decide these edge effects. The objective of this analysis was to validate the model and the new contact detection algorithm against the results presented by Warner (Warner, 2000).

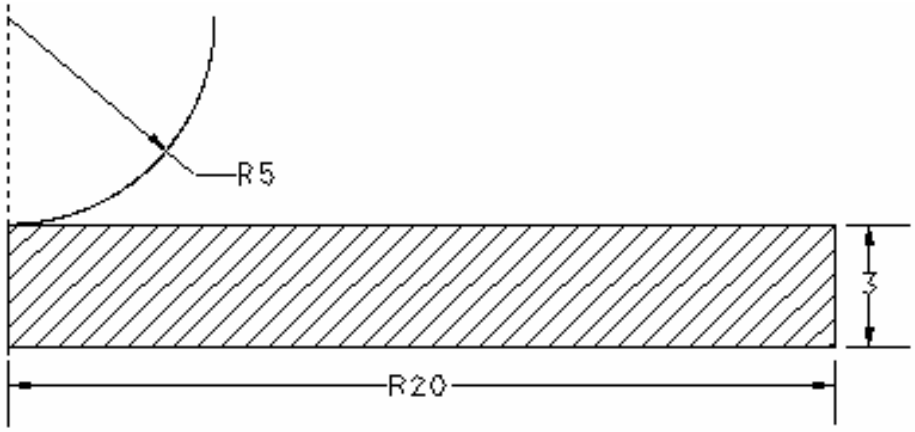

Figure 2-3 Axisymmetric model of articular cartilage with a rigid spherical indenter

Table 2-1 Material properties used in the model of articular cartilage indentation with a rigid spherical indenter

Parameter	Value
Aggregate modulus, H_A	0.55 MPa
Poisson's ratio, $\nu_{cartilage}$	0.08
Permeability, k	4.0 x 10^{-15} m^4/Ns
Void ratio, e	4.0 (80 % interstitial fluid)
Co-efficient of friction, μ	0.02
Seepage co-efficient, k_s	1 mm^3/Ns – Flow 0 mm^3/Ns – No flow

The material properties (Table 2-1) used were taken from Spilker and colleagues' work (Spilker *et al.*, 1992a) and correspond to the normal human cartilage. These properties were also used by Warner (Warner, 2000) in his study against which this model was validated. The value of 0.02 is the maximum value of the range (0.002 – 0.02) given by most of the researchers (Mow and Lai, 1980; Macirowski *et al.*, 1994; Warner, 2000).

The aggregate modulus and Young's modulus are related by Eq. 2-5

$$H_A = E(1-\upsilon)/(1+\upsilon)(1-2\upsilon) \qquad \textbf{2-5}$$

Hence, Young's modulus, $E_{cartilage}$ = 0.54 MPa. This is within the range of values (0.79±0.36 MPa) for normal human cartilage (Nordin and Frankel, 1989).

H_A, $E_{cartilage}$ and $\nu_{cartilage}$ in all the cartilage models are effective elastic properties of the solid phase used to model the cartilage.

The cartilage consisted of 3200 (200 × 16) CAX4RP (4-node bilinear displacement and pore pressure, reduced integration with hourglass control) elements as shown in Figure 2-4. The rigid spherical indenter was modelled as an analytical rigid body with reference point at its centre.

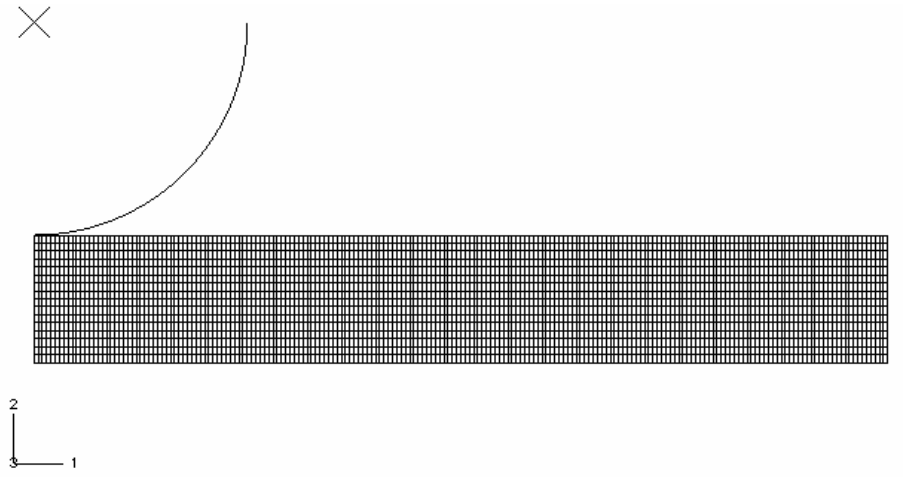

Figure 2-4 Finite element mesh of an axisymmetric model of articular cartilage with a rigid spherical indenter

The comparisons were made with CAX8RP (8-node biquadratic displacement bilinear pore pressure, reduced integration) model for choosing the type of elements. Mesh sensitivity analysis was also carried out. The graded mesh was not created and was intentionally developed as the same model was to be used for sliding contact model and was not an issue for 2-dimensional modelling as far as computational time is concerned.

Boundary and interface conditions were imposed on the cartilage according to Spilker and colleagues' model (Spilker *et al.*, 1992a). The bottom nodes were constrained in both horizontal and vertical directions. The nodes on the axis were constrained in horizontal direction. The pore pressure on the nodes of the outer edge was maintained at zero so to have unrestricted fluid flow. Flow was prevented from the bottom surface as well as from the surface on the vertical axis of symmetry. The reference node/point of the spherical indenter was constrained in the horizontal direction. Its rotation was also constrained.

Three different surface flow conditions were implemented and compared: free flow, no flow or sealed and flow according to the development of the contact, i.e. contact dependent flow by changing seepage co-efficient and/or sink pore pressure in the FLOW subroutines. No changes were made to other ABAQUS files.

Automatic time increments using UTOL parameter ("specifying the allowed maximum pore pressure change in one increment" for transient analysis) (Goldsmith *et al.*, 1995; ABAQUS., 2005) as well as fixed time increments were used. Automatic time incrementation was implemented using a typically small value of 600 kPa for UTOL (Goldsmith *et al.*, 1995). Whenever fixed time increments were used care was taken that this time increment would be well within the minimum

time increment used by ABAQUS if automatic time increments were to be used with UTOL of 600 kPa. This value was found to give acceptable results.

Both stress-relaxation and creep-deformation were simulated. The stress-relaxation was carried out by applying 10% deformation over a ramp time of 2 seconds and maintaining the indenter in that position for further 1000 seconds. Creep-deformation was carried out by applying the load of 0.9N (this would give approximately 10 % deformation) over a ramp time of 2 seconds and maintaining that load for further 1000 seconds.

2.2.2 Joint contact mechanics of two cartilages

Two contacting cartilages mounted on cortical bone supports were modelled. This model was exactly reproduced from the work of Federico and colleagues (Federico *et al.*, 2004) in order to validate the model in the current study. The thickness of each cartilage was 1 mm and radius of curvature was 400 mm. Both cartilages were symmetric about horizontal plane passing through their initial point of contact on the vertical axis of symmetry.

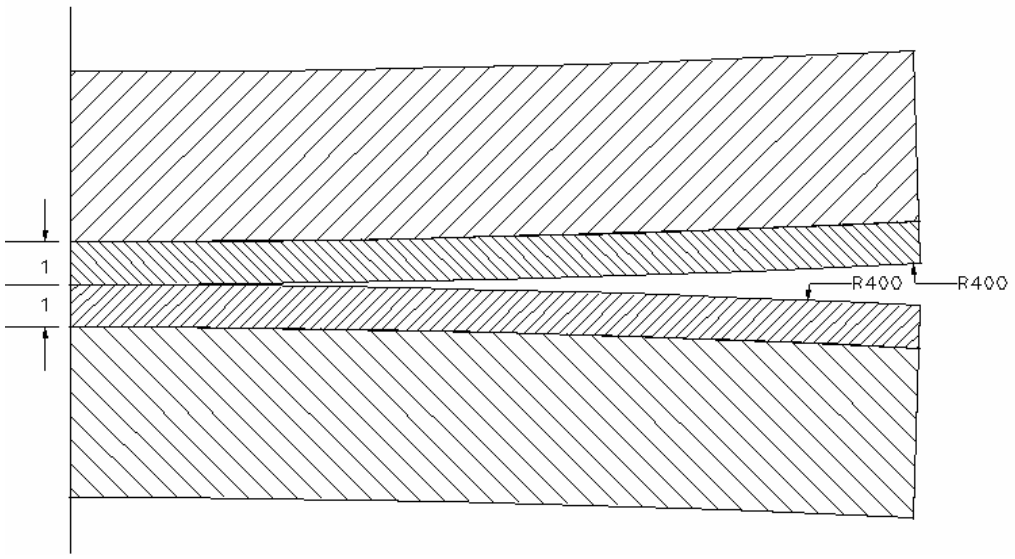

Figure 2-5 Axisymmetric model of joint contact mechanics of articular cartilages

Non-linear permeability in the form of void ratio dependent permeability (VRDP) was also implemented in this model. The permeability was derived using the following *k-e* relationship (Holmes and Mow, 1990; Wu and Herzog, 2000):

$$k = k_0 \left(\frac{e}{e_0} \right)^{\kappa} \exp^{o} \left(\frac{M}{2} \left[\left(\frac{1+e}{1+e_0} \right)^2 - 1 \right] \right) \quad \textbf{2-6}$$

where,

k – Permeability, and

e – Void ratio

Other terms are explained in Table 2-2

The contact was assumed frictionless to correctly model validation process along with the following material properties (Federico *et al.*, 2004):

Table 2-2 Material properties used in the model of joint contact mechanics of articular cartilages

Parameter		Value
Young's modulus of cartilage, $E_{cartilage}$		0.450 MPa
Poisson's ratio of cartilage, $\nu_{cartilage}$		0.106
Initial permeability, k_o		1.16 x 10^{-3} mm^4/Ns
Initial void ratio, e_o		4.2 (approx. 80.75 % interstitial fluid)
Material parameter for *k-e* relationship (Eq. 2-6)	M	4.638
	κ	0.0848
Seepage co-efficient, k_s		1 mm^3/Ns – Flow 0 mm^3/Ns – No flow
Young's modulus of bone, E_{bone}		2 GPa
Poisson's ratio of bone, ν_{bone}		0.20

The properties used in this model were different as compared to those used in spherical indenter and cartilage model for the validation purpose since the models against which the current models were compared used different sets of properties.

Each cartilage was modelled with 200 (20 × 10) CAX4P (4-node bilinear displacement and pore pressure) elements. The bone was modelled using 100 (20 × 5) CAX4 (4-node bilinear) elements.

An axisymmetric model of two cartilages in contact and attached to subchondral bone had the same geometry and the same number of elements as those used by Federico and colleagues (Federico *et al.*, 2004) except the type of elements. Federico used 8-node elements whereas in the current study 4-node elements were used. This effectively removed the mid-side nodes from Federico's model keeping everything else same, i.e. node spacing (distance between the adjacent nodes on the element edges) was doubled.

An observation point/node N1 was marked in the lower cartilage, 0.2 mm below the surface and on the axis. The same point was used by Federico and colleagues. All the mechanical parameters were monitored at this node.

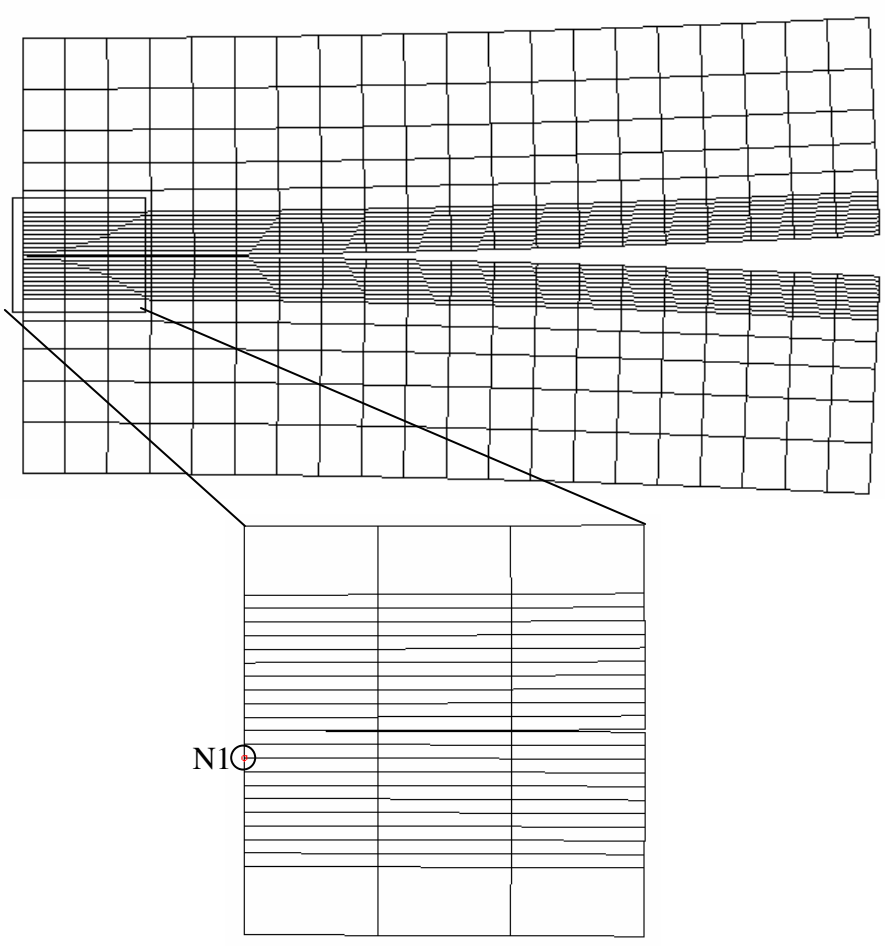

Figure 2-6 Finite element mesh of an axisymmetric model of joint mechanics of cartilages with node N1 0.2 mm below lower cartilage surface

The nodes on the base of the lower bone were constrained in horizontal and vertical directions. The nodes on the axis on lower as well as upper cartilage-bone component and those on the base of the upper bone were prevented from moving in horizontal direction. Fluid flow was prevented from the cartilage surfaces on the vertical axis of symmetry. The pore pressure on the nodes of the outer edge of each cartilage was maintained at zero to have unrestricted fluid flow.

The contact detection was done by the new algorithm developed for cartilage-cartilage configuration. The automatic time incrementation was implemented using UTOL of 600 kPa as this value was found to give acceptable results.

Stress-relaxation was carried out by applying 0.3 mm displacement to the base of the upper bone which was equivalent to 15% deformation in each cartilage. Deformation was applied over a ramp time of 10 seconds and was maintained for further 300 seconds.

An equivalent model as proposed by Ateshian and colleagues (Ateshian *et al.*, 1994a) was developed to represent two identical and symmetrical cartilage-bone components. The two cartilages modelled here had the same material and geometric properties and the deformation was in the linear range. Hence the upper cartilage was replaced by a steel block modelled with 300 (20 × 15) CAX4 (4-node bilinear) elements. The 15% deformation was applied using 0.15 mm displacement on the base of the steel block.

The same boundary and interface conditions were maintained for lower cartilage-bone component. The nodes on the axis and the base of the steel block were constrained in the horizontal direction.

The objective of this analysis was to validate the model and the new contact detection algorithm against the results presented by Federico and colleagues (Federico *et al.*, 2004). The contact was assumed frictionless in both the models in order to compare the results of the two.

2.2.3 Cartilage indentation with a rigid plane ended cylindrical indenter

This model was created to quantify material parameters of the bovine cartilage used in the experiments currently being addressed at the University of Leeds (Katta *et al.*, 2006).

Cartilage of 2 mm thickness and 20 mm radius mounted on the bone was modelled with a rigid plane ended cylindrical indenter of 3 mm diameter. The indenter was modelled with a large fillet radius of 0.5 mm to avoid stress concentration at the sharp edge.

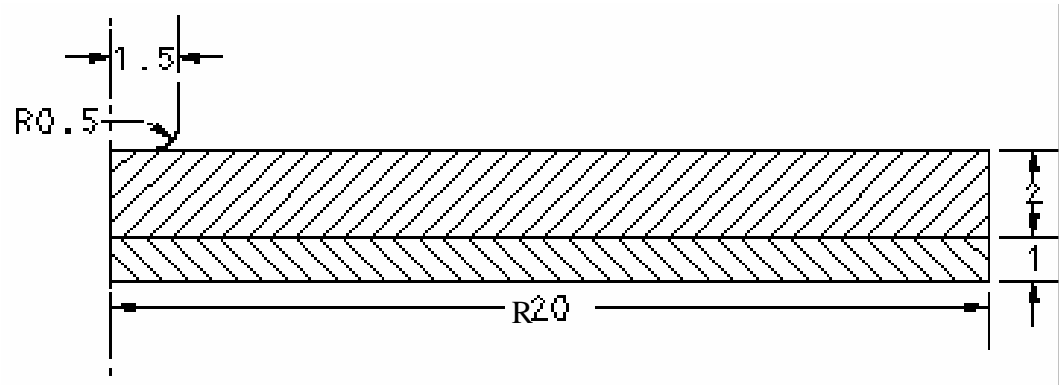

Figure 2-7 Axisymmetric model of articular cartilage with a rigid plane ended cylindrical indenter

The following material properties were used:

Table 2-3 Material properties used in the model of articular cartilage indentation with a plane ended cylindrical indenter

Parameter	Value
Poisson's ratio of cartilage, $\nu_{cartilage}$	0.0 (Jin *et al.*, 2000)
Void ratio, e	4.0 (80 % interstitial fluid) (Warner, 2000)
Co-efficient of friction, μ	0.02 (Warner, 2000)
Young's modulus of bone, E_{bone}	2 GPa (Federico *et al.*, 2004)
Poisson's ratio of bone, ν_{bone}	0.20 (Federico *et al.*, 2004)
Seepage co-efficient, k_s	1 mm^3/Ns – Flow 0 mm^3/Ns – No flow

The cartilage was modelled with 2000 (200 × 10) CAX4RP elements. The bone was modelled using 1000 (200 × 5) CAX4R (4-node bilinear, reduced integration with hourglass control) elements. Indenter was modelled as analytical rigid with its reference point at a node on the cartilage surface on the vertical axis of symmetry.

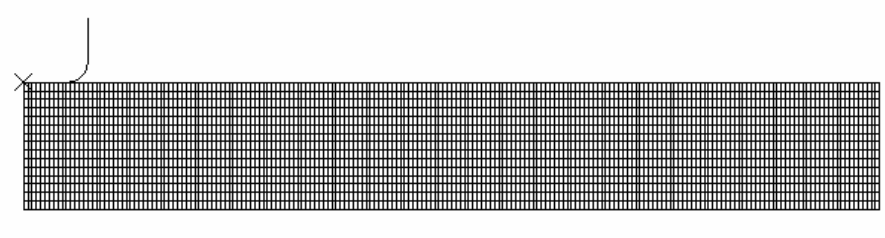

Figure 2-8 Finite element mesh of an axisymmetric model of articular cartilage with a plane ended cylindrical indenter

The boundary and interface conditions imposed on the bone and the cartilage were the same as those imposed on the lower cartilage-bone component in the joint contact mechanics model of two cartilages. The indenter was constrained in the same way as mentioned in the cartilage indentation model with a rigid spherical indenter.

The contact changed only at the fillet during simulation and was detected using the contact detection algorithm developed. Automatic time incrementation was used with UTOL of 600 kPa as this value was found to give acceptable results.

The load of 1.88N was applied at the indenter reference point over a ramp time of 2 seconds and was maintained for further 3000 seconds. The deformation was observed at a node on the cartilage surface coinciding with the indenter reference point. The FE creep-deformation predictions were compared with the experimental results and, aggregate modulus and permeability were calculated.

2.3 Sliding models and materials

These models were used as the applications to reproduce experimental cartilage behaviour considered by many researchers (McCutchen, 1962; Maroudas, 1967; Walker *et al.*, 1968; Mow and Lai, 1979; Krishnan *et al.*, 2005) and also to model physiologically relevant joint conditions that exists in hemiarthroplasty which has been addressed in a number of experimental and clinical studies (Brown and Shaw, 1983; Hodge *et al.*, 1986; Wan *et al.*, 2006). The current study did not exactly try to address the issues in these studies but was an exercise to merely lay the foundation for future studies.

The sliding models used plane strain CPE4RP (4-node bilinear displacement and pore pressure reduced integration with hourglass control) elements for cartilage and plane strain CPE4R (4-node bilinear, reduced integration with hourglass control) elements for bone, if modelled.

Ideally the sliding models should be three dimensional as they are more realistic. However, three dimensional models are computationally more expensive and hence two dimensional plane strain models were considered for the current study.

2.3.1 Rigid plate sliding over cartilage surface

The cartilage with bone support was modelled. The cartilage was 2 mm thick and 9 mm long (Forster and Fisher, 1999). The plate was 25 mm in length and covered the entire surface of the cartilage.

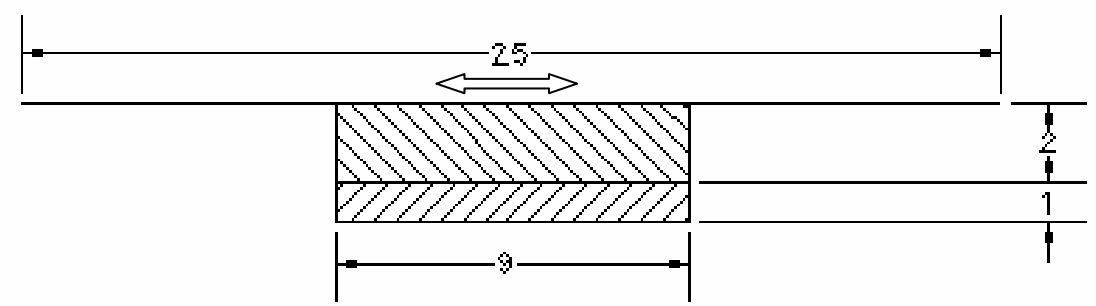

Figure 2-9 Model of a rigid plate sliding over cartilage surface

The contact was assumed frictionless. The bone was modelled as elastic with a high Young's modulus and the cartilage was biphasic with following material properties (Goldsmith *et al.*, 1995; Warner, 2000):

Table 2-4 Material and kinematic properties used in the model of a rigid plate sliding over cartilage

Parameter	Value
Young's modulus, $E_{cartilage}$	0.54 MPa
Poisson's ratio, $\nu_{cartilage}$	0.08
Permeability, k	4.0 x 10^{-15} m^4/Ns
Void ratio, e	4.0 (80 % interstitial fluid)
Young's modulus of bone, E_{bone}	2 GPa (Federico *et al.*, 2004)
Poisson's ratio of bone, ν_{bone}	0.20 (Federico *et al.*, 2004)
Sliding velocity, V	4 mm/s (Forster and Fisher, 1999)
Sliding distance, d	±4 mm about the mean position
Seepage co-efficient, k_s	1 mm^3/Ns – Flow 0 mm^3/Ns – No flow

The bone was modelled with 36 (18 × 2) CPE4R elements and the cartilage with 72 (18 × 4) CPE4RP elements. The rigid plate was modelled as analytical rigid solid with reference point at its left hand side end point.

An observation point/node N1 was marked exactly in the centre of the cartilage surface where the mechanical parameters were monitored. It was also the mean position about which indenter reciprocated.

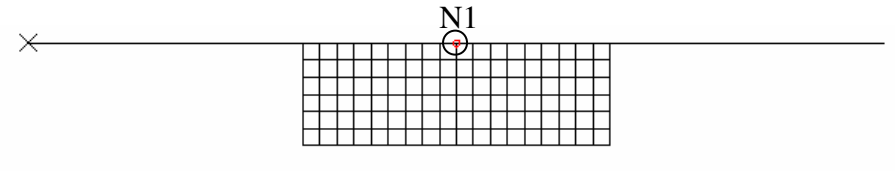

Figure 2-10 Finite element mesh for the model of a rigid plate sliding over cartilage covering its surface entirely

The base of the bone was constrained in horizontal and vertical directions. The pore pressure was maintained at zero at the nodes on the outer edges of the cartilage to allow unrestricted fluid flow. The rotation of the reference node/point of the plate was also constrained.

The surface flow conditions, though the surface was closed at all the times, was implemented using contact detection algorithm validated earlier for consolidation problem. Automatic time incrementation with UTOL of 600 kPa was used as this value was found to give acceptable results.

The load of 2N/mm was applied at the reference point of the plate over a ramp time of 2 seconds and then held constant for further 600 seconds. During the 600 seconds period the indenter was made to slide in a reciprocating motion over the cartilage with the velocity of 4 mm/s.

The same model was also investigated for creep-deformation over 600 seconds instead of sliding and the results were compared.

2.3.2 Rigid cylindrical indenter sliding over cartilage surface

The cartilage of 3 mm thickness and 25 mm length was modelled. The rigid cylindrical indenter was of 5 mm radius.

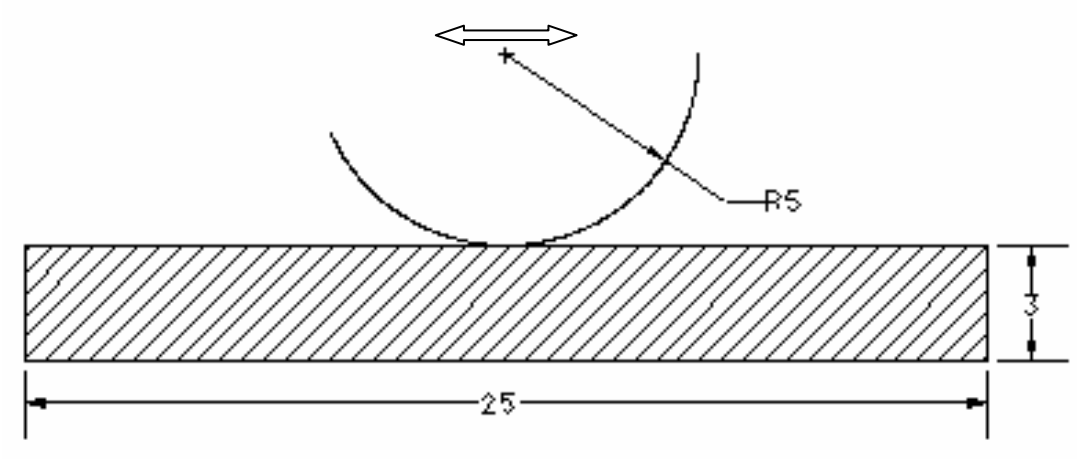

Figure 2-11 Model of a rigid cylindrical indenter on cartilage surface

The cartilage material and kinematic properties used were the same as used in plane strain element model of a rigid plate sliding over cartilage surface.

The cartilage was modelled using 1920 (120 × 16) CPE4RP elements. The cylindrical indenter was modelled as analytical rigid solid with reference point at its centre.

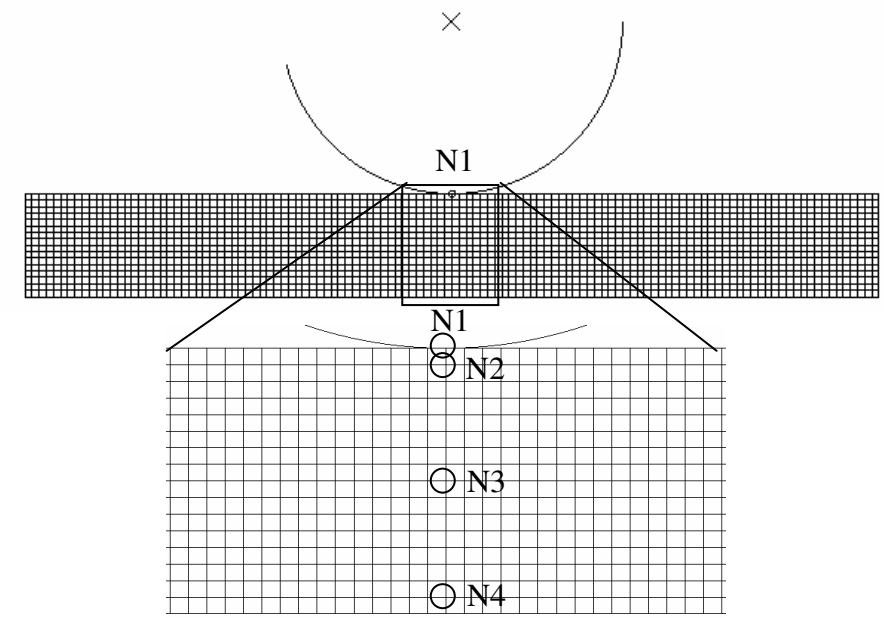

Figure 2-12 Finite element mesh for the model of a rigid cylindrical indenter sliding over cartilage

The observation points/nodes N1, N2, N3 and N4 as shown in Figure 2-12 were marked exactly in the centre of the cartilage where the mechanical parameters were monitored. It was also the mean position about which indenter reciprocated. The nodes N1 and N2 were in the STZ, N1 being on the cartilage surface and N2 being at a distance 93.75% of total height from the bottom. N3 was in the mid-zone and exactly in the centre of the cartilage. N4 was in the deep zone at a distance of 6.25% of the total height from the bottom.

The base of the cartilage was constrained in horizontal and vertical directions. Moreover no flow was allowed through the bottom surface of the cartilage. The pore pressure was maintained at zero at the nodes on the outer edges of the cartilage to allow unrestricted fluid flow. The rotation of the reference node/point of the indenter was also constrained.

The surface flow conditions at the top were detected using the algorithm discussed before. The surface conditions at a particular node within the indenter stroke length changed throughout the simulation as the indenter was reciprocating. Automatic time incrementation with UTOL of 600 kPa was used.

The load of 0.5N/mm and 0.1N/mm were applied at the reference point of the indenter over a ramp time of 2 seconds and then held constant for further duration. After the 2 seconds period the indenter was made to slide in a reciprocating motion over the cartilage with the velocity of 4 mm/s.

Chapter 3 Consolidation Results and Discussion

3.1 cartilage indentation with a rigid spherical indenter

3.1.1 4-node element v/s 8-node elements

The choice of element type was examined after stress-relaxation simulations using 800 (100 × 8) CAX8RP, 800 (100 × 8) CAX4RP and 3200 (200 × 16) CAX4RP elements. The node spacing in the models with 800 CAX8RP elements and 3200 CAX4RP elements was kept same whereas the model with 800 CAX4RP elements was coarser as node spacing was doubled and was considered here owing to the same number of elements as those used in CAX8RP model.

Figure 3-1 shows the contact pressure distribution on the surface. The model with 8-node elements predicted distorted pressure distribution within the contact region. The contact pressure at the surface node on the vertical axis of symmetry was zero. As against this both 4-node element models predicted very smooth distribution of the contact pressure. The discussion on mesh sensitivity is deferred till the next section.

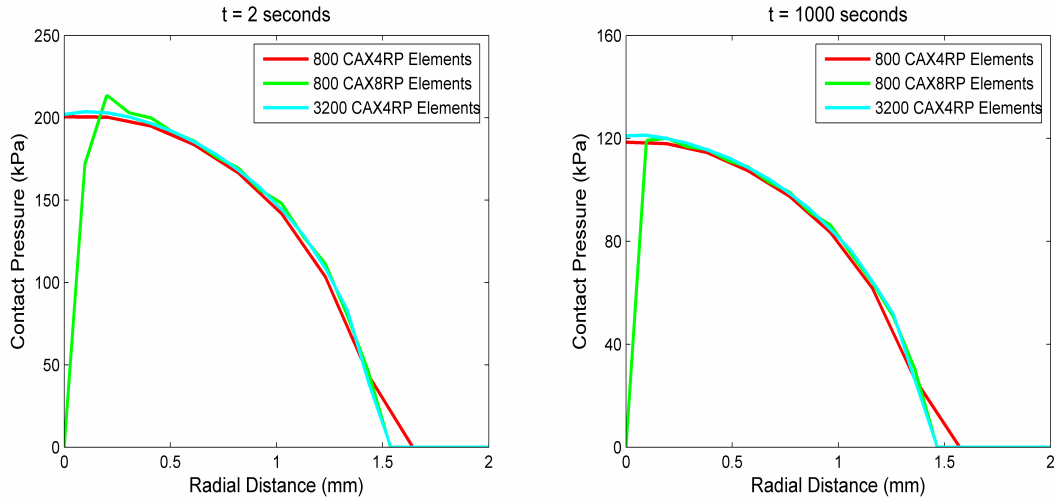

Figure 3-1 Contact pressure distribution at the cartilage surface at different times

The same was true for pore pressure distribution (Figure 3-2). The pore pressure predicted after 2 seconds of ramp deformation at the surface node on the vertical axis of symmetry for 8-node element model was 50 kPa as against 170 kPa

predicted by both 4-node element models. Similar observations were made after 1000 seconds of consolidation.

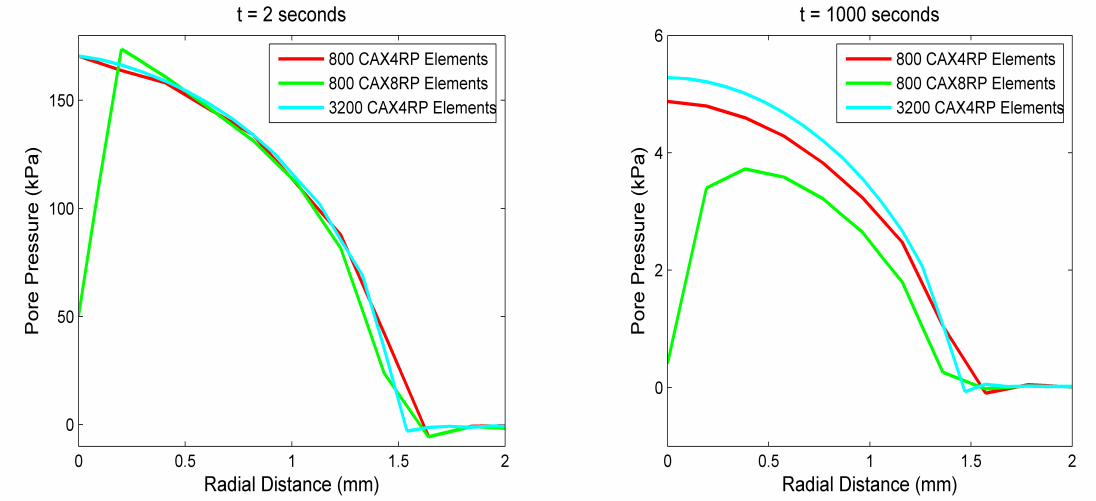

Figure 3-2 Pore pressure distribution at the cartilage surface at different times

The compressive axial stress distribution at the cartilage surface after 2 seconds of ramp deformation was also not smooth for 8-node element model with higher value at the surface node on the vertical axis of symmetry. The distribution after 1000 seconds seemed to be smooth and consistent with 4-node element models except a small tensile stress peak at the edge of the contact (Figure 3-3).

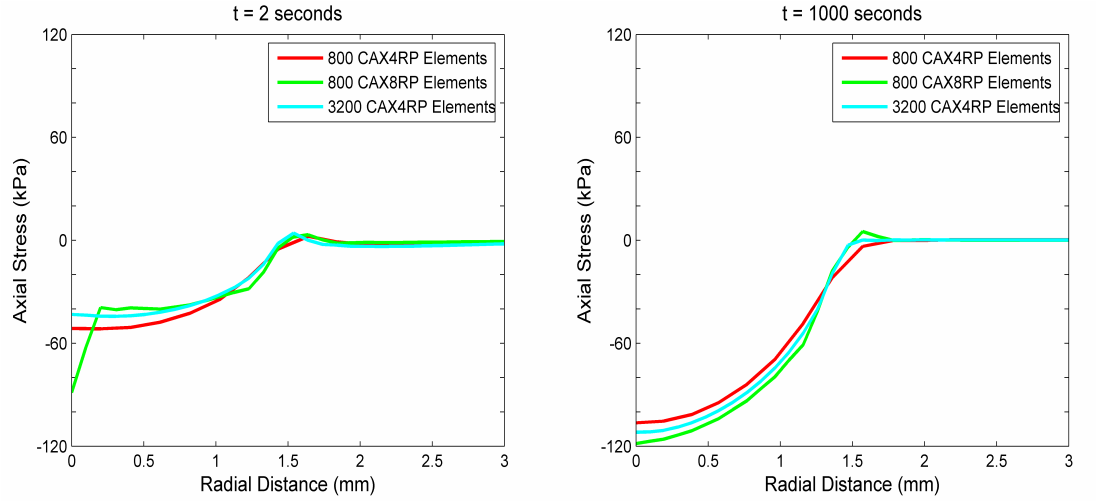

Figure 3-3 Axial stress distribution at the cartilage surface at different times

Radial stress at the surface node on the vertical axis of symmetry after 2 seconds of ramp deformation was compressive for 8-node element model as against tensile radial stress in 4-node element models. The stress distribution after 1000 seconds appeared to be smooth and showed higher values compared to 4-node element models (Figure 3-4).

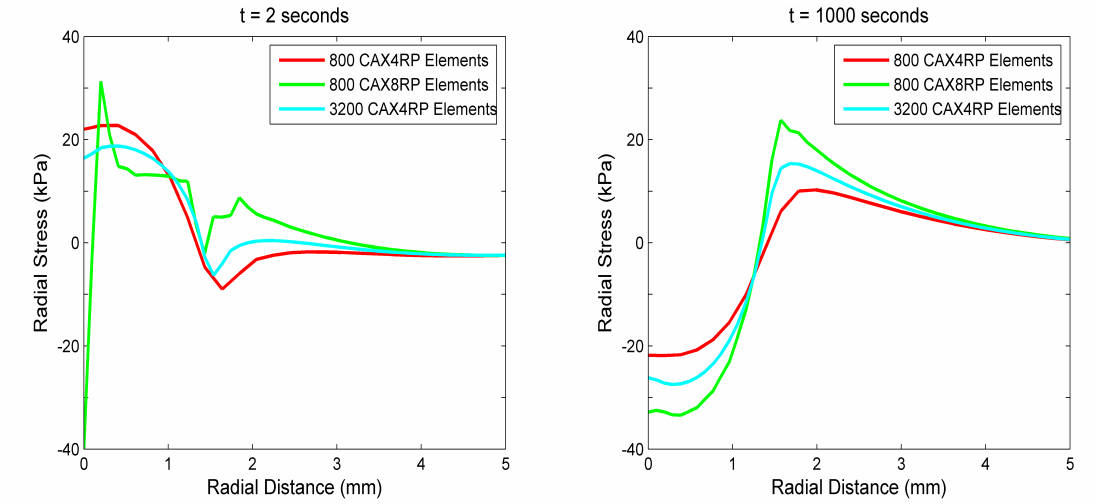

Figure 3-4 Radial stress distribution at the cartilage surface at different times

The results with 8-node element model showed significant distortions in distributions. Warner had used multi point constraint at the cartilage surface node on the vertical axis of symmetry which coincided with the point on the indenter. No such constraints were used here. It is also to be noted that no attempt was made to correct the 8-node model to give smooth distributions which was possible. The only change made in the ABAQUS input file was with respect to the element type keeping all the other parameters constant. The objective here was to study the effect of changing the element type from 4-node to 8-node.

It was inferred from these observations that 8-node elements though being widely used in cartilage FE modelling research were not the ideal type to be used in contact simulations. As far as possible first-order elements should be used for slave surfaces in contact simulations (ABAQUS., 2005) because of the way the contact stresses are calculated at the nodes. Second-order elements like CAX8RP may create problems in calculating the "consistent nodal loads for constant pressure" (See Figure 3-5 where P is the pressure and A is the area on which it acts). ABAQUS uses these nodal forces to take important decisions during contact simulation and it becomes difficult to decide whether the nodal forces are because of the constant pressure or it is the actual variation of the pressure across the element. It was thus decided to use 4-node CAX4RP elements in subsequent analyses for the current study.

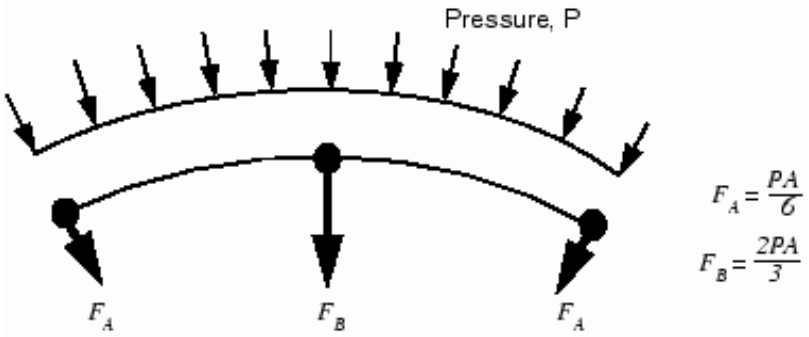

Figure 3-5 Equivalent nodal loads for a constant pressure on a two-dimensional second-order element (ABAQUS., 2005)

3.1.2 Mesh sensitivity analysis

Mesh sensitivity analysis was carried out by reducing the mesh size by half and by increasing it by a factor of 2.

The mesh that was finally used had 3200 (200 × 16) CAX4RP elements. The denser mesh had 12800 (400 × 32) elements and coarser one had 800 (100 × 8) elements.

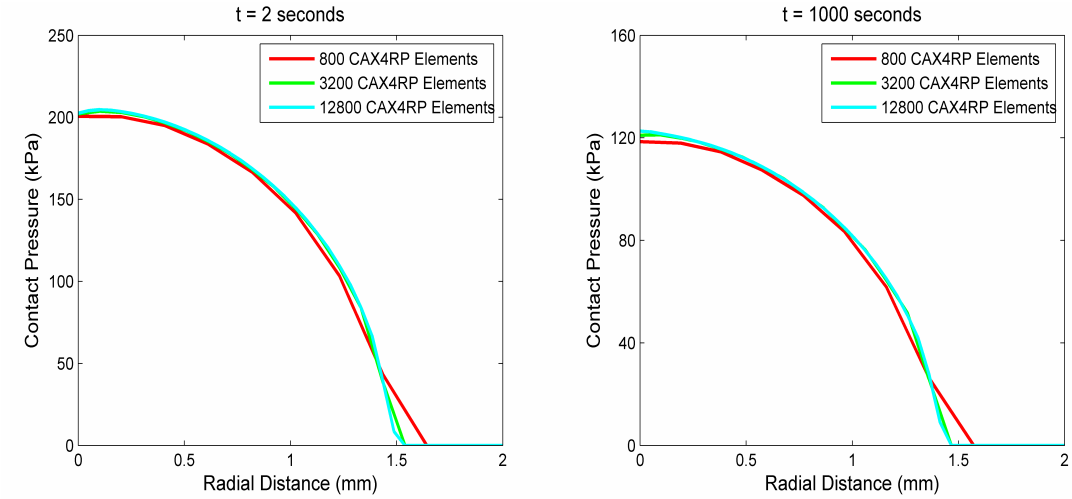

Figure 3-6 Contact Pressure distribution at the cartilage surface at different times

The contact pressure distributions after 2 seconds of ramp deformation and 1000 seconds of consolidation did not show significant difference except that in case of coarser mesh the contact zone was not captured precisely. This could be seen by the curve for 800 elements being slightly outside than those for other mesh densities (Figure 3-6). The mesh being coarser did not have sufficient nodes to cover the precise contact zone.

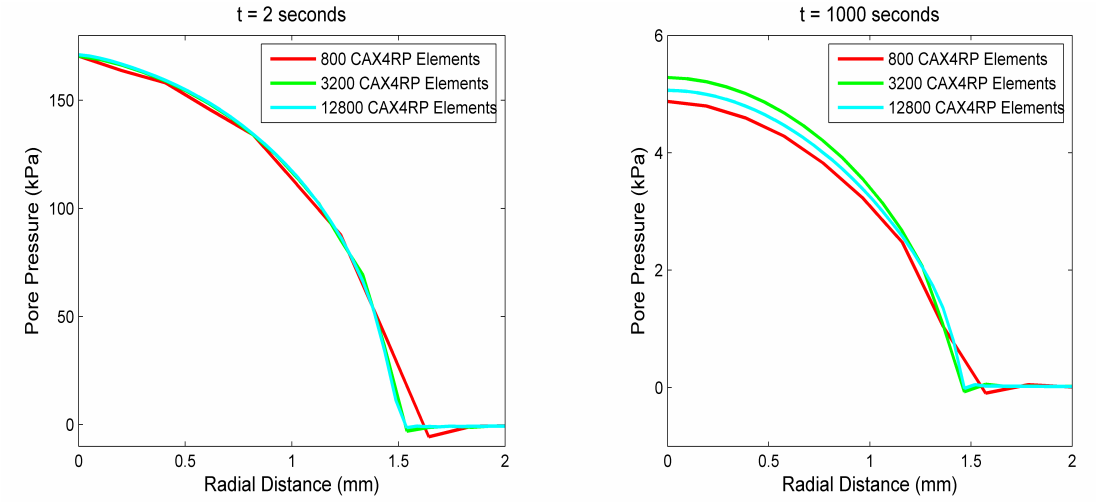

Figure 3-7 Pore pressure distribution at the cartilage surface at different times

Pore pressure at the edge of the contact after 2 seconds of ramp deformation showed a little more negative value for coarser mesh than the other mesh densities (Figure 3-7). This was due to numerical errors and lesser number of nodes at the contact edge in lower density mesh.

Pore pressure distribution after 1000 seconds of consolidation with the lowest density mesh showed lower values than the other two meshes. The reduction in pore pressure due to stress-relaxation was captured differently by all the three mesh densities. The change in maximum pore pressures with the increasing mesh density was also not consistent. The lowest density mesh could not correctly predict the pore pressure at the contact edge (Figure 3-7).

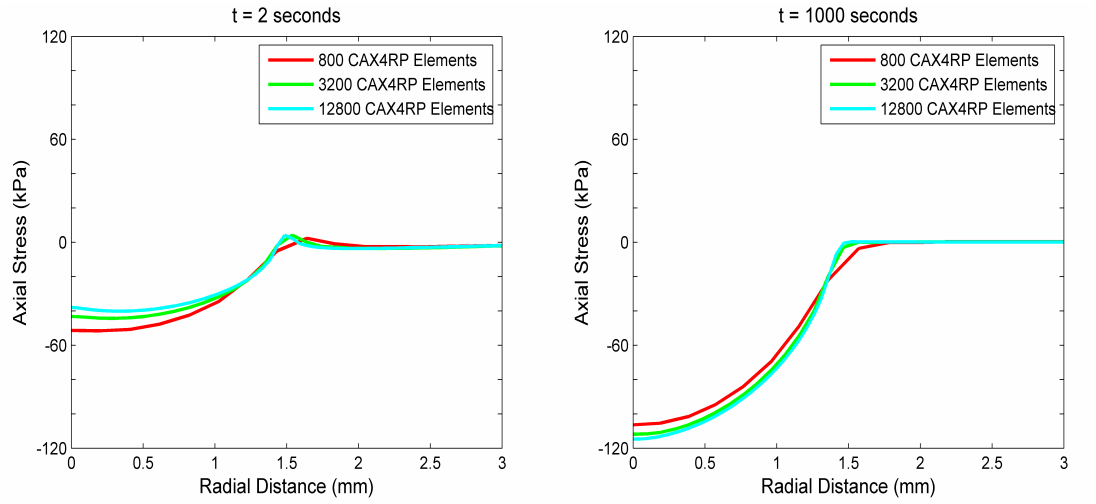

Figure 3-8 Axial stress distribution at the cartilage surface at different times

Axial stress distribution at the cartilage surface showed that the lowest density mesh failed to accurately capture the stress-relaxation from 2 seconds of ramp deformation till the period of 1000 seconds of consolidation. The reduction in axial stress was found to be lesser in coarser mesh compared to other two mesh densities. The two higher density meshes predicted almost similar axial stresses (Figure 3-8).

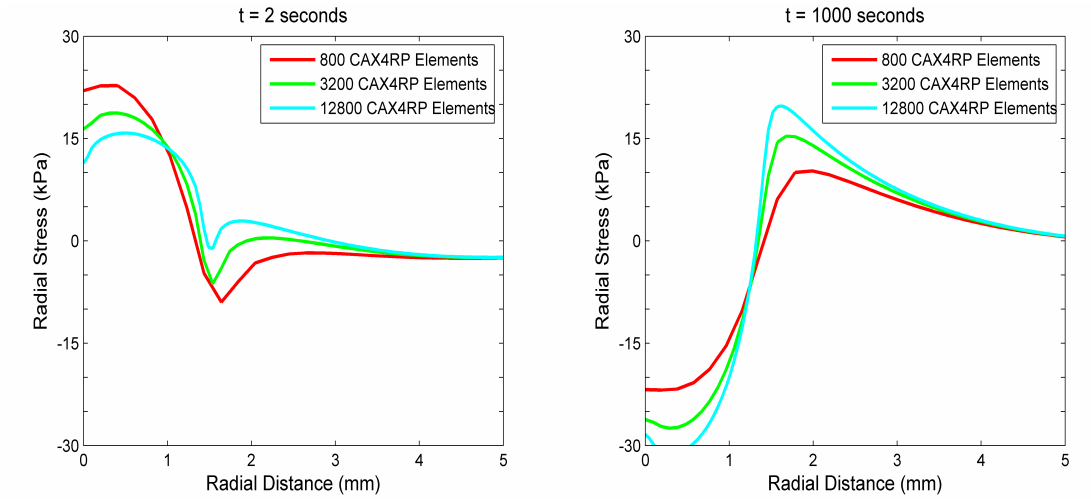

Figure 3-9 Radial stress distribution at the cartilage surface at different times

Radial stress distribution at the surface showed gradual improvement with the increase in the mesh density for both 2 seconds of ramp deformation as well as 1000 seconds of consolidation (Figure 3-9).

As was shown by the mesh sensitivity analysis the highest density mesh was able to give better results compared to the other two. The mesh with the lowest density could not represent the contact zone precisely. The stress-relaxation behaviour shown by both higher density meshes was almost the same as can be seen from pore pressure and axial stress curves. Moreover, 12800 elements mesh involved more computational efforts giving better results for the radial stresses and pore pressure. It was thus decided to use the mesh with 3200 elements.

3.1.3 Use of NLGEOM

Another important factor in FE simulations using ABAQUS is the inclusion of NLGEOM parameter which is used to represent geometric nonlinearities and finite deformation. The articular cartilage generally undergoes large deformation under

normal physiological conditions (Kwan *et al.*, 1990). NLGEOM parameter models this large deformation behaviour.

In this small study, the effect of using NLGEOM parameter on different parameters was studied to decide whether to include this parameter in the current research work where cartilage was being deformed minimum by 10%.

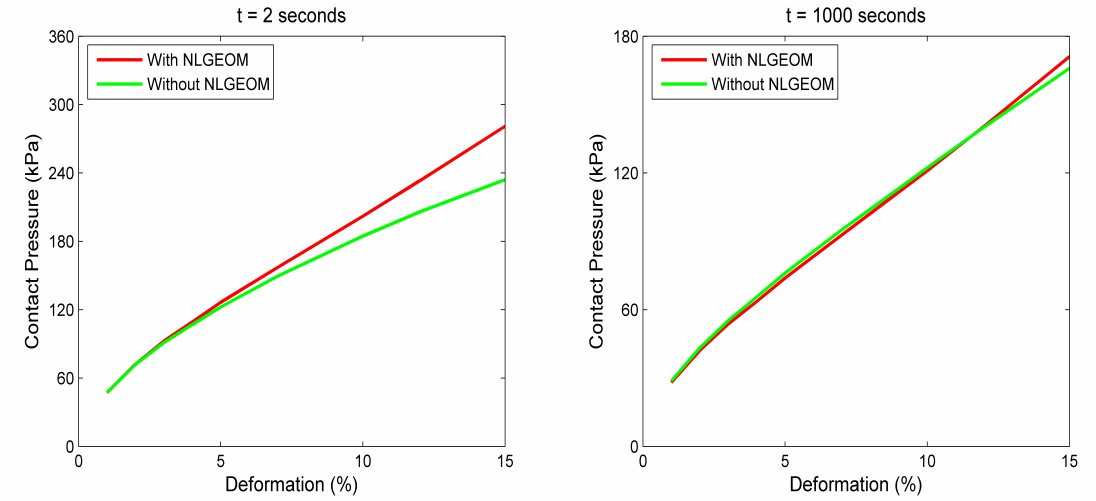

Figure 3-10 Contact pressure at the surface node on the axis for various deformations at different times

The effect of using NLGEOM on contact pressure at the surface was higher contact stresses after 2 seconds of ramp deformation for deformations of approximately 8% and higher. There was very less difference between the two curves after 1000 seconds of consolidation (Figure 3-10).

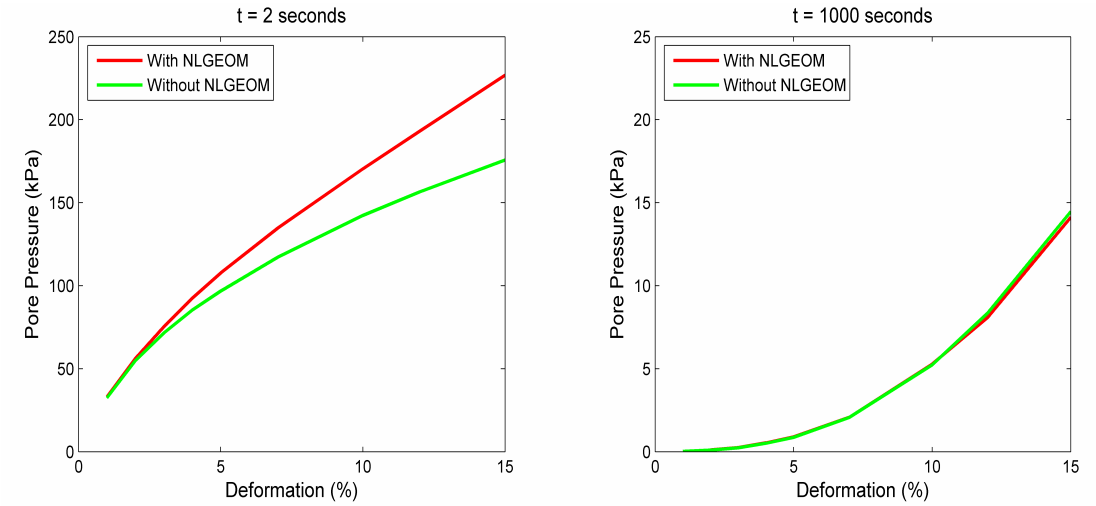

Figure 3-11 Pore pressure at the surface node on the axis for various deformations at different times

Pore pressure distribution at the cartilage surface showed higher values after approximately 5% deformation after 2 seconds of ramp deformation. Such a trend was not seen after 1000 seconds of consolidation (Figure 3-11).

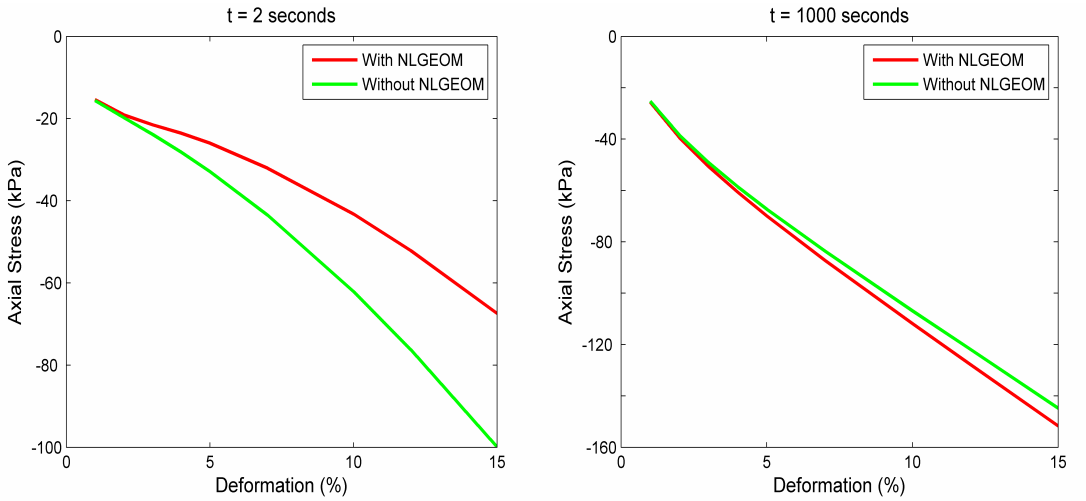

Figure 3-12 Axial stress at the surface node on the axis for various deformations at different times

Compressive axial stress at the cartilage surface seemed to predict lower values with NLGEOM after 2 seconds of ramp deformation for the values of approximately 3% deformation and higher. Unlike in contact pressure and pore pressure graphs, the deviation in two curves is also seen after 1000 seconds of consolidation as well. NLGEOM gives higher values of compressive axial stresses than those without after approximately 6% of deformation and higher (Figure 3-12).

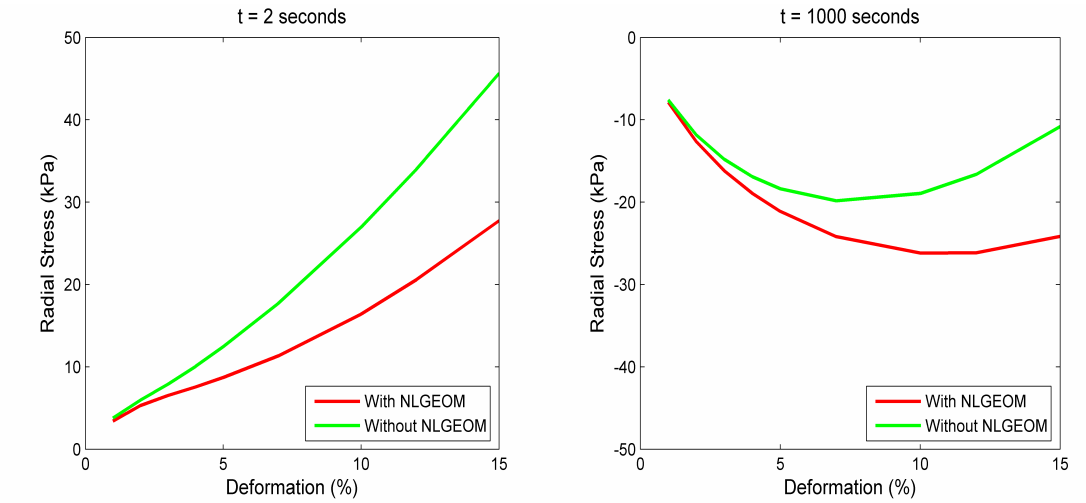

Figure 3-13 Radial stress at the surface node on the axis for various deformations at different times

The deviations in the radial stresses at the cartilage surface showed a marked difference for both 2 seconds of ramp deformation as well as 1000 seconds of consolidation. This deviation was seen right from the deformation of around 3% (Figure 3-13).

NLGEOM parameter affected the contact and pore pressure distributions at the cartilage surface after 2 seconds of ramp deformation and the difference between the values with and without NLGEOM went on increasing as the deformation increased. The values when NLGEOM was used were higher than the ones without NLGEOM. The difference after 1000 seconds of consolidation was negligible.

Unlike in the cases of contact pressure and pore pressure, both axial and radial stress distribution deviated after 1000 seconds of consolidation. This difference was in addition to that seen after 2 seconds of ramp deformation. It could be inferred from the presented results that any cartilage FE model with deformations of more than 5% should include NLGEOM parameter. Hence it is used in all the studies presented here except in joint contact mechanics of two identical cartilages which was used for validation purpose based on the study of Federico and colleagues (Federico *et al.*, 2004) who did not use it.

3.1.4 Stress-relaxation

NLGEOM parameter was used in these simulations not only for the reasons cited before but also because it was used by Warner against whose model these validations were carried out.

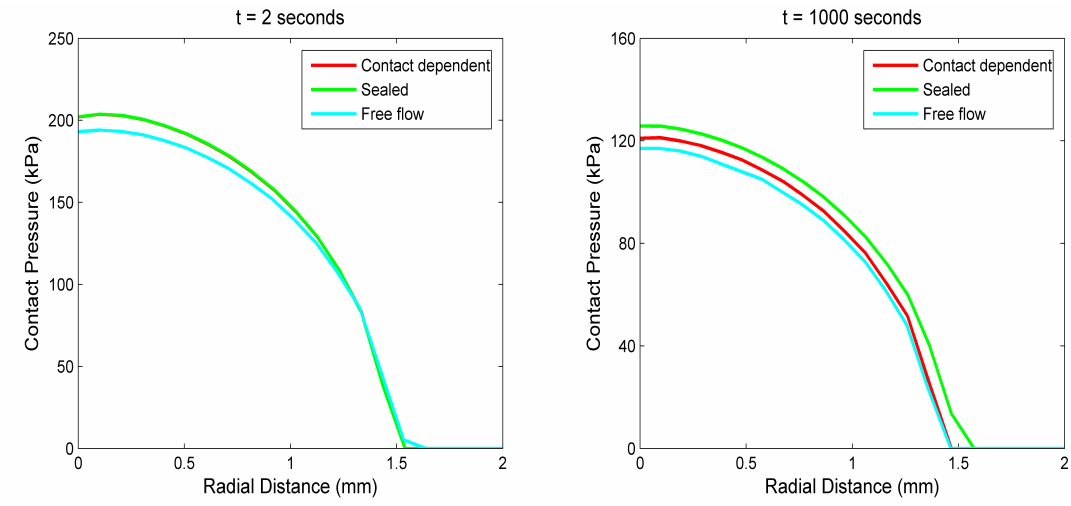

Figure 3-14 Contact pressure distribution at the cartilage surface at different times

The Figure 3-14 shows the contact pressure distribution at the cartilage surface after 2 seconds of ramp deformation and 1000 seconds of consolidation. Contact pressure for all the three surface conditions was found to be almost similar with free flow surface showing lesser value of the three. Contact pressure decreased after 1000 seconds of consolidation mainly due to the reduction in load at the cartilage-indenter interface. Thus surface conditions did not make much difference as far as contact stresses were concerned.

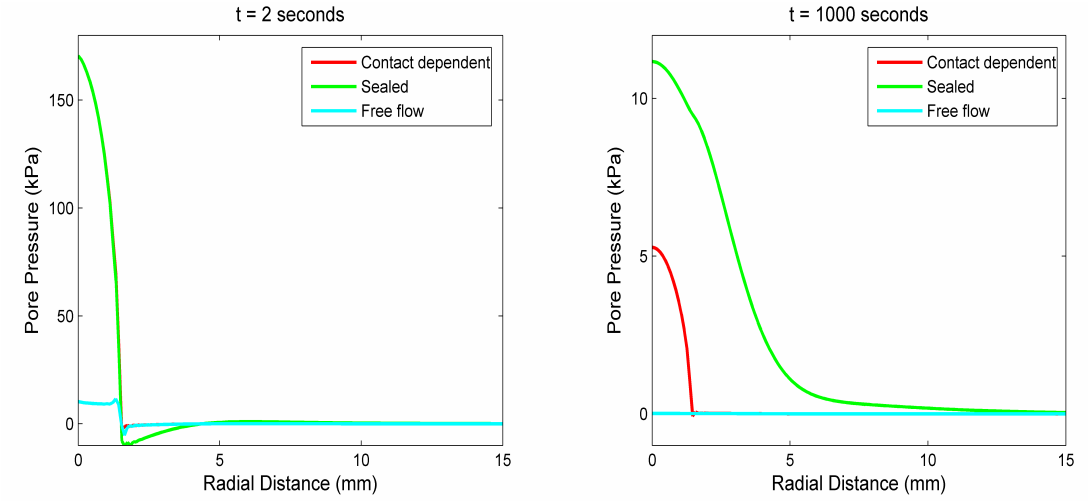

Figure 3-15 Pore pressure distribution at the cartilage surface at different times

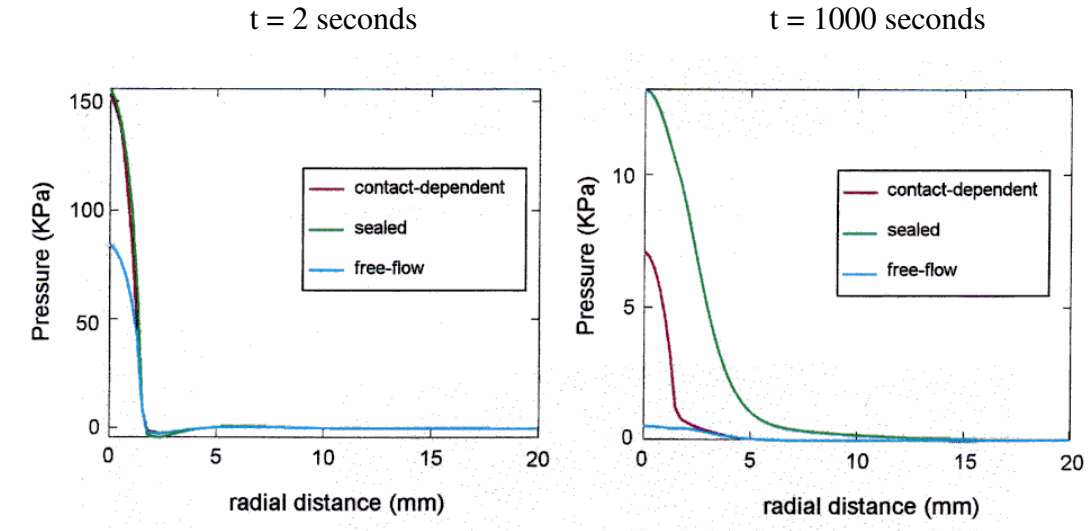

Figure 3-16 Pore pressure distribution at the cartilage surface at different times (Warner, 2000)

The pore pressure distributions for all the three surface conditions from present study were compared to those of Warner (Figure 3-15 and Figure 3-16). The results

agreed well with those provided by Warner (Warner, 2000) except in the case of free flow condition. Porous indenter was used for free flow surface condition by Warner (Warner *et al.*, 2001b) whereas for the other two conditions impermeable rigid indenter with properties of stainless steel was used. However, it was not clear as to how the displacement was applied; whether indenter was assigned the properties of porous material or whether distributed deformation was used mimicking indenter curvature. If porous material was used, then the data for the same was not provided by Warner. Thus in the current study the indenter was kept rigid impermeable to be consistent throughout all three surface conditions and the free flow was allowed at the surface which predicted very low values for the pore pressure after 2 seconds of ramp deformation (10 kPa at a surface node on vertical axis of symmetry) unlike in Warner's study (Warner, 2000) which predicted value as high as 80 kPa at a surface node on vertical axis of symmetry.

Suh and Spilker found that for free flow conditions the pore pressure at the cartilage surface was always zero for porous plane ended cylindrical indenter (Suh and Spilker, 1994) for both slow as well as fast compression rates.. Thus it was obvious that for porous spherical indenter as well, the surface pore pressure would be zero as contact was developed over a period of time unlike in plane ended cylindrical indenter where the contact was developed all at once. The formulation here, in spite of contradictions (surface condition was free flow whereas indenter was rigid impermeable), showed remarkably low values after 2 seconds of ramp loading.

The results of pore pressure after 1000 seconds of consolidation and those of other parameters after both 2 seconds and 1000 seconds were in good agreement to those of Warner. This condition of free flow, the way it was modelled here (free flow on the surface with contradicting rigid impermeable indenter), does not have any physical significance and hence will not be discussed in detail.

The pore pressure distributions on the cartilage surface after 2 seconds of ramp deformation were same for both sealed and contact dependent flow conditions within the contact zone. Outside the contact zone negative pore pressure was recorded very close to the contact edge in case of sealed conditions which was also observed in contact dependent flow but over a very small area. The reduction in pore pressure could be seen in all three cases after 1000 seconds of consolidation with contact dependent flow conditions showing more reduction than sealed conditions owing to the free flow surface outside the contact. The values after 2 seconds of ramp deformation for contact dependent and sealed conditions were higher than those presented by Warner. This could be due to the reasons such as element type,

mesh density and contact detection algorithm which were different in these studies. The corresponding values were lower after 1000 seconds of consolidation.

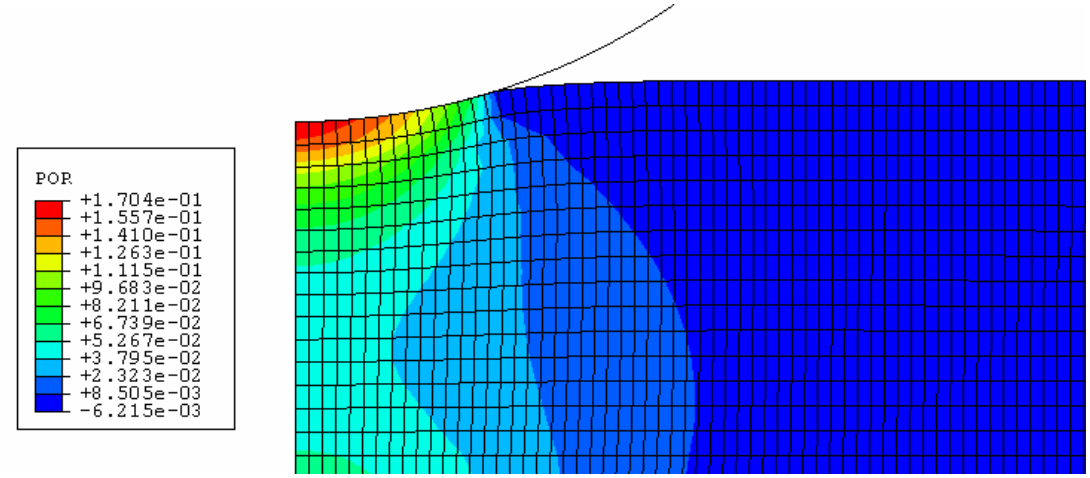

Figure 3-17 Pore pressure (MPa) contour plot for contact dependent flow after 2 seconds

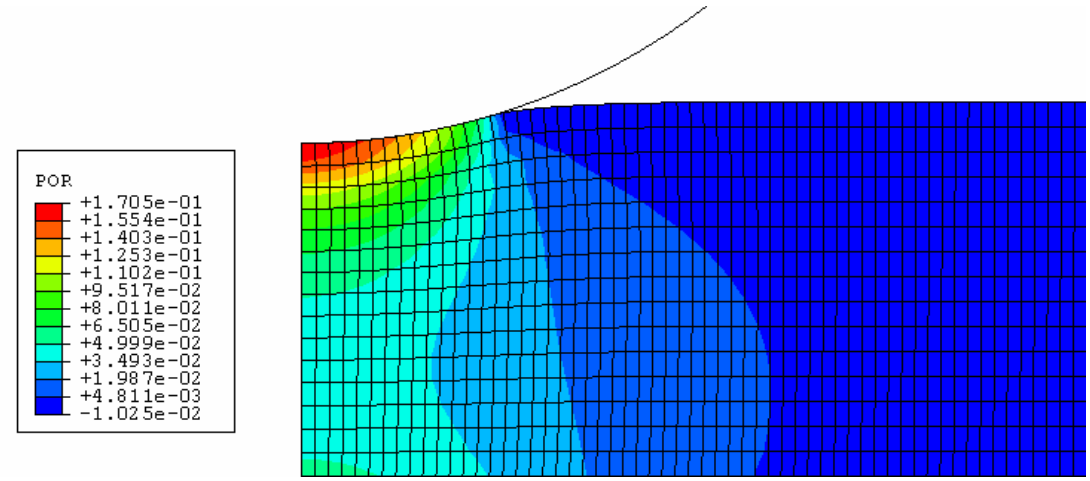

Figure 3-18 Pore pressure (MPa) contour plot for sealed flow after 2 seconds

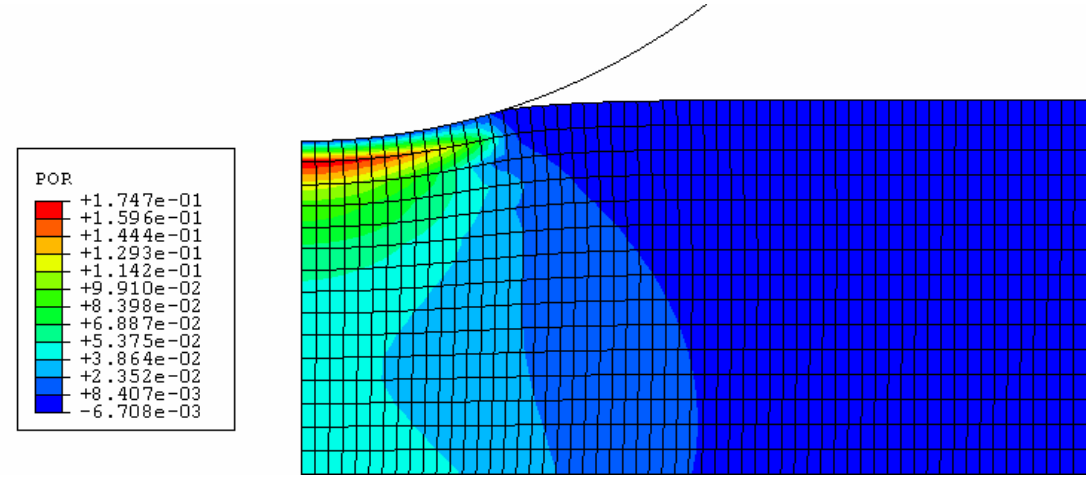

Figure 3-19 Pore pressure (MPa) contour plot for free flow after 2 seconds

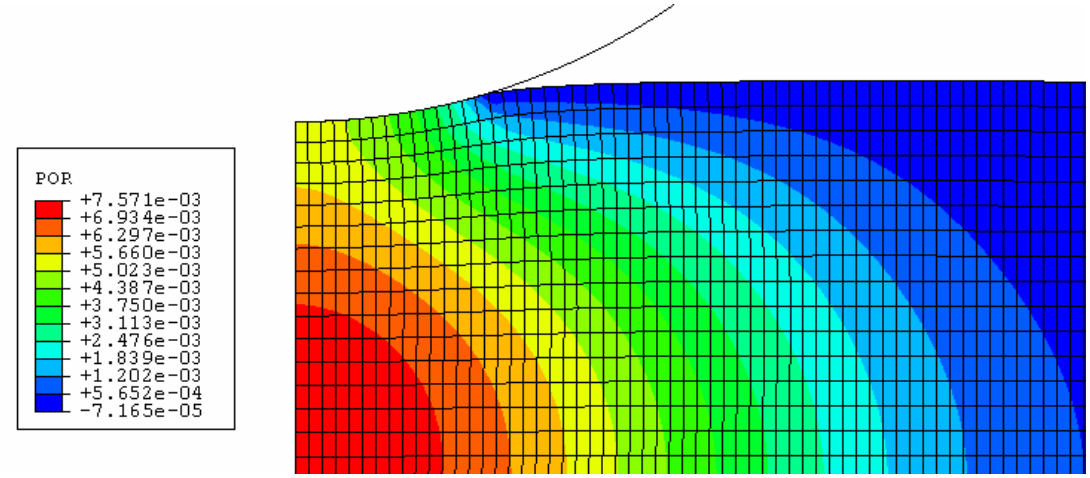

Figure 3-20 Pore pressure (MPa) contour plot for contact dependent flow after 1000 seconds

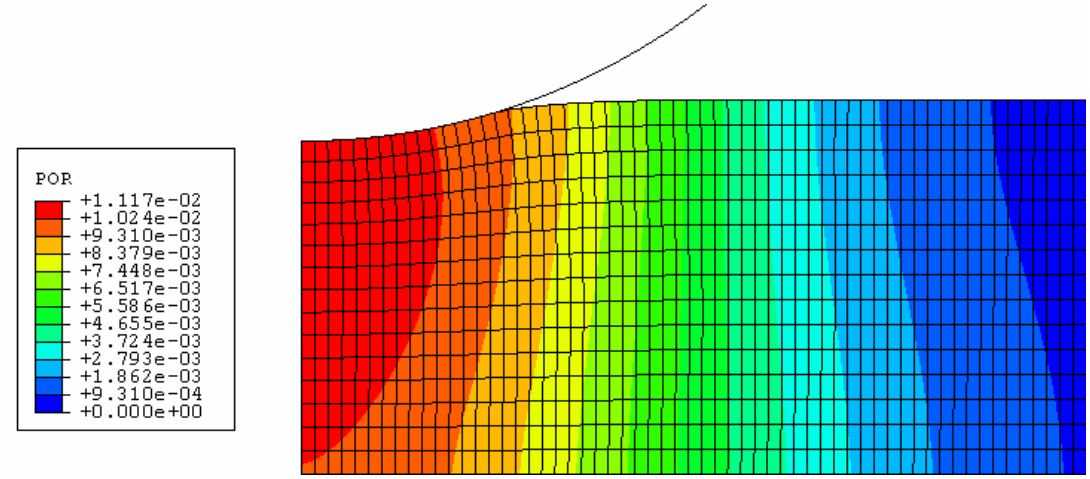

Figure 3-21 Pore pressure (MPa) contour plot for sealed flow after 1000 seconds

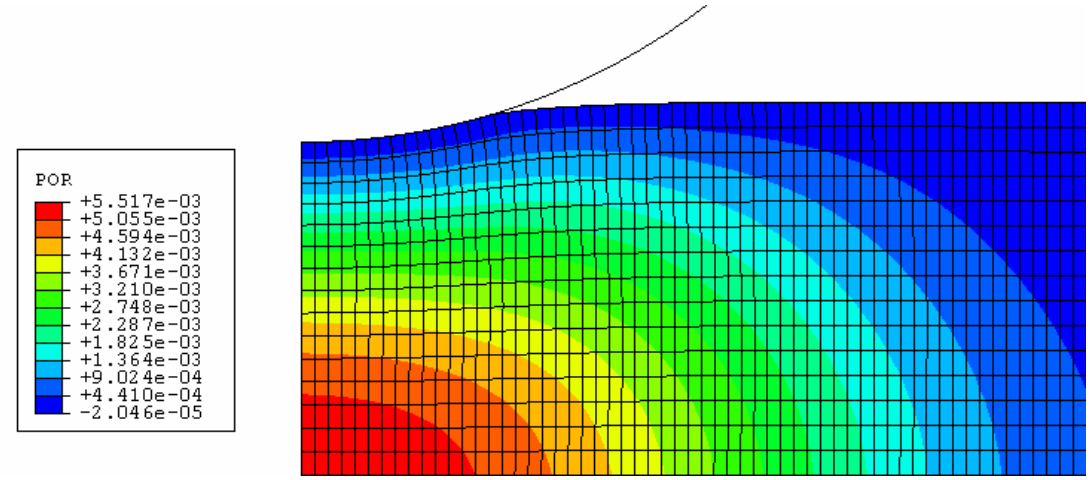

Figure 3-22 Pore pressure (MPa) contour plot for free flow after 1000 seconds

The contour plots after 2 seconds (Figure 3-17, Figure 3-18 and Figure 3-19) and 1000 seconds (Figure 3-20, Figure 3-21 and Figure 3-22) gave better visualization of the pore pressure distribution within the cartilage layer. The contour plots after 1000 seconds of consolidation for sealed and contact dependent flow conditions were significantly different.

Table 3-1 Pore pressure in the cartilage predicted after 2 seconds of ramp deformation

Surface Flow Condition	Minimum Value (kPa)	Maximum Value (kPa)	Reference
Contact dependent	-6.2	+170.4	Current study
	-3.8	+168.0	(Warner, 2000)
Sealed	-10.3	+170.5	Current study
	-4.2	+158.0	(Warner, 2000)

The maximum pore pressure for both the sealed and contact dependent flow, after 2 seconds of ramp deformation, was found at the centre of indentation near the cartilage surface. The contact dependent and sealed flow conditions predicted similar values as the cartilage surface is sealed under indentation centre for both the flow conditions. The maximum values presented by Warner for sealed and contact dependent flow conditions were different possibly because of contact detection algorithm where the entire element surface was sealed once the contact stresses at the mid-side node crossed the threshold value. The difference in pore pressure between Warner's and the current study was also probably due to the same reason.

The stress shielding phenomenon of articular cartilage in the form of interstitial fluid pressurization had been discussed in literature survey chapter. The high pore pressure (Figure 3-15) and low axial stresses (Figure 3-23) observed after 2 seconds of ramp deformation in the current study clearly demonstrated this phenomenon. The axial stress results were also in good agreement with those given by Warner (Warner, 2000) whose axial stress results are shown in Appendix A.

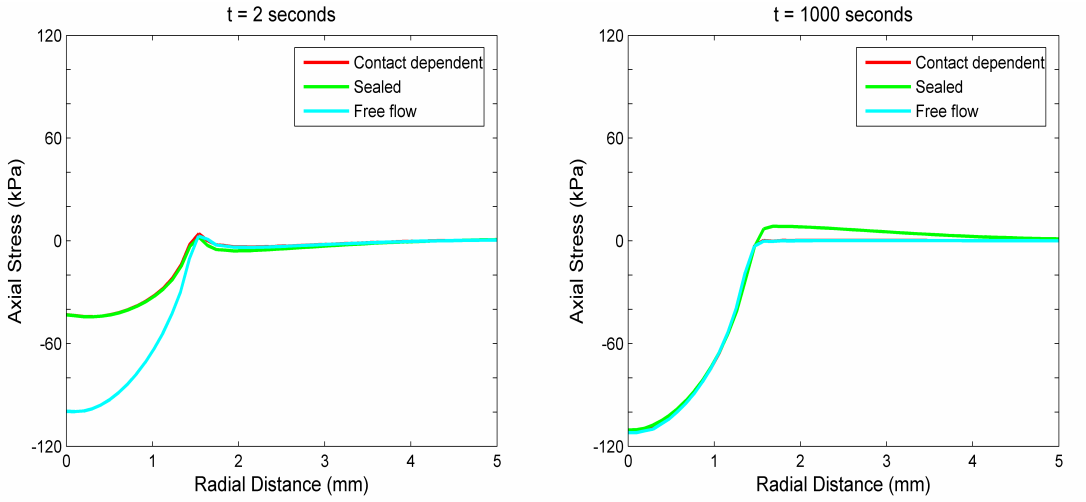

Figure 3-23 Axial stress distribution at the cartilage surface at different times

The maximum reduction in axial stress was shown by sealed and contact dependent flow conditions. The pore pressure at this point had significantly dropped down (Figure 3-15) as the maximum load was now supported by solid matrix. Small tensile stress zone was observed next to the contact edge for sealed conditions.

The axial stress contour plot after 2 seconds showed similar axial stress distribution as observed by Warner. The plots of the current study for contact dependent flow after 2 seconds and 1000 seconds are presented in Appendix A.

Table 3-2 Axial stresses in the cartilage predicted after 2 seconds of ramp deformation

Surface Flow Condition	Minimum Value (kPa)	Maximum Value (kPa)	Reference
Contact dependent	-81.9	+4.2	Current study
	-82.4	+4.9	(Warner, 2000)
Sealed	-81.9	+3.5	Current study
	-82.8	+5.39	(Warner, 2000)

The difference observed in Table 3-2 may be due to the difference in the contact detection algorithms and the type of elements used.

The radial stress distributions at the cartilage surface after 2 seconds of ramp deformation and 1000 seconds of consolidation also showed good agreement with those of Warner. The current study, however, showed lower tensile radial stresses after 2 seconds of ramp deformation and higher compressive radial stresses after 1000 seconds of consolidation (Figure 3-24 and Figure 3-25).

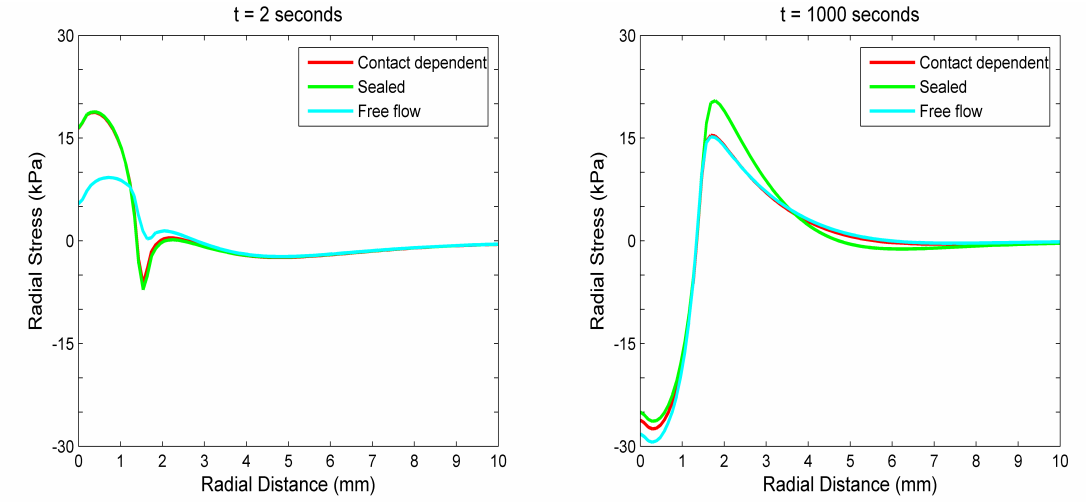

Figure 3-24 Radial stress distribution at the cartilage surface at different times

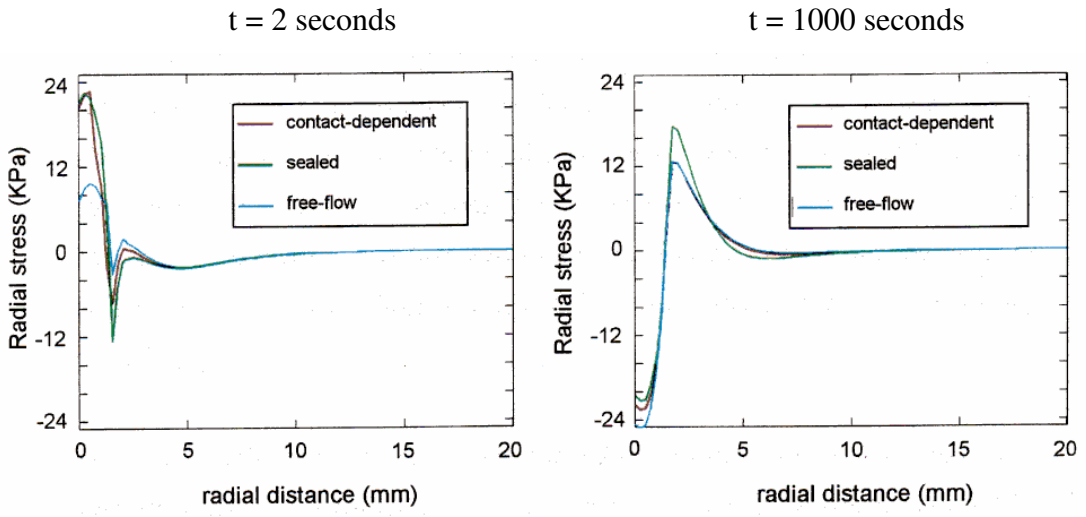

Figure 3-25 Radial stress distribution at the cartilage surface at different times (Warner, 2000)

Table 3-3 Radial stresses in the cartilage predicted after 2 seconds of ramp deformation

Surface Flow Condition	Minimum Value (kPa)	Maximum Value (kPa)	Reference
Contact dependent	-20.0	+41.1	Current study
	-21.7	+41.5	(Warner, 2000)
Sealed	-20.0	+41.1	Current study
	-19.0	+38.4	(Warner, 2000)

The values of compressive radial stresses were lower than compressive axial stresses but the tensile radial stresses were higher compared to tensile axial stresses. This was observed by Warner as an important factor owing to tissue failure mostly under tensile loading (Warner, 2000). The transition from tensile radial stresses to compressive radial stresses at the surface was also observed as was done by Warner. The contour plot at 2 seconds of ramp deformation for contact dependent flow is given in Appendix A.

From this discussion it can be inferred that sealed and contact dependent flow conditions did not make much of a difference after 2 seconds of ramp deformation. Similarly, as far as axial stresses, radial stresses, and contact pressure on the surface were concerned, there was not much difference between free flow and contact dependent flow conditions after 1000 seconds of consolidation. The difference was clearly seen in all the three cases in pore pressure distribution after 1000 seconds. Contact dependent flow was able to predict realistic cartilage behaviour as compared to the other two after both 2 seconds and 1000 seconds. The similar observations were made by Warner with the exception of pore pressure distribution after 2 seconds of ramp deformation in free flow surface condition.

3.1.4 Creep-deformation

The contact pressure distribution on the surface after 2 seconds of ramp loading was found to be similar to that of stress-relaxation after 2 seconds of ramp deformation. After 1000 seconds of consolidation, the contact stresses reduced due to the increase in the contact area, load remaining constant. The surface flow conditions did not make much of a difference (Figure 3-26).

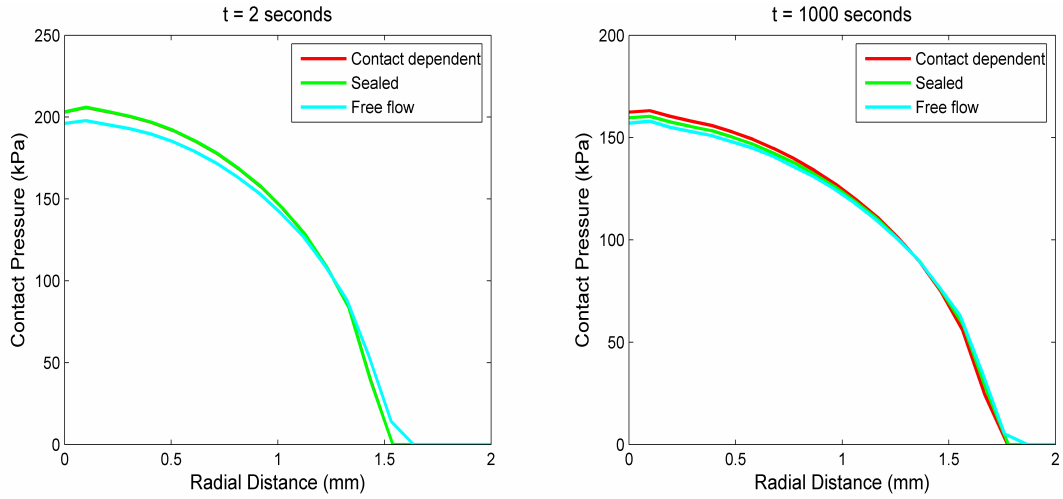

Figure 3-26 Contact pressure distribution at the cartilage surface at different times

It was obvious from the results presented for stress-relaxation (Figure 3-14) and creep-deformation (Figure 3-26) that the increase in the contact area was seen only in creep-deformation.

The pore pressure, axial stress and radial stress distributions were similar to those observed in stress-relaxation and the graphs for the same are given in Appendix B.

The results from both stress-relaxation and creep-deformation did indicate the effectiveness of using contact dependent flow conditions rather than assuming either free flow or sealed flow conditions.

3.2 Joint contact mechanics of two cartilages

NLGEOM parameter was not used in these simulations in order to validate with the model presented by Federico and colleagues (Federico *et al.*, 2004) who had not used it as well.

3.2.1 Stress-relaxation

The steel block over cartilage configuration (Plane/Cart) was considered by Federico (Federico, 2006) whereas the current study analysed both steel block over cartilage and identical cartilage over cartilage configurations (Cart/Cart).

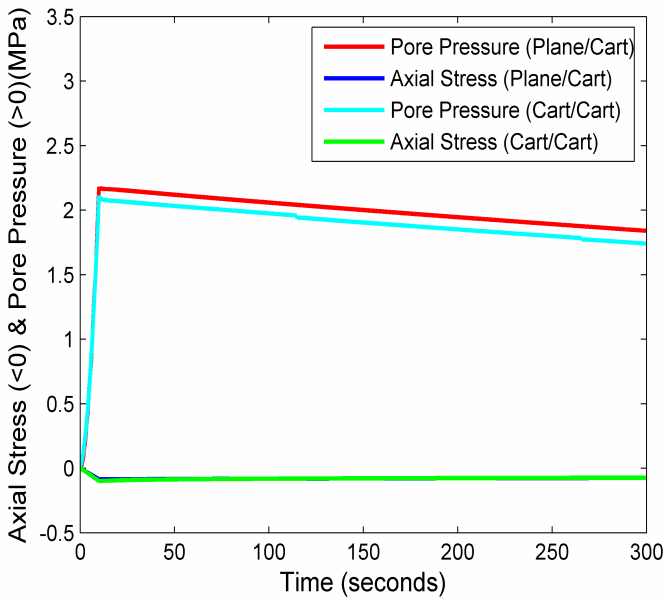

Figure 3-27 Fluid pore pressure and solid compressive axial stress over time at node N1 for steel block over cartilage (Plane/Cart) and cartilage over cartilage (Cart/Cart) configuration

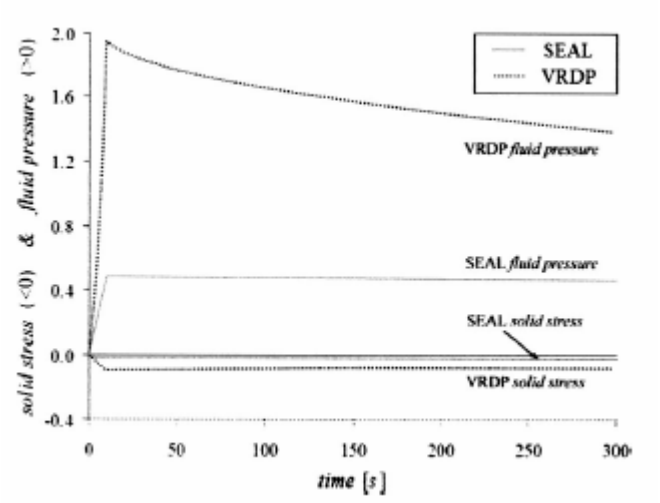

Figure 3-28 Fluid pore pressure and solid compressive axial stress over time at node N1 (Federico *et al.*, 2004; Federico *et al.*, 2005)

VRDP, shown in Figure 3-28, was used in both the current study as well that by Federico. The *k-e* relationship of Eq. 2-6 was used to get the different values of permeability from the values given in Table 2-2.

SEAL in the Figure 3-28 which meant sealed surface condition was implemented by Federico and colleagues using non-porous elastic elements above the cartilage surface. This was not included in the current study.

The time response of the steel block over cartilage was in good agreement with the results presented by Federico and colleagues (Federico *et al.*, 2004; Federico *et al.*, 2005). The small difference of predicted maximum pore pressure (2.18 MPa in Figure 3-27 versus 2.0 MPa in Figure 3-28) may be due to the differences in formulations. Federico had used 8-node elements whereas in the current study 4-node elements were used. Moreover, the contact detection algorithms used were different (Federico, 2006).

The steel block over cartilage configuration in the current study gave higher values of pore pressure throughout as compared to cartilage over cartilage. The maximum pore pressure for the block over cartilage model (2.18 MPa) was found to be around 3.3% higher than the maximum (2.11 MPa) predicted for cartilage over cartilage configuration. The difference in the axial stresses at the current scale used

for Figure 3-27 was negligible. Theoretically both the pore pressure results should have been the same (Ateshian *et al.*, 1994a). This deviation was probably due to the difference in formulations in ABAQUS.

Firstly, the pressure-overclosure surface behaviour for block over cartilage model was formulated to be hard whereas for cartilage over cartilage model it was exponentially soft. The soft surface formulation was not used for block over cartilage model as it gave unacceptable levels of overclosure. Hard surface formulation could not be used for cartilage over cartilage model because of numerical problems. The soft surface formulation is recommended by ABAQUS when modelling soft thin layer of material as well as for better contact detection when impact loads are not involved (ABAQUS., 2005) as in this case. Even with the hard surface formulation for cartilage over cartilage which failed to converge after ramp loading, the overall ramp deformation of 30% did not translate into exact 15% deformation in each cartilage which theoretically should have been the case. It did so only for very small deformations and the results for the same are not presented here.

Secondly, the formulation of slave and master surfaces in ABAQUS for the identical mesh and stiffness properties did not permit the nodes displacement to be exactly symmetrical in cartilage over cartilage configuration. This was confirmed by interchanging the master-slave surface definitions.

For the steel block over cartilage configuration the contact detection algorithm validated earlier using rigid spherical indenter over cartilage was used whereas for cartilage over cartilage configuration the contact detection algorithm developed for two cartilage surfaces in contact was used. The results presented earlier in this section indicated the validity of this second algorithm and also the validity of the joint contact mechanics formulation.

3.3 Cartilage indentation with a rigid plane ended cylindrical indenter

The creep-deformation predictions from FE simulation were compared to the experimental results as shown in Figure 3-29. The deformation at 3000 seconds was maintained at 0.19 mm by altering the Young's modulus and then the permeability was changed to fit the initial part of the curve. Young's modulus was observed to be 2.38 MPa and since the Poisson's ratio was kept at 0.0 to allow maximum compressibility (Jin *et al.*, 2000) aggregate modulus was also calculated to be 2.38 MPa. Permeability was also calculated and was found to be 1.2×10^{-15} m^4/Ns.

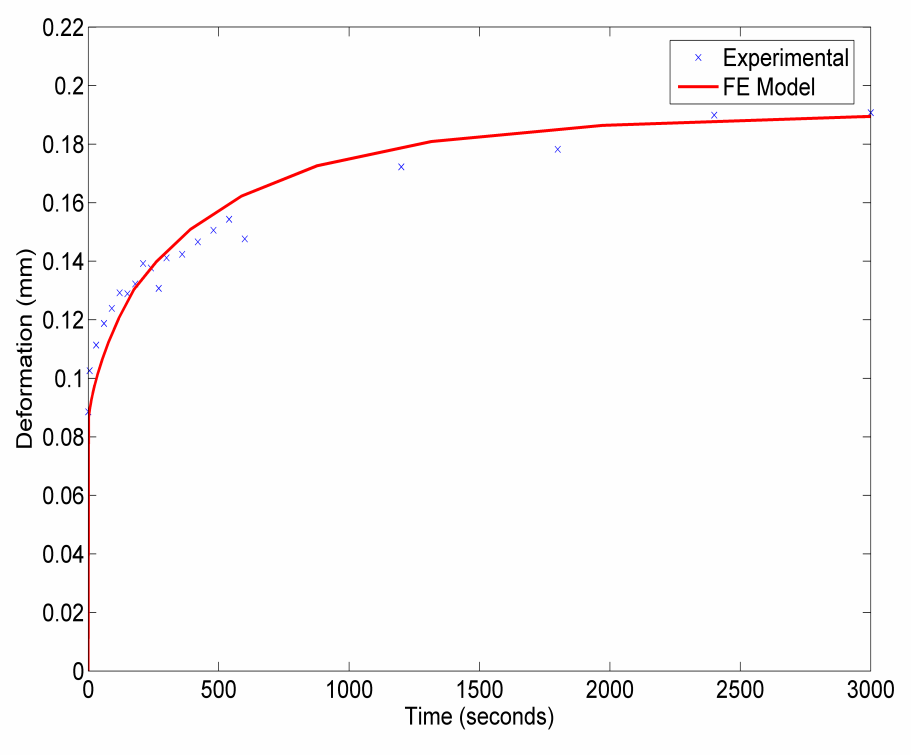

Figure 3-29 Comparison of experimental measurements (Katta *et al.*, 2006) with FE predictions

This model was to demonstrate the capability of the FE model to predict mechanical parameters of the cartilage. The values of these mechanical parameters derived in this study were only indicative of the experimental measurements.

Chapter 4 Sliding Results and Discussion

4.1 Rigid plate sliding over cartilage surface

The Figure 4-1 shows the pore pressure and compressive axial stress at a central node N1 on the cartilage surface for sliding as well as consolidation in creep-deformation. Both the pore pressure and axial stress distribution showed remarkably similar values for sliding as well as consolidation. This was as expected because the entire cartilage surface was constantly covered by the plate and the effects of sliding or consolidation would be similar (friction was assumed to be zero).

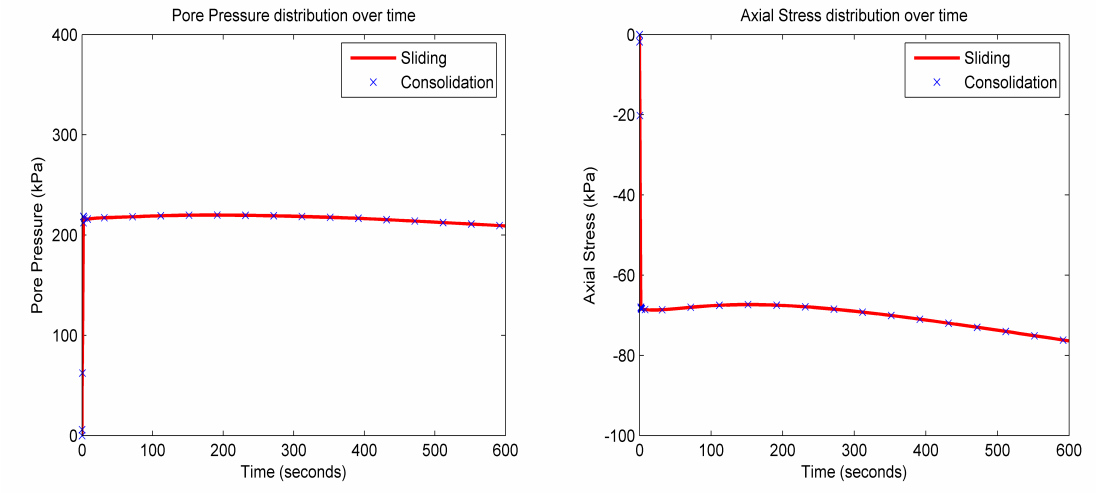

Figure 4-1 Pore pressure and axial stress distribution at central node on cartilage surface

It was observed that during the ramp loading and up to around 200 seconds of sliding the pore pressure increased and compressive axial stresses decreased before following the normal trend of consolidation and that it would take relatively a long time before complete consolidation occurs. This increase in interstitial fluid pressurization during sliding was also observed by Jin and colleagues (Jin *et al.*, 2000) when load was applied for increasing time durations. In their study, this was seen as a dip in the effective co-efficient of friction for loads applied for less than 5 minutes.

It was also observed that during the ramp loading and up to the period of around 200 seconds the interstitial fluid flowed towards the loaded surface around the cartilage centre (Figure 4-2).

The flow slowly became parallel to the surface as more and more fluid escaped through the free draining cartilage sides (Figure 4-3). This was in good agreement with the weeping lubrication observed by McCutchen and Macirowski (McCutchen, 1959; McCutchen, 1962; Macirowski *et al.*, 1994) at least in the initial stages of load application.

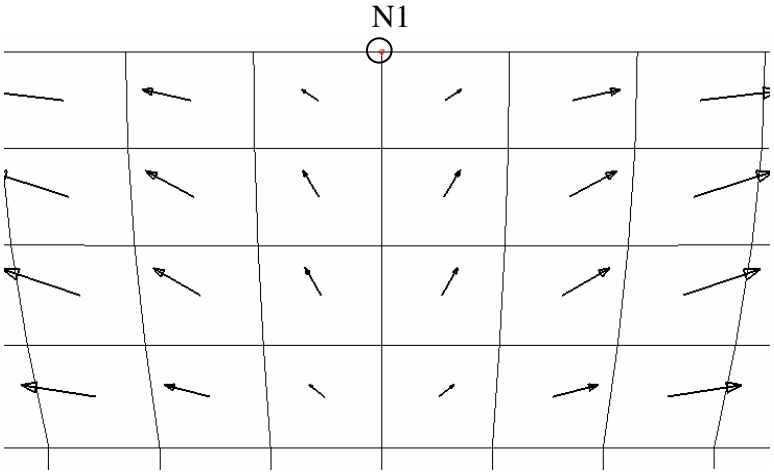

Figure 4-2 Direction of fluid flow at 149.6 seconds of sliding near the cartilage centre

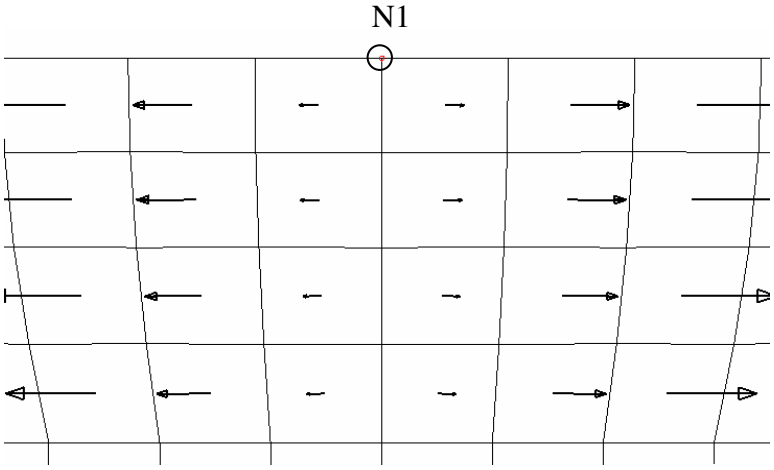

Figure 4-3 Direction of fluid flow at 600 seconds of sliding near the cartilage centre

4.2 Rigid cylindrical indenter sliding over cartilage surface

NLGEOM parameter was used in these simulations. The pore pressure and axial stress at N1, N2, N3 and N4 were plotted against time at which the indenter comes exactly at its mean position for two loading conditions; 0.1N/mm and 0.5N/mm which would give approximately 3.3% and 10% deformations respectively after ramp loading. The simulation with 0.5N/mm load could run only for 395 seconds due to numerical errors and mesh distortion thereafter. This was a very preliminary study and further analysis is required. This was meant to be the simplification of hemiarthroplasty as in the case of a hip joint where the artificial metallic femoral head would get engaged with the natural articular cartilage in acetabulum. The mesh distortion after 394 seconds of sliding is shown in Figure 4-4

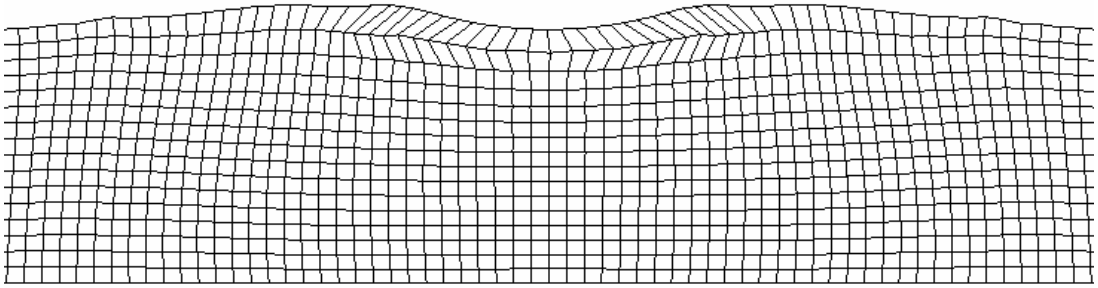

Figure 4-4 Cartilage mesh distortion after 394 seconds of sliding (load = 0.5 N/mm)

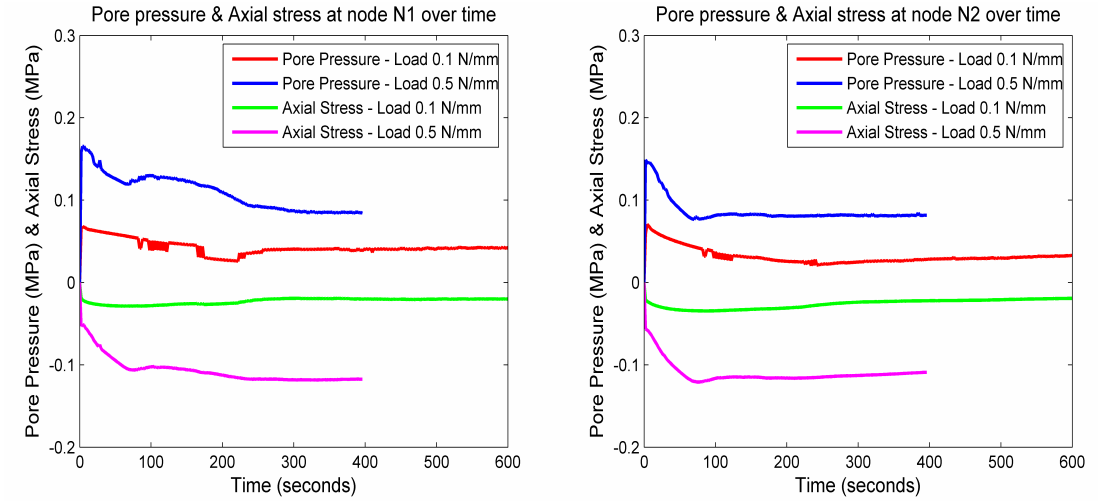

Figure 4-5 Pore pressure and axial Fluid pore pressure and solid compressive axial stress over time at nodes N1 (on surface) and N2 (just below surface)

The pore pressure at the nodes N1 and N2 (Figure 4-5) clearly showed the decreasing trend with time before it more or less stabilized at a constant value which was well above zero. In the configuration studied here, the most of the cartilage surface was open where both exudation and imbibition was allowed.

The pore pressure at the surface initially showed higher value as the load was being applied directly on the surface and the majority of the load was being taken by the fluid phase (Figure 4-5). The little bulge in the pore pressure (and axial stress) at node N1 between 100 and 200 seconds could be because of numerical errors. This needs to be investigated further.

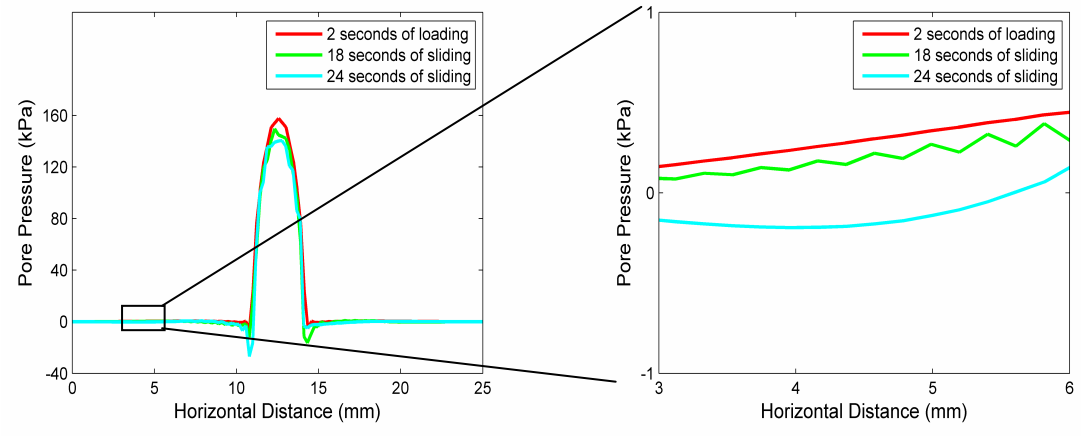

Figure 4-6 Pore pressure distribution on the cartilage sliding (load = 0.5 N/mm)

Figure 4-7, Figure 4-8 and Figure 4-9 show the fluid flow direction in the cartilage after 2 seconds of ramp loading, 18 seconds of sliding and 24 seconds of sliding respectively. The pore pressure on the most of the cartilage surface was either positive or zero after 2 seconds of loading (Figure 4-10) and the upward deformation of the cartilage was not much (Figure 4-13). The pore pressure immediately outside the cartilage contact zone was negative over a small area (Figure 4-6). The fluid flow exudation occurred wherever the pore pressure was positive and imbibition took place wherever the pore pressure was negative or if the area was loaded by the indenter. The fluid exudation was observed at the contact edges as the indenter loaded the contact area where the fluid could either flow inside the cartilage or exude from the path of least resistance. Thus fluid could be seen to exude from both the leading and trailing contact edges whereas there was fluid imbibition within the contact zone. The fluid could also be seen exuding a little farther from the contact

zone whereas the fluid imbibition took place over a small area outside the contact zone.

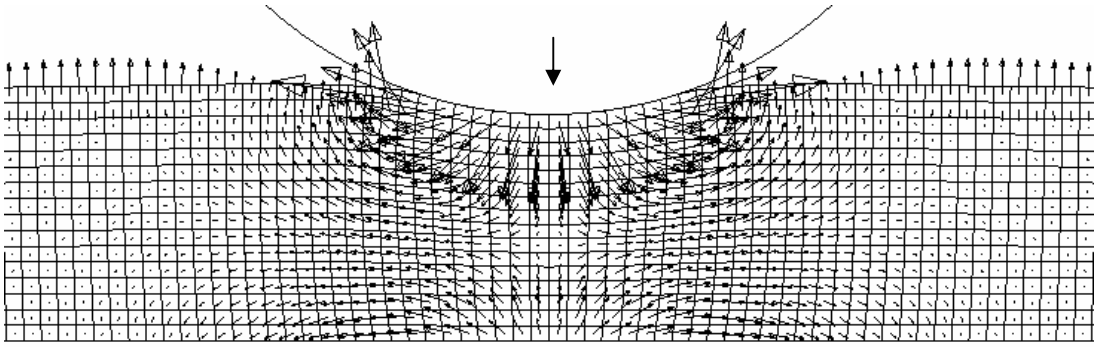

Figure 4-7 Direction of fluid flow after 2 seconds of ramp loading (load = 0.5 N/mm)

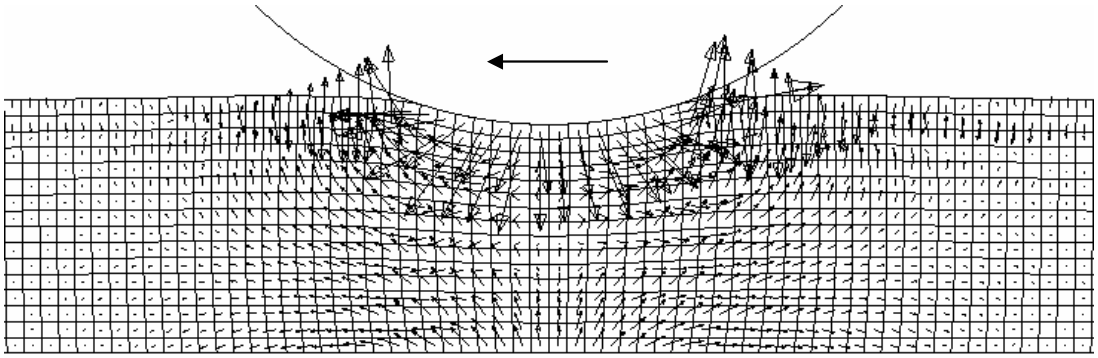

Figure 4-8 Direction of fluid flow after indenter reached its mean position after 18 seconds of sliding and moving towards left (load = 0.5 N/mm)

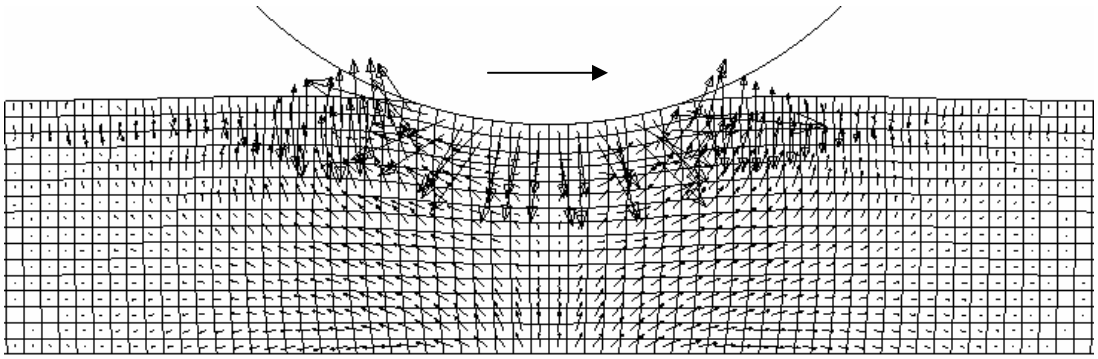

Figure 4-9 Direction of fluid flow after indenter reached its mean position after 24 seconds of sliding and moving towards right (load = 0.5 N/mm)

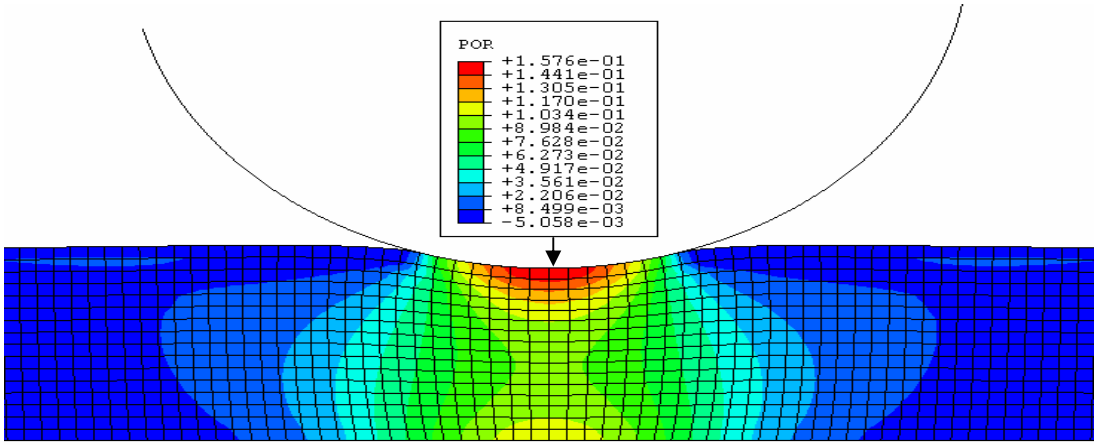

Figure 4-10 Pore pressure (MPa) distribution after 2 seconds of ramp loading (load = 0.5 N/mm)

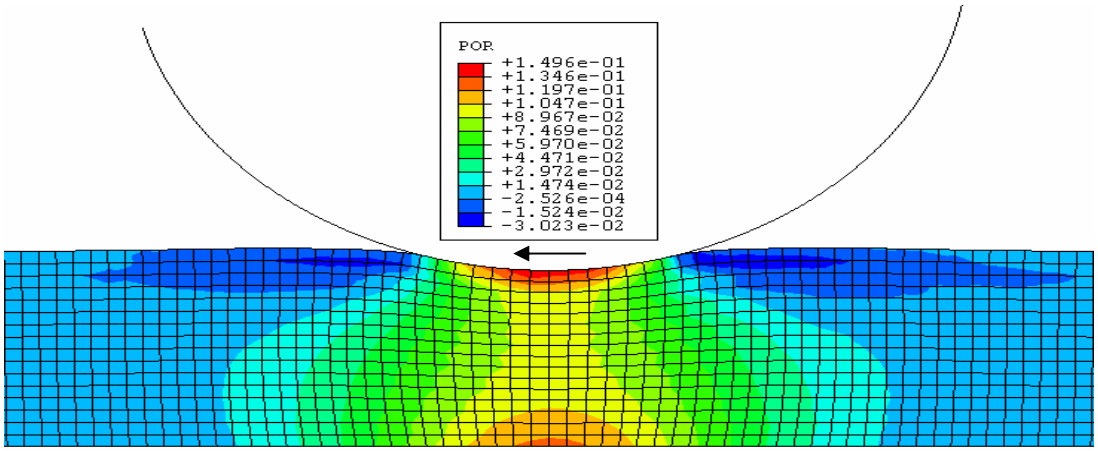

Figure 4-11 Pore pressure (MPa) distribution after indenter reached its mean position after 18 seconds of sliding and moving towards left (load = 0.5 N/mm)

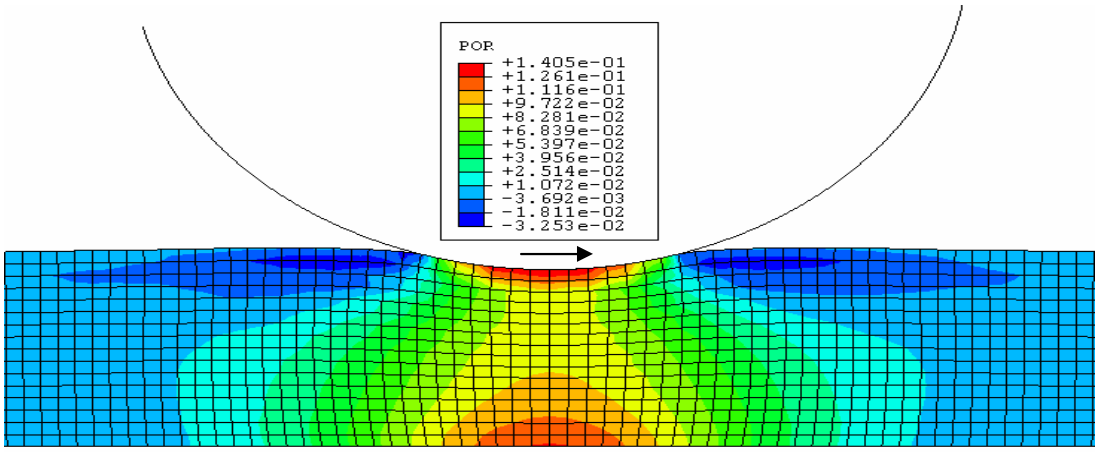

Figure 4-12 Pore pressure (MPa) distribution after indenter reached its mean position after 24 seconds of sliding and moving towards right (load = 0.5 N/mm)

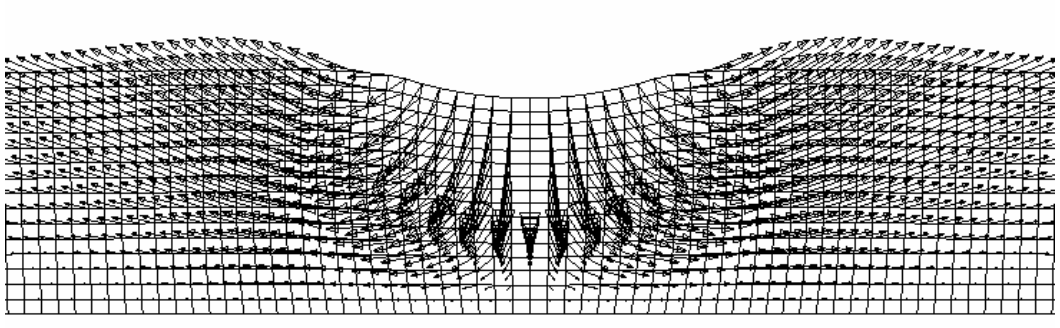

Figure 4-13 Direction of cartilage deformation after 2 seconds of ramp loading (load = 0.5 N/mm)

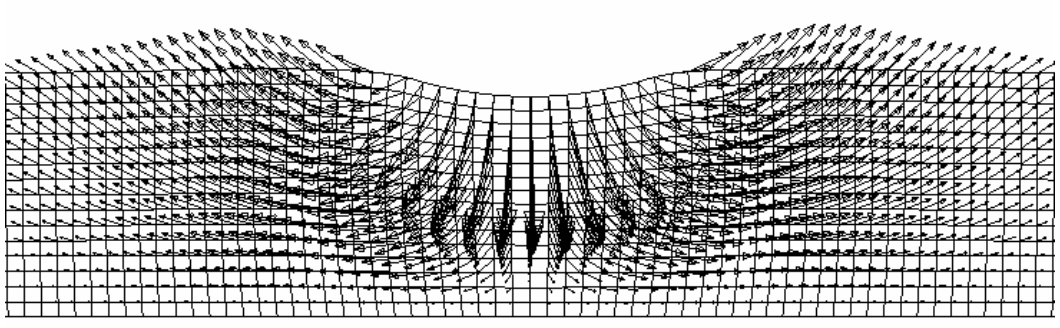

Figure 4-14 Direction of cartilage deformation after indenter reached its mean position after 18 seconds of sliding and moving towards left (load = 0.5 N/mm)

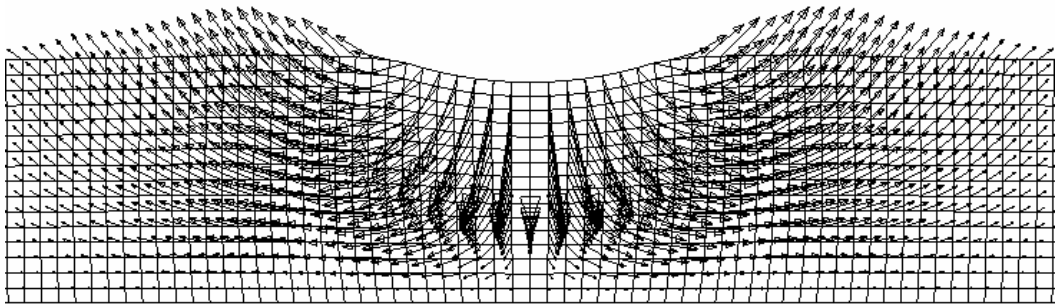

Figure 4-15 Direction of cartilage deformation after indenter reached its mean position after 24 seconds of sliding and moving towards right (load = 0.5 N/mm)

The upward deformation of the cartilage increased as the sliding continued (Figure 4-14 and Figure 4-15). This caused the pore pressure at the majority of cartilage surface to be negative causing fluid imbibition into the cartilage (Figure 4-6). In the contact zone it always remained positive (Figure 4-11 and Figure 4-12). The fluid continued to exude at the leading and trailing contact edges and imbibition took place over larger surface. The pore pressure on the surface was found to decrease slowly with time before attaining almost constant value (Figure 4-6, Figure 4-10, Figure 4-11 and Figure 4-12).

This fluid exudation at the contact edges was self generating lubrication mechanism observed by Mow and Lai (Mow and Lai, 1980). As Mow and Lai suggested the fluid exudation at the leading edge could be providing the lubricating fluid.

This was also indicative of boosted lubrication (Maroudas, 1967; Walker *et al.*, 1968) where the lubricating fluid flows inside the cartilage leaving behind hyaluronic acid – protein complex providing lubricating properties to the cartilage.

The pore pressure, however, did not remain constant at the initial value as the fluid imbibition rate possibly was low and the movement of the fluid from other parts of the cartilage to the surface was also low because of low permeability of the cartilage. This did not allow the cartilage to be fully saturated before the indenter came back during its reciprocating motion. Hence the pore pressure went on decreasing before it attained a steady value when imbibition and exudation rates possibly became equal. It was remarkable that this constant value of the pore pressure was significantly higher than zero.

The compressive axial stress showed the increasing trend before attaining the stable value thus depicting the stress shielding phenomenon under sliding conditions.

The steady interstitial fluid pressurization, in the current study, over a long time intervals confirmed that the low effective co-efficient of friction observed in cartilage was due to the interstitial fluid pressurization phenomenon.

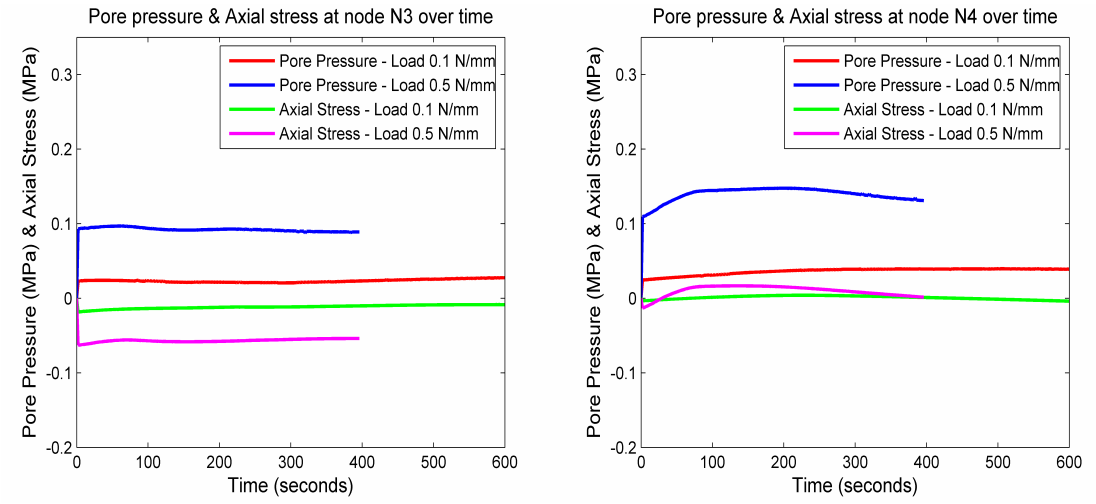

Figure 4-16 Pore pressure and axial Fluid pore pressure and solid compressive axial stress over time at nodes N3 (in mid-zone) and N4 (in deep zone)

In the mid zone, both the pore pressure and axial stress remained more or less constant at the values attained soon after loading (Figure 4-16). The initial pore pressure in the mid zone was found to be lesser than that at the STZ and the initial axial pressure at mid zone was higher than the corresponding value at STZ. This was more clearly visible for the loading of 0.5N/mm.

The fluid flow directions in Figure 4-7, Figure 4-8 and Figure 4-9 clearly showed the fluid flow pattern inside the cartilage. As the indenter comes over a region, the fluid was pushed inside towards the mid zone. At the same time, the fluid from the deep zone was found to rise up. Both these flows were found to diminish from the centre of indentation. When the indenter travelled away from this zone the fluid in the mid zone flowed away from this zone and hence the mid zone in this area (node N3) comparatively showed stable values of both pore pressure and axial stress even over large time intervals.

In the deep zone the pore pressure was found to increase in the initial stages of sliding for up to around 200 seconds for the loading of 0.5N/mm before it started decreasing (Figure 4-16). It could not be verified whether it attained the stable value or not. In case of 0.1N/mm load, after this initial increase in the pore pressure it was found to attain the steady value without decreasing (Figure 4-16). The bottom surface of the cartilage was sealed and no fluid was allowed to flow through it. As the indenter moved away from the contact region, the fluid in the deep zone under the new contact region seemed to flow towards the mid zone and surrounding deep zones. This could be the reason for the increase in the pore pressure in the deep zone. The similar observation was not made at the surface zone as some of the fluid was always lost in spite of imbibition. This very small but continued fluid loss did not allow the fluid pressure to increase or remain constant at the surface in the initial stages of sliding. There was a clear shift in the maximum pore pressure zone from STZ to the deep zone (Figure 4-10, Figure 4-11 and Figure 4-12).

The compressive axial stress during this period decreased and there was a brief transition to tensile stress which was seen for both the loading conditions. This could be the reason for the vertical fissures observed in OA in the deep zone. This needs to be investigated further as it could be a numerical error.

This study was not complete and hence needs to be investigated further, especially over a very long time intervals and with a very stable formulation. The surface pore pressure curve though showed stable values, a lot of fluctuations were seen especially in the initial stages. The same is left for future studies.

Chapter 5 Overall Discussion and Conclusions

Biphasic poroelastic finite element models of articular cartilage were developed, validated and analysed in this study under different experimental and physiologically relevant configurations. The new contact detection algorithms with general applicability for indenter on cartilage and cartilage on cartilage configurations were also developed, validated, and applied. Soils consolidation procedure of ABAQUS FE software package (ABAQUS., 2005) version 6.5-5 was used throughout to model the biphasic cartilage.

The contact detection algorithm, making use of URDFIL and FLOW subroutines of ABAQUS, was an improvement over the one developed by Warner (Warner, 2000). Warner had used 8-node elements and his algorithms used the contact stress on the mid-side node to detect whether an element surface was in contact or not and accordingly changed the flow conditions either stopping or allowing the interstitial fluid flow from that element surface. The one presented in this study, though depended on the contact stresses, had a general applicability. It used the contact stress at a node to determine whether that node was in contact or not and changed the flow conditions accordingly only at that node and not for the entire element surface. This gave an advantage of using it for 4-node as well as for 8-node element axisymmetric and two-dimensional models. It could be used for 3-dimensional problems as well after some modifications, though it was not tested in the current study.

The decision to use 4-node or 8-node elements was taken based on the study conducted with 3 different axisymmetric models. First and third models had 4-node axisymmetric elements with latter model having half the node spacing than the former. The second model had 8-node elements but with the same node spacing as the third one. This study was carried out for cartilage under stress-relaxation.

It was found that the 8-node elements were not always the best type of elements to be used in contact simulations, especially because of the way the surface nodal forces were calculated by ABAQUS (ABAQUS., 2005). It was also found that without the added improvements, especially at a surface node on the vertical axis of symmetry, 8-node elements could not be used to accurately model the cartilage indentation. This model gave unrealistic results at this node for contact stresses, pore pressure, axial stress and radial stress, mostly, immediately after 2 seconds of ramp deformation. On the other hand, both 4-node element models showed realistic results

at this node without any changes being made to input files except the type of element. It was thus decided to use 4-node element mesh throughout this study.

Mesh sensitivity studies were carried out to find the mesh with acceptable level of accuracy in the results and at the same time to reduce the computational time. Three axisymmetric models with different mesh densities were used in this study, First model had 800 4-node elements, second had 3200 4-node elements and the third one had 12800 4-node elements. This study was carried out for cartilage under stress-relaxation.

The results from all the three mesh models were very close except in case of radial stresses. The least dense mesh gave higher values of compressive axial stress after 2 seconds of ramp deformation. Moreover, this mesh could not capture the contact zone as accurately as the other two denser meshes due to lesser number of surface nodes. It also showed a more negative pore pressure just outside the contact zone. The model with highest mesh density differed with the intermediate mesh density model mostly in radial stress values, distribution trend remaining the same. The other parameters were very close and hence it was decided to use the mesh with 3200 elements to reduce the computational time.

NLGEOM parameter in ABAQUS is used to model finite deformation (ABAQUS., 2005) which is observed in articular cartilage. The small study was conducted to analyze the effect of this parameter at different levels of deformation. The model with 3200 4-node axisymmetric elements was used with and without NLGEOM parameter. This study was also carried out for cartilage under stress-relaxation.

The significant changes in the values of contact pressures, pore pressures, axial stresses and radial stresses were observed approximately around and after 5% of deformation. There was no significant difference in contact and pore pressures after 1000 seconds of consolidation. The contact and pore pressures after 2 seconds of ramp deformation showed higher values with NLGEOM as the deformation increased. In case of axial and radial stresses the values with NLGEOM were lower after 2 seconds of ramp deformation and were higher after 1000 seconds of consolidation. It also meant that NLGEOM was able to model consolidation better. Thus NLGEOM was used for all the studies except for joint contact model with cartilage over cartilage which was used to validate the model and contact detection algorithm by comparing the results to those of Federico and colleagues (Federico *et al.*, 2004) which did not make use of this parameter.

The rigid spherical indenter on cartilage model and the contact detection algorithm for this configuration was validated using the problem studied by Warner

under three different surface flow conditions, viz. contact dependent, sealed and free flow. All these three different surface flow conditions were implemented by changing the FLOW subroutine and input files were not changed in any way. This study was carried out for cartilage under stress-relaxation.

The results showed a remarkable similarity with those of Warner except in case of pore pressure for free flow conditions after 2 seconds of ramp deformation. It was not clear exactly how free flow conditions were implemented by Warner, though it was mentioned that porous indenter was used (Warner *et al.*, 2001b). The pore pressure values presented in his study after 2 seconds of ramp deformation were very high with the peak value around 80 kPa at a node on the vertical axis of symmetry. Suh and Spilker (Suh and Spilker, 1994) had made an observation that the surface pore pressure would be zero with porous indenter for both slow as well as fast compression rates.

The stress shielding phenomenon of the cartilage was clearly seen as the consolidation proceeded. Initially the majority of the load was taken by the fluid which slowly shifted to the solid during consolidation. Thus during the initial stages fluid phase clearly shielded the solid from stresses and towards the end of the consolidation, solid phase took up the majority of the load.

The small differences in the absolute values of different parameters monitored in the current study and that by Warner were mainly because of differences in element type, mesh density and contact detection algorithm used in these studies. In the current study, the sealed and contact dependent flow conditions predicted similar results in the contact zone after 2 seconds of ramp deformation whereas in the study conducted by Warner a small difference could be seen. This difference could be attributed to the different contact detection algorithms used. In qualitative terms, the results, their trends and distribution agreed well with those of Warner. The findings observed with creep-deformation were similar to those of stress-relaxation studies.

These results clearly demonstrated that the proposed 4-node element axisymmetric model and the new contact detection algorithm could produce reliable results and demonstrate correctly the cartilage behaviour under stress-relaxation and creep-deformation. It also showed that though sealed condition could produce the same results as the contact dependent flow after 2 seconds of ramp deformation/loading, it could not do the same during transient phase of consolidation. The contact dependent flow conditions could give more realistic results not only immediately after deformation/loading but also during consolidation phase.

Axisymmetric joint contact mechanics model of cartilage over cartilage was validated against the results of Federico and colleagues (Federico *et al.*, 2004) who used 8-node axisymmetric elements. The radius of curvature of each cartilage attached to the bone was 400 mm. The model was symmetric about horizontal plane and hence one cartilage could be replaced by a frictionless plane (Ateshian *et al.*, 1994a). The upper cartilage was replaced by a frictionless plane and was modelled as a steel block with its lower edge touching the cartilage. This was necessary as the contact detection algorithm validated earlier could be used. The same trends as observed by Federico were seen here except that the pore pressure values were a little higher. This could be due the differences in the element types and contact detection algorithms used in these two studies, though the material data and the geometry were exactly the same.

The cartilage on cartilage configuration was then modelled, analyzed and results compared with plane on cartilage configuration. The second version of contact detection algorithm was used. This algorithm was specifically developed for two cartilages in contact and could take care of jump condition required at the cartilage-cartilage contact interface.

The absolute values of pore pressure were lower as compared to the configuration with plane on cartilage but were still higher compared with those of Federico. This difference was not seen in axial stresses. Both the pore pressure and axial stress trends were similar in all the models.

Theoretically, the results for plane on cartilage and cartilage on cartilage configurations should have been the same. The reason for lower pore pressure values in case of cartilage over cartilage configuration could be due to the combination of factors. Firstly, the pressure-overclosure surface behaviour for block over cartilage was formulated to be hard whereas for cartilage over cartilage it was exponentially soft due to numerical convergence and excessive overclosure problems. Even with the hard surface formulation for cartilage over cartilage which failed to converge after ramp loading, the overall ramp deformation of 30% did not translate into exact 15% deformation in each cartilage which should have been the case theoretically. Secondly, the formulation of slave and master surfaces in ABAQUS for the identical mesh and stiffness properties did not permit the nodes displacement to be exactly symmetrical in cartilage over cartilage configuration. The refinement of mesh also could not be of much help. The difference in the peak pore pressure between plane over cartilage and cartilage over cartilage was found to be around 3.3%.

The cartilage over cartilage model coupled with the contact detection algorithm for this configuration gave reasonable results.

The determination of mechanical properties is one of the important uses of FE models (Mow *et al.*, 1989; Kwan *et al.*, 1990). The indentation experiments using plane ended cylindrical indenter were conducted at the University (Katta *et al.*, 2006). The FE model was created for the same. FE model predictions were then compared to the experimental deformation results and important properties like aggregate modulus and permeability were derived.

A brief study was conducted of two sliding configurations; one with a rigid plate sliding over a cartilage fully covering it in its motion and the other with a rigid cylindrical indenter sliding over the cartilage. The contact detection algorithm for indenter over cartilage configuration was used in both these cases.

The configuration of the rigid plate sliding over the cartilage was found to be similar to the cartilage consolidation when that plate completely covered the cartilage throughout the duration of sliding. The contact was frictionless and hence no additional loads were applied as sliding began under the initially applied load. This effectively gave the same configuration as used in consolidation where the load was held constant without sliding and plate covering the entire cartilage surface. Both the consolidation curves of pore pressure were found to be exactly similar showing slight increase in the initial stages. This increase was found to be due to the fluid rushing towards the surface as was found by McCutchen (McCutchen, 1959; McCutchen, 1962) in his weeping lubrication mechanism.

In case of a rigid cylindrical indenter sliding over the cartilage, the remarkable property of cartilage to maintain interstitial fluid pressurization was seen. Interstitial fluid pressurization has been linked to the frictional characteristics of the cartilage (Forster *et al.*, 1995; Krishnan *et al.*, 2005). In these studies, the co-efficient of friction was found to decrease with the increasing fluid pressurization. The cartilage is also known to maintain its remarkable lubricating characteristics over a long time period (Mow and Huiskes, 2005).

This preliminary study clearly demonstrated that even after a long time of loading and sliding the pore pressure initially decreased and attained a constant value which was significantly higher than zero. This was possible as the fluid imbibition at the surface took place along with the exudation. In the initial stages of sliding some fluid was always lost probably due to the imbalance in the fluid imbibition and exudation rates. In the latter stages of sliding these rates probably became equal thus maintaining the fluid pressurization and providing the lubricating properties over a long range of time intervals. The increase in the pore pressure was not seen at the surface as was seen in the deep zone also because of continuous loss of fluid from the surface.

The small transition to tensile axial stress seen in the deep zone could be either due to numerical error or if it was not then it could potentially explain the deep zone vertical fissures observed in OA.

The self generating lubrication mechanism observed by Mow and Lai (Mow and Lai, 1980) was also seen here. Fluid was seen to be flowing downwards in the contact zone as the indenter moved over a region. Both at the leading and trailing edges of the contact zone, fluid was found to be exuding, fluid flow at the leading edge providing the lubricating fluid. The downward fluid flow at the cartilage surface in the contact zone also pointed to the boosted lubrication mechanism (Maroudas, 1967; Walker *et al.*, 1968).

This study was aimed at understanding the joint contact mechanics of articular cartilage through finite element modelling and having the basis for future studies. The results achieved in terms of new contact detection algorithm, model validations and some new analysis like indenter sliding over cartilage have put the basic foundation to build upon.

Chapter 6 Possibilities for the Future

The future possibilities can be broadly classified into two categories: improvements specific to the current work and extension of the current work. Both are discussed in the following sections.

6.1 Improvements specific to the current work

The joint contact mechanics model with cartilage over cartilage was not entirely accurate, especially when compared with an equivalent plane on cartilage model. Though the difference was too small and the reasons like soft surface formulation and slave/master surfaces formulation were pointed out for this difference, it still needs to be looked into further in order to gain enough confidence in using soft surface formulation as against the hard formulation.

The analysis of cylindrical indenter sliding over cartilage needs to be carried out over a longer time period. The tensile stresses observed in the deep zone need to be further investigated as it is potentially one of the deciding factors for the vertical fissures seen in OA.

The fluctuations seen in the pore pressure and axial stress curves for cylindrical indenter sliding over cartilage also need to be addressed. There are several unanswered questions which may be due to the numerical errors. Mesh distortion was also observed especially for higher loads. Hence more stable formulation is needed to increase the confidence level in the results.

6.2 Extension of the current work

The contact detection algorithm proposed here is yet to be tested for 3-dimesnional models. This will be useful in 3-dimensional indentation and sliding models.

The most of the models presented in this work used fixed permeability except in the model of cartilage over cartilage. The logical extension of the other models is to incorporate strain dependent permeability, non-homogeneity and material anisotropy into these models to make them more realistic.

The model with cartilage over cartilage did not use finite deformation parameter (NLGEOM) provided by ABAQUS in order to compare it with the results against which the model was validated. An attempt was made in this study to

incorporate NLGEOM but the analysis could not converge. This will be a good problem to look at in the future.

The cartilage over cartilage consolidation configuration also needs to be modelled using hard surface formulation not only to compare it with soft formulation but also to look into the problems of numerical errors encountered in using hard formulation in this study. Another option may be to try and use slideline elements available in ABAQUS as was done by van der Voet (van der Voet, 1992).

Hemiarthroplasty is one of the major remedies for the people with OA. The sliding problems discussed above were limited applications of FE in understanding artificial joints. The problem was also not treated in terms of joint replacements but exclusively from the model formulation point of view. More realistic geometries like those exist in artificial joints need to be modelled and analyzed. Moreover 3-dimensional models need to be studied in detail as they are physiologically more realistic.

The studies of varying or cyclic loading conditions were not carried out in sliding models. Moreover, the friction was not considered in any of the sliding models. These need to be analyzed in the future studies.

The models of cartilage sliding over cartilage though attempted were not successfully analyzed in this study mainly because of inappropriate formulations which failed to give acceptable pore pressure distribution over the cartilage surface. These need to be looked into in the future.

8-node elements were not used in this study. In cartilage sliding over cartilage or consolidation problems the effect of nodal forces calculations as mentioned earlier took the form of uneven contact stresses which was not observed with 4-node elements. It was thus decided to keep the uniformity throughout this study by using 4-node elements. Many researchers have been using 8-node element library provided by ABAQUS. Understanding the internal problem formulation in ABAQUS was out of scope of this study. Hence the new studies need to be conducted taking into consideration the mathematical problem formulation in ABAQUS.

References

ABAQUS. Version 6.5, in *Manuals.* 2005, ABAQUS, Inc.: Pawtucket, RI, USA.

Adeeb, S.M., Ahmed, E.Y.S., Matyas, J., Hart, D.A., Frank, C.B. and Shrive, N.G. Congruency effects on load bearing in diarthrodial joints. *Computer Methods in Biomechanics and Biomedical Engineering*, 2004. **7**(3): p. 147-157.

Anderson, D.D., Brown, T.D., Yang, K.H. and Radin, E.L. A dynamic finite-element analysis of impulsive loading of the extension-splinted rabbit knee. *Journal of Biomechanical Engineering-Transactions of the ASME*, 1990. **112**(2): p. 119-128.

Anderson, D.D., Brown, T.D. and Radin, E.L. Stress wave effects in a finite element analysis of an impulsively loaded articular joint. *Proceedings of the Institution of Mechanical Engineers. Part H-Journal of Engineering in Medicine.*, 1991. **205**(1): p. 27-34.

Appleyard, R.C., Ghosh, P. and Swain, M.V. Biomechanical, histological and immunohistological studies of patellar cartilage in an ovine model of osteoarthritis induced by lateral meniscectomy. *Osteoarthritis and Cartilage*, 1999. **7**: p. 281 - 294.

Armstrong, C.G. and Mow, V.C. Variations in the intrinsic mechanical properties of human articular cartilage with age, degeneration, and water content. *Journal of Bone and Joint Surgery-American Volume*, 1982. **64**(1): p. 88-94.

Ateshian, G.A., Soslowsky, L.J. and Mow, V.C. Quantitation of articular surface topography and cartilage thickness in knee joints using stereophotogrammetry. *Journal of Biomechanics*, 1991. **24**(8): p. 761-776.

Ateshian, G.A., Lai, W.M., Zhu, W.B. and Mow, V.C. An asymptotic solution for the contact of two biphasic cartilage layers. *Journal of Biomechanics*, 1994a. **27**(11): p. 1347 - 1360.

Ateshian, G.A., Kwak, S.D., Soslowsky, L.J. and Mow, V.C. A stereophotogrammetric method for determining in situ contact areas in diarthrodial

joints, and a comparison with other methods. *Journal of Biomechanics*, 1994b. **27**(1): p. 111-124.

Ateshian, G.A. and Wang, H. A theoretical solution for the frictionless rolling contact of cylindrical biphasic articular cartilage layers. *Journal of Biomechanics*, 1995. **28**(11): p. 1341 - 1355.

Ateshian, G.A. and Wang, H. Rolling resistance of articular cartilage due to interstitial fluid flow. *Proceedings of the Institution of Mechanical Engineers, Part H (Journal of Engineering in Medicine)*, 1997. **211**: p. 419 - 424.

Ateshian, G.A. A theoretical formulation for boundary friction in articular cartilage. *Journal of Biomechanical Engineering*, 1997. **119**(1): p. 81-86.

Ateshian, G.A., Wang, H.Q. and Lai, W.M. The role of interstitial fluid pressurization and surface porosities on the boundary friction of articular cartilage. *Journal of Tribology-Transactions of the ASME*, 1998. **120**(2): p. 241-248.

Ateshian, G.A., Soltz, M.A., Mauck, R.L., Basalo, I.M., Hung, C.T. and Lai, W.M. The role of osmotic pressure and tension-compression nonlinearity in the frictional response of articular cartilage. *Transport in Porous Media*, 2003. **50**(1-2): p. 5-33.

Balazs, E.A., Watson, D., Duff, I.F. and Roseman, S. Hyaluronic acid in synovial fluid .I. molecular parameters of hyaluronic acid in normal and arthritic human fluids. *Arthritis and Rheumatism*, 1967. **10**(4): p. 357-376.

Batra, R.C. Elements of continuum mechanics. 1st ed. AIAA Education Series, ed. Schetz, J.A. 2006, Chichester, West Sussex, U.K.: John Wiley & Sons, Ltd. Pages: 325.

Bell, C.J., Fisher, J., Ingham, E., Forsey, R., Thompson, J.I. and Stone, M.H. Tribology of therapeutic lubricants. In 48th Annual Meeting of the Orthopaedic Research Society. 2002. Dallas, Texas.

Bell, C.J., Ingham, E. and Fisher, J. Influence of hyaluronic acid on the time-dependent friction response of articular cartilage under different conditions. *Proceedings of Institution of Mechanical Engineers - Part H*, 2006. **220**: p. 23 - 31.

Belytschko, T., Kulak, R.F., Schultz, A.B. and Galante, J.O. Finite element stress analysis of an intervertebral disc. *Journal of Biomechanics*, 1974. **7**(3): p. 277-285.

Best, B.A., Guilak, F., Setton, L.A., Zhu, W., Saed-Nejad, F., Ratcliffe, A., Weidenbaum, M. and Mow, V.C. Compressive mechanical properties of the human anulus fibrosus and their relationship to biochemical composition. *Spine*, 1994. **19**(2): p. 212-221.

Biot, M.A. General theory of three-dimensional consolidation. *Journal of Applied Physics*, 1941. **12**: p. 155 - 164.

Brekelmans, W.A.M., Poort, H.W. and Slooff, T.J.J.H. A new method to analyse the mechanical behaviour of skeletal parts. *Acta Orthopaedica Scandinavica*, 1972. **43**: p. 301 - 317.

Brown, T.D. and Shaw, D.T. In vitro contact stress distributions in the natural human hip. *Journal of Biomechanics*, 1983. **16**(6): p. 373 - 384.

Brown, T.D. and DiGioia, A.M., III. A contact-coupled finite element analysis of the natural adult hip. *Journal of Biomechanics*, 1984. **17**(6): p. 437 - 448.

Brown, T.D., Radin, E.L., Martin, R.B. and Burr, D.B. Finite-element studies of some juxtarticular stress changes due to localized subchondral stiffening. *Journal of Biomechanics*, 1984. **17**(1): p. 11-&.

Caravia, L., Dowson, D., Fisher, J., Corkhill, P.H. and Tighe, B.J. A comparison of friction in hydrogel and polyurethane materials for cushion-form joints. *Journal of Materials Science: Materials in Medicine*, 1993. **4**(5): p. 515-520.

Carter, D.R., Rapperport, D.J., Fyhrie, D.P. and Schurman, D.J. Relation of coxarthrosis to stresses and morphogenesis - a finite-element analysis. *Acta Orthopaedica Scandinavica*, 1987. **58**(6): p. 611-619.

Carter, D.R., Beaupre, G.S., Wong, M., Smith, R.L., Andriacchi, T.P. and Schurman, D.J. The mechanobiology of articular cartilage development and degeneration. *Clinical Orthopaedics and Related Research*, 2004. **427S**: p. S69 - S77.

Chand, R., Haug, E. and Rim, K. Stresses in the human knee joint. *Journal of Biomechanics*, 1976. **9**(6): p. 417-420.

Charnley, J. The lubrication of animal joints. In Symposium on Biomechanics. 1959. London: Institution of Mechanical Engineers.

Charnley, J. The lubrication of animal joints in relation to surgical reconstruction by arthroplasty. *Annals of the Rheumatic Diseases*, 1960. **19**: p. 10-19.

Chen, X., Chen, Y. and Hisada, T. Development of a finite element procedure of contact analysis for articular cartilage with large deformation based on the biphasic theory. *JSME International Journal Series C-Mechanical Systems Machine Elements and Manufacturing*, 2005. **48**(4): p. 537-546.

Chen, Y.A., Chen, X.A. and Hisada, T. Non-linear finite element analysis of mechanical electrochemical phenomena in hydrated soft tissues based on triphasic theory. *International Journal for Numerical Methods in Engineering*, 2006. **65**(2): p. 147-173.

Clift, S.E. Finite-element analysis in cartilage biomechanics. *Journal of Biomedical Engineering*, 1992. **14**(3): p. 217-221.

Cohen, B., Lai, W.M. and Mow, V.C. A transversely isotropic biphasic model for unconfined compression of growth plate and chondroepiphysis. *Journal of Biomechanical Engineering-Transactions of the ASME*, 1998. **120**(4): p. 491-496.

Crowninshield, R.D., Johnston, R.C., Andrews, J.G. and Brand, R.A. A biomechanical investigation of the human hip. *Journal of Biomechanics*, 1978. **11**(1-2): p. 75-77.

Cruess, R., Kwok, D., Duc, P., Lecavalier, M. and Dang, G. The response of articular cartilage to weight-bearing against metal. A study of hemiarthroplasty of the hip in the dog. *The Journal of Bone & Joint Surgery (Br)*, 1984. **66-B**(4): p. 592-597.

Czichos, H. Tribology. Tribology Series. Vol. 1. 1978, Amsterdam: Elsevier Scientific Publishing Company. Pages: 400.

Dalldorf, P.G., Banas, M.P., Hicks, D.G. and Pellegrini, V.D. Rate of degeneration of human acetabular cartilage after hemiarthroplasty. *Journal of Bone and Joint Surgery-American Volume*, 1995. **77A**(6): p. 877-882.

Davis, W.H., Lee, S.L. and Sokoloff, L. Proposed model of boundary lubrication by synovial-fluid - structuring of boundary water. *Journal of Biomechanical Engineering-Transactions of the Asme*, 1979. **101**(3): p. 185-192.

Dintenfass, L. Lubrication in synovial joints. *Nature*, 1963a. **197**(486): p. 496-497.

Dintenfass, L. Lubrication in synovial joints - a theoretical analysis - a rheological approach to the problems of joint movements and joint lubrication. *Journal of Bone and Joint Surgery-American Volume*, 1963b. **45**(6): p. 1241-1256.

Donzelli, P.S. and Spilker, R.L. A contact finite element formulation for biological soft hydrated tissues. *Computer Methods in Applied Mechanics and Engineering*, 1998. **153**: p. 63-79.

Donzelli, P.S., Spilker, R.L., Ateshian, G.A. and Mow, V.C. Contact analysis of biphasic transversely isotropic cartilage layers and correlations with tissue failure. *Journal of Biomechanics*, 1999. **32**(10): p. 1037-1047.

Dowson, D. Basic tribology, in Introduction to the biomechanics of joints and joint replacement., Dowson, D. and Wright, V., Editors. 1981, Mechanical Engineering Publications Ltd.: London. p. 49 - 60.

Dowson, D. and Jin, Z.-M. Micro-elastohydrodynamic lubrication of synovial joints. In Biomechanics of Osteoarthrosis. 1986 Annual Conference on Growing Points on the Biomechanics of Human Joints, Jan. 1986. Engineering in Medicine. 1986. Leeds, UK.

Eberhardt, A.W., Keer, L.M., Lewis, J.L. and Vithoontien, V. An analytical model of joint contact. *Journal of Biomechanical Engineering-Transactions of the ASME*, 1990. **112**(4): p. 407-413.

Eberhardt, A.W., Lewis, J.L. and Keer, L.M. Contact of layered elastic spheres as a model of joint contact - effect of tangential load and friction. *Journal of Biomechanical Engineering-Transactions of the ASME*, 1991a. **113**(1): p. 107-108.

Eberhardt, A.W., Lewis, J.L. and Keer, L.M. Normal contact of elastic spheres with two elastic layers as a model of joint articulation. *Journal of Biomechanical Engineering*, 1991b. **113**(4): p. 410-417.

Ehlers, W. and Markert, B. A linear viscoelastic biphasic model for soft tissues based on the theory of porous media. *Journal of Biomechanical Engineering-Transactions of the Asme*, 2001. **123**(5): p. 418-424.

Elmore, S.M., Sokoloff, L., Norris, G. and Carmeci, P. Nature of "imperfect" elasticity of articular cartilage. *Journal of Applied Physiology*, 1963. **18**(2): p. 393-396.

El'Sheikh, H.F., MacDonald, B.J. and Hashmi, M.S.J. Finite element simulation of the hip joint during stumbling: a comparison between static and dynamic loading. *Journal of Materials Processing Technology. Proceedings of the International Conference on the Advanced Materials Processing Technology, 2001.*, 2003. **143-144**: p. 249-255.

Federico, S., La Rosa, G., Herzog, W. and Wu, J.Z. Effect of fluid boundary conditions on joint contact mechanics and applications to the modeling of osteoarthritic joints. *Journal of Biomechanical Engineering*, 2004. **126**(2): p. 220-225.

Federico, S., Herzog, W. and Wu, J.Z. Erratum: ``Effect of Fluid Boundary Conditions on Joint Contact Mechanics and Applications to the Modelling of Osteoarthritic Joints," J. Biomech. Eng., 126(2), pp. 220--225. *Journal of Biomechanical Engineering*, 2005. **127**(1): p. 208-209.

Federico, S. Personal communication on "Effect of fluid boundary conditions on joint contact mechanics and applications to the modeling of osteoarthritic joints". Pawaskar, S.S., Editor. 2006: Leeds, UK.

Forster, H., Fisher, J., Dowson, D. and Wright, V. The effect of stationary loading on the friction and boundary lubrication of articular cartilage in the mixed lubrication regime. In Proceedings of the 21st Leeds/Lyon Symposium on Tribology, Lubrication and Lubricants. 1995: Elsevier Science, Amsterdam.

Forster, H. and Fisher, J. The influence of loading time and lubricant on the friction of articular cartilage. *Proceedings of Institution of Mechanical Engineers. Part H - Journal of Engineering in Medicine*, 1996. **210**(2): p. 109-119.

Forster, H. and Fisher, J. The influence of continuous sliding and subsequent surface wear on the friction of articular cartilage. *Proceedings of Institution of Mechanical Engineers - Part H*, 1999. **213**: p. 329 - 345.

Frijns, A.J.H., Huyghe, J.M. and Janssen, J.D. A validation of the quadriphasic mixture theory for intervertebral disc tissue. *International Journal of Engineering Science*, 1997. **35**(15): p. 1419-1429.

Goldsmith, A.A.J., Hayes, A. and Clift, S.E. Modelling the response of biomaterials and soft, hydrated biological tissues using soils consolidation theory. In ABAQUS User's Conference. 1995. Paris, France.

Goldsmith, A.A.J., Hayes, A. and Clift, S.E. Application of finite elements to the stress analysis of articular cartilage. *Medical Engineering and Physics*, 1996. **18**(2): p. 89 - 98.

Graindorge, S., Ferrandez, W., Jin, Z., Ingham, E., Grant, C., Twigg, P. and Fisher, J. Biphasic surface amorphous layer lubrication of articular cartilage. *Medical Engineering & Physics*, 2005. **27**(10): p. 836-844.

Graindorge, S.L., Jin, Z.M., Fisher, J., Grant, C.A., Twigg, P., Mitchell, W. and Ingham, E. Biphasic surface layer lubrication of articular cartilage - a finite element study. In 49th Annual Meeting of the Orthopaedic Research Society. 2003. New Orleans, Louisiana.

Graindorge, S.L., Jin, Z., Fisher, J., Ferrandez, W., Twigg, P.C., Grant, C.A. and Ingham, E. Biphasic amorphours surface layer lubrication of articular cartilage under "dynamic" loading conditions. In 50th Annual Meeting of the Orthopaedic Research Society. 2004. San Francisco, California.

Guilak, F., Jones, W.R., Ting-Beall, H.P. and Lee, G.M. The deformation behavior and mechanical properties of chondrocytes in articular cartilage. *Osteoarthritis and Cartilage*, 1999. **7**: p. 59 - 70.

Hale, J.E., James Rudert, M. and Brown, T.D. Indentation assessment of biphasic mechanical property deficits in size-dependent osteochondral defect repair. *Journal of Biomechanics*, 1993. **26**(11): p. 1319-1325.

Hall, R.M. and Unsworth, A. Friction in hip prostheses. *Biomaterials*, 1997. **18**(15): p. 1017-1026.

Hayes, W.C. and Mockros, L.F. Viscoelastic properties of human articular cartilage. *Journal of Applied Physiology*, 1971. **31**(4): p. 562-568.

Hayes, W.C., Keer, L.M., Herrmann, G. and Mockros, L.F. A mathematical analysis for indentation tests of articular cartilage. *Journal of Biomechanics*, 1972. **5**(5): p. 541-551.

Hayes, W.C. and Bodine, A.J. Flow-independent viscoelastic properties of articular cartilage matrix. *Journal of Biomechanics*, 1978. **11**(8-9): p. 407-419.

Herzog, W., Diet, S., Suter, E., Mayzus, P., Leonard, T.R., Muller, C., Wu, J.Z. and Epstein, M. Material and functional properties of articular cartilage and patellofemoral contact mechanics in an experimental model of osteoarthritis. *Journal of Biomechanics*, 1998. **31**(12): p. 1137-1145.

Higginson, G.R., Litchfield, M.R. and Snaith, J. Load-displacement-time characteristics of articular cartilage. *International Journal of Mechanical Sciences*, 1976. **18**(9-10): p. 481-486.

Higginson, G.R. and Unsworth, A. The lubrication of natural joints., in Tribology of Natural and Artificial Joints, Dumbleton, J.H., Editor. 1981, Elsevier: Amsterdam. p. 47 - 72.

Hills, B.A. Oligolamellar lubrication of joints by surface-active phospholipid. *Journal of Rheumatology*, 1989. **16**(1): p. 82-91.

Hills, B.A. Boundary lubrication in vivo. *Proceedings of the Institution of Mechanical Engineers. Part H-Journal of Engineering in Medicine*, 2000. **214**(H1): p. 83-94.

Hills, B.A. and Crawford, R.W. Normal and prosthetic synovial joints are lubricated by surface-active phospholipid: a hypothesis. *The Journal of Arthroplasty*, 2003. **18**(4): p. 499-505.

Hirsch, C. and Frey, H.D. A contribution to the pathogenesis of chondromalacia of the patella; a physical, histologic and chemical study, by Carl Hirsch. Acta chirurgica Scandinavica (Supplementum). Vol. 83. 1944, Stockholm: Kungl. boktryckeriet, P. A. Norstedt & soner. Pages: 106.

Hodge, W.A., Fijan, R.S., Carlson, K.L., Burgess, R.G., Harris, W.H. and Mann, R.W. Contact pressures in the human hip joint measured in vivo. *Proceedings of the National Academy of Sciences of the United States of America*, 1986. **83**(9): p. 2879-2883.

Holmes, M.H., Lai, W.M. and Mow, V.C. Singular perturbation analysis of the nonlinear, flow-dependent compressive stress relaxation behavior of articular cartilage. *Journal of Biomechanical Engineering*, 1985. **107**(3): p. 206-218.

Holmes, M.H. A theoretical-analysis for determining the nonlinear hydraulic permeability of a soft-tissue from a permeation experiment. *Bulletin of Mathematical Biology*, 1985. **47**(5): p. 669-683.

Holmes, M.H. Finite deformation of soft-tissue - analysis of a mixture model in uniaxial compression. *Journal of Biomechanical Engineering-Transactions of the ASME*, 1986. **108**(4): p. 372-381.

Holmes, M.H. and Mow, V.C. The nonlinear characteristics of soft gels and hydrated connective tissues in ultrafiltration. *Journal of Biomechanics*, 1990. **23**(11): p. 1145-1156.

Hou, J.S., Holmes, M.H., Lai, W.M. and Mow, V.C. Boundary-conditions at the cartilage-synovial fluid interface for joint lubrication and theoretical verifications. *Journal of Biomechanical Engineering-Transactions of the ASME*, 1989. **111**(1): p. 78-87.

Huiskes, R. and Chao, E.Y.S. A survey of finite element analysis in orthopedic biomechanics: the 1st decade. *Journal of Biomechanics*, 1983. **16**(6): p. 385 - 409.

Huyghe, J.M. and Janssen, J.D. Quadriphasic mechanics of swelling incompressible porous media. *International Journal of Engineering Science*, 1997. **35**(8): p. 793-802.

Jin, Z.M., Dowson, D. and Fisher, J. Analysis of fluid film lubrication in artificial hip joint replacements with surfaces of high elastic modulus. *Proceedings of the Institution of Mechanical Engineers Part H-Journal of Engineering in Medicine*, 1997. **211**(3): p. 247-256.

Jin, Z.M., Pickard, J.E., Forster, H., Ingham, E. and Fisher, J. Frictional behaviour of bovine articular cartilage. *Biorheology*, 2000. **37**(1 - 2): p. 57 - 63.

Johnson, G.R., Dowson, D. and Wright, V. The elastic behaviour of articular cartilage under a sinusoidally varying compressive stress. *International Journal of Mechanical Sciences*, 1977. **19**(5): p. 301-308.

Katta, J., Pawaskar, S.S., Jin, Z., Ingham, E. and Fisher, J. Effect of load variation on the friction properties of articular cartilage. In 33rd Leeds-Lyon Symposium on Tribology. To be published in Proceedings of the Institution of Mechanical Engineers, Part J, Journal of Engineering Tribology. 2006. Leeds, U.K.: Professional Engineering Publishing **(under review)**.

Kelkar, R. and Ateshian, G.A. Contact creep response between a rigid impermeable cylinder and a biphasic cartilage layer using integral transforms. In 1995 Bioengineering Conference. 1995. New York: ASME.

Kempson, G.E., Freeman, M.A.R. and Swanson, S.A.V. The determination of a creep modulus for articular cartilage from indentation tests on the human femoral head. *Journal of Biomechanics*, 1971. **4**(4): p. 239-250.

Kerin, A.J., Wisnom, M.R. and Adams, M.A. The compressive strength of articular cartilage. *Proceedings of the Institution of Mechanical Engineers. Part H - Journal of Engineering in Medicine*, 1998. **212**(H4): p. 273-280.

Krishnan, R., Park, S., Eckstein, F. and Ateshian, G.A. Inhomogeneous cartilage properties enhance Superficial interstitial fluid support and frictional properties, but do not provide a homogeneous state of stress. *Transactions of the ASME. Journal of Biomechanical Engineering*, 2003. **125**(5): p. 569-77.

Krishnan, R., Mariner, E.N. and Ateshian, G.A. Effect of dynamic loading on the frictional response of bovine articular cartilage. *Journal of Biomechanics*, 2005. **38**: p. 1665 - 1673.

Kwan, M.K., Lai, W.M. and Mow, V.C. Fundamentals of fluid transport through cartilage in compression. *Annals of Biomedical Engineering*, 1984. **12**(6): p. 537-558.

Kwan, M.K., Lai, W.M. and Mow, V.C. A finite deformation theory for cartilage and other soft hydrated connective tissues - I. equilibrium results. *Journal of Biomechanics*, 1990. **23**(2): p. 145 - 155.

Lai, W.M. and Mow, V.C. Drag-induced compression of articular-cartilage during a permeation experiment. *Biorheology*, 1980. **17**(1-2): p. 111-123.

Lai, W.M., Mow, V.C. and Roth, V. Effects of non-linear strain-dependent permeability and rate of compression on the stress behavior of articular-cartilage. *Journal of Biomechanical Engineering-Transactions of the ASME*, 1981. **103**(2): p. 61-66.

Lai, W.M., Hou, J.S. and Mow, V.C. A triphasic theory for the swelling and deformation behaviours of articular cartilage. *Journal of Biomechanical Engineering*, 1991. **113**: p. 245-258.

Levanon, D. and Stein, H. The articular cartilage of the rabbit knee: a scanning electron microscopy study. *Cells and Materials*, 1991. **1**(3): p. 219 - 229.

Lewis, P.R. and McCutchen, C.W. Mechanism of animal joints: experimental evidence for weeping lubrication in mammalian joints., in *Nature*. 1959. p. 1285.

Li, G.A., DeFrate, L.E., Park, S.E., Gill, T.J. and Rubash, H.E. In vivo articular cartilage contact kinematics of the knee - an investigation using dual-orthogonal fluoroscopy and magnetic resonance image-based computer models. *American Journal of Sports Medicine*, 2005. **33**(1): p. 102-107.

Li, L.P., Soulhat, J., Buschmann, M.D. and Shirazi-Adl, A. Nonlinear analysis of cartilage in unconfined ramp compression using a fibril reinforced poroelastic model. *Clinical Biomechanics*, 1999. **14**(9): p. 673-682.

Li, L.P., Shirazi-Adl, A. and Buschmann, M.D. Alterations in mechanical behaviour of articular cartilage due to changes in depth varying material properties--a nonhomogeneous poroelastic model study. *Computer Methods in Biomechanics & Biomedical Engineering*, 2002. **5**(1): p. 45 - 52.

Li, L.P. and Herzog, W. The role of viscoelasticity of collagen fibers in articular cartilage: theory and numerical formulation. *Biorheology*, 2004. **41**(3-4): p. 181-194.

Linn, F.C. Lubrication of animal joints : II the mechanism. *Journal of Biomechanics*, 1968. **1**(3): p. 193-205.

Lipshitz, H., Etheredge, R., 3rd and Glimcher, M.J. In vitro wear of articular cartilage. *The Journal Of Bone And Joint Surgery. American Volume*, 1975. **57**(4): p. 527-534.

Lipshitz, H. and Glimcher, M.J. In vitro studies of the wear of articular cartilage II. Characteristics of the wear of articular cartilage when worn against stainless steel plates having characterized surfaces. *Wear*, 1979. **52**(2): p. 297-339.

Liu, Y., Kerdok, A.E. and Howe, R.D. A nonlinear finite element model of soft tissue indentation, in Proceedings of Medical Simulation. 2004. p. 67-76.

Loret, B. and Simoes, F.M.F. Articular cartilage with intra- and extrafibrillar waters: a chemo-mechanical model. *Mechanics of Materials*, 2004. **36**(5-6): p. 515-541.

Lozada, C.J. and Steigelfest, E. Osteoarthritis. in *eMedicine*, Varga, J., Talavera, F., Diamond, H.S., Mechaber, A.J. and Weinstein, A., Editors. http://www.emedicine.com/MED/topic1682.htm, Accessed on 13/07/2006, 2006, WebMD.

Macintosh, D.L. Hemiarthroplasty of the knee using a space occupying prosthesis for painful varus and valgus deformities. *Journal of Bone and Joint Surgery-American Volume*, 1958. **40**(6): p. 1431-1431.

Macirowski, T., Tepic, S. and Mann, R.W. Cartilage stresses in the human hip-joint. *Journal of Biomechanical Engineering-Transactions of the Asme*, 1994. **116**(1): p. 10 - 18.

Mak, A.F. The apparent viscoelastic behavior of articular-cartilage - the contributions from the intrinsic matrix viscoelasticity and interstitial fluid-flows. *Journal of Biomechanical Engineering-Transactions of the ASME*, 1986. **108**(2): p. 123-130.

Maroudas, A. Hyaluronic acid films. *Proceedings of Institution of Mechanical Engineers*, 1967. **181**: p. 122 - 124.

Maroudas, A. Physicochemical properties of cartilage in the light of ion exchange theory. *Biophysical Journal*, 1968. **8**(5): p. 575-95.

McCutchen, C.W. Mechanism of animal joints: sponge-hydrostatic and weeping bearings., in *Nature*. 1959. p. 1284 - 1285.

McCutchen, C.W. The frictional properties of animal joints. *Wear*, 1962. **5**(1): p. 1 - 17.

Ming, Z., Zheng, Y.P. and Mak, A.F.T. Estimating the effective young's modulus of soft tissues from indentation tests--nonlinear finite element analysis of effects of friction and large deformation. *Medical Engineering & Physics*, 1997. **19**(6): p. 512-517.

Mizrahi, J., Maroudas, A., Lanir, Y., Ziv, I. and Webber, T.J. The instantaneous deformation of cartilage - effects of collagen fiber orientation and osmotic-stress. *Biorheology*, 1986. **23**(4): p. 311-330.

Morrell, K.C., Hodge, W.A., Krebs, D.E. and Mann, R.W. Corroboration of in vivo cartilage pressures with implications for synovial joint tribology and osteoarthritis causation. *Proceedings of the National Academy of Sciences of the United States of America*, 2005. **102**(41): p. 14819-14824.

Mow, V.C., Lai, W.M. and Redler, I. Some surface characteristics of articular cartilage--I. a scanning electron microscopy study and a theoretical model for the dynamic interaction of synovial fluid and articular cartilage. *Journal of Biomechanics*, 1974. **7**(5): p. 449-456.

Mow, V.C. and Lai, W.M. The optical sliding contact analytical rheometer (OSCAR) for flow visualization at the articular surface. In 1979 Advances in

Bioengineering. Winter Annual Meeting of the American Society of Mechanical Engineers, 2-7 Dec. 1979. 1979. New York, NY, USA: ASME.

Mow, V.C., Kuei, S.C., Lai, W.M. and Armstrong, C.G. Biphasic creep and stress relaxation of articular cartilage in compression: theory and experiments. *Transactions of ASME, Journal of Biomechanical Engineering*, 1980. **102**: p. 73-84.

Mow, V.C. and Lai, W.M. Recent developments in synovial joint biomechanics. *SIAM Review*, 1980. **22**(3): p. 275 - 317.

Mow, V.C., Holmes, M.H. and Lai, W.M. Fluid transport and mechanical properties of articular cartilage: a review. *Journal of Biomechanics*, 1984. **17**(5): p. 377 - 394.

Mow, V.C., Gibbs, M.C., Lai, W.M., Zhu, W.B. and Athanasiou, K.A. Biphasic indentation of articular cartilage - II. a numerical algorithm and an experimental study. *Journal of Biomechanics*, 1989. **22**(8/9): p. 853 - 861.

Mow, V.C., Ratcliffe, A. and Poole, A.R. Cartilage and diarthrodial joints as paradigms for hierarchical materials and structures. (Review). *Biomaterials*, 1992. **13**(2): p. 67 - 97.

Mow, V.C. and Huiskes, R., eds. Basic Orthopaedic Biomechanics and Mechano-Biology. Third ed. 2005, Lippincott Williams & Wilkins: Philadelphia. Pages: 720.

Neer, C.S. Articular replacement for the humeral head. *Journal of Bone and Joint Surgery-American Volume*, 1955. **37**(2): p. 215-228.

Nordin, M. and Frankel, V.H. Basic biomechanics of the musculoskeletal system. 2nd ed. 1989, Philadelphia: Lippincott Williams & Wilkins. Pages: 323.

Oloyede, A. and Broom, N.D. Is classical consolidation theory applicable to articular cartilage deformation? *Clinical Biomechanics*, 1991. **6**(4): p. 206-212.

Olsen, S. and Oloyede, A. A finite element analysis methodology for representing the articular cartilage functional structure. *Computer Methods in Biomechanics & Biomedical Engineering*, 2002. **5**(6): p. 377 - 386.

Orford, C.R. and Gardner, D.L. Ultrastructural histochemistry of the surface lamina of normal articular cartilage. *The Histochemical Journal*, 1985. **17**(2): p. 223-233.

Owen, D.R.J. and Hinton, E. A simple guide to finite elements. 1st ed. 1980, Swansea, U.K.: Pineridge Press Limited. Pages: 136.

Park, S., Krishnan, R., Nicoll, S.B. and Ateshian, G.A. Cartilage interstitial fluid load support in unconfined compression. *Journal of Biomechnics*, 2003. **36**: p. 1785 - 1796.

Parsons, J.R. and Black, J. The viscoelastic shear behavior of normal rabbit articular cartilage. *Journal of Biomechanics*, 1977. **10**(1): p. 21-29.

Persson, B.N.J. Sliding friction. Second ed. 2000, Berlin: Springer-Verlag. Pages: 515.

Radin, E.L., Swann, D.A. and Weisser, P.A. Separation of a hyaluronate-free lubricating fraction from synovial fluid. *Nature*, 1970. **228**(5269): p. 377-&.

Rhee, D.K., Marcelino, J., Baker, M.A., Gong, Y.Q., Smits, P., Lefebvre, V., Jay, G.D., Stewart, M., Wang, H.W., Warman, M.L. and Carpten, J.D. The secreted glycoprotein lubricin protects cartilage surfaces and inhibits synovial cell overgrowth. *Journal of Clinical Investigation*, 2005. **115**(3): p. 622-631.

Roth, V. and Mow, V.C. Finite element analysis of contact problems for indentation of articular cartilage. In Advances in Bioengineering. 1977. New York: American Society of Mechanical Engineers.

Saikko, V. A simulator study of friction in total replacement hip joints. *Proceedings of Institution of Mechanical Engineers - Part H*, 1992. **206**(H1): p. 201 - 211.

Seller, P.C., Dowson, D. and Wright, V. The rheology of synovial fluid. *Rheologica Acta*, 1971. **10**(1): p. 2-7.

Setton, L.A., Zhu, W. and Mow, V.C. The biphasic poroviscoelastic behavior of articular cartilage: Role of the surface zone in governing the compressive behavior. *Journal of Biomechanics*, 1993. **26**(4-5): p. 581-592.

Setton, L.A., Elliott, D.M. and Mow, V.C. Altered mechanics of cartilage with osteoarthritis: human osteoarthritis and an experimental model of joint degeneration. *Osteoarthritis and Cartilage*, 1999. **7**: p. 2 - 14.

Shirazi, R. and Shirazi-Adl, A. Analysis of articular cartilage as a composite using non-linear membrane elements for collagen fibrils. *Medical Engineering and Physics*, 2005. **27**(10): p. 827-835.

Simon, W.H. Scale effects in animal joints. I. articular cartilage thickness and compressive stress. *Arthritis & Rheumatism*, 1970. **13**(3): p. 244-255.

Sokoloff, L. Elasticity of aging cartilage., in Federation proceedings. 1966, Federation Of American Societies For Experimental Biology: United States. p. 1089 - 1095.

Soltz, M.A. and Ateshian, G.A. Experimental verification and theoretical prediction of cartilage interstitial fluid pressurization at an impermeable contact interface in confined compression. *Journal of Biomechanics*, 1998. **31**(10): p. 927-934.

Soreide, O., Skjaerven, R. and Alho, A. The risk of acetabular protrusion following prosthetic replacement of the femoral-head. *Acta Orthopaedica Scandinavica*, 1982. **53**(5): p. 791-794.

Spilker, R.L., Suh, J.-K. and Mow, V.C. A finite element formulation of the nonlinear biphasic model for articular cartilage and hydrated soft tissues including strain-dependent permeability. In Computational Methods in Bioengineering, BED. 1988. New York: ASME.

Spilker, R.L., Suh, J.K. and Mow, V.C. Effects of friction on the unconfined compressive response of articular-cartilage - a finite-element analysis. *Journal of Biomechanical Engineering-Transactions of the ASME*, 1990. **112**(2): p. 138-146.

Spilker, R.L., Suh, J.K. and Mow, V.C. A finite-element analysis of the indentation stress-relaxation response of linear biphasic articular-cartilage. *Journal of Biomechanical Engineering-Transactions of the ASME*, 1992a. **114**(2): p. 191-201.

Spilker, R.L., Dealmeida, E.S. and Donzelli, P.S. Finite-element methods for the biomechanics of soft hydrated tissues - nonlinear-analysis and adaptive-control of meshes. *Critical Reviews in Biomedical Engineering*, 1992b. **20**(3-4): p. 279-313.

Suh, J.K. and Spilker, R.L. Indentation analysis of biphasic articular-cartilage - nonlinear phenomena under finite deformation. *Journal of Biomechanical Engineering-Transactions of the ASME*, 1994. **116**(1): p. 1-9.

Suh, J.-K., Spilker, R.L. and Mow, V.C. Finite element analysis of the indentation problem for articular cartilage using a finite deformation biphasic model. *Advances in Bioengineering, American Society of Mechanical Engineers, Bioengineering Division (Publication) BED*, 1990. **17**: p. 215 - 218.

Suh, J.-K., Spilker, R.L. and Holmes, M.H. A penalty finite element analysis for nonlinear mechanics of biphasic hydrated soft tissue under large deformation. *International Journal for Numerical Methods in Engineering*, 1991. **32**(7): p. 1411-1439.

Sun, D.D., Guo, X.E., Likhitpanichkul, M., Lai, W.M. and Mow, V.C. The influence of the fixed negative charges on mechanical and electrical behaviors of articular cartilage under unconfined compression. *Journal of Biomechanical Engineering-Transactions of the ASME*, 2004. **126**(1): p. 6-16.

Sun, D.N., Gu, W.Y., Guo, X.E., Lai, W.M. and Mow, V.C. A mixed finite element formulation of triphasic mechano-electrochemical theory for charged, hydrated biological soft tissues. *International Journal for Numerical Methods in Engineering*, 1999. **45**(10): p. 1375-1402.

Swann, D.A. and Radin, E.L. The molecular basis of articular lubrication. I. purification and properties of a lubricating fraction from bovine synovial fluid. *Journal of Biological Chemistry*, 1972. **247**(24): p. 8069-8073.

Swann, D.A., Radin, E.L. and Hendren, R.B. Lubrication of articular-cartilage by synovial-fluid glycoproteins. *Arthritis and Rheumatism*, 1979. **22**(6): p. 665-666.

Swann, D.A., Hendren, R.B., Radin, E.L., Sotman, S.L. and Duda, E.A. The lubricating activity of synovial fluid glycoproteins. *Arthritis and Rheumatism*, 1981a. **24**(1): p. 22-30.

Swann, D.A., Slayter, H.S. and Silver, F.H. The molecular structure of lubricating glycoprotein-I, the boundary lubricant for articular cartilage. *Journal of Biological Chemistry*, 1981b. **256**(11): p. 5921-5925.

Swann, D.A., Silver, F.H., Slayter, H.S., Stafford, W. and Shore, E. The molecular-structure and lubricating activity of lubricin isolated from bovine and human synovial-fluids. *Biochemical Journal*, 1985. **225**(1): p. 195-201.

Tortora, G.J. and Grabowski, S.R. Introduction to the human body: the essentials of anatomy and physiology. Sixth ed. 2004, USA: John Wiley & Sons, Inc. Pages: 619.

van der Meulen, M.C.H., Beaupré, G.S., Smith, R.L., Giddings, V.L., Allen, W.A., Athanasiou, K.A., Zhu, C.F., Song, Y., Mandell, J.A., Poser, R.D. and Goodman, S.B. Factors influencing changes in articular cartilage following hemiarthroplasty in sheep. *Journal of Orthopaedic Research*, 2002. **20**(4): p. 669-675.

van der Voet, A.F. Finite element modelling of load transfer through articular cartilage In *Civil Engineering*. PhD Thesis. 1992, University of Calgary: Canada. p. 267

van der Voet, A.F., Shrive, N.G. and S., S.N. Numerical modelling of articular cartilage in synovial joints: poroelasticity and boundary conditions., in Recent Advances in Computer Methods in Biomechanics and Biomedical Engineering. 1992, Books and Journals International Ltd.: Swansea. p. 200 - 209.

Walker, P.S., Dowson, D., Longfield, M.D. and Wright, V. "Boosted lubrication" in synovial joints by fluid entrapment and enrichment. *Annals of the Rheumatic Diseases*, 1968. **27**(6): p. 512-520.

Walker, P.S., Yildirim, G., Sussman-Fort, J. and Klein, G.R. Relative positions of the contacts on the cartilage surfaces of the knee joint. *The Knee*, 2006. **In Press, Corrected Proof**.

Wan, L., de Asla, R.J., Rubash, H.E. and Li, G. Determination of in-vivo articular cartilage contact areas of human talocrural joint under weightbearing conditions. *Osteoarthritis and Cartilage*, 2006. **In Press, Corrected Proof**.

Wang, H. and Ateshian, G.A. The normal stress effect and equilibrium friction coefficient of articular cartilage under steady friction shear. *Journal of Biomechanics*, 1997. **30**(8): p. 771-776.

Warner, M.D. Finite element biphasic modelling of articular cartilage: an investigation into crystal induced damage. PhD Thesis. 2000, University of Bath. p. 177

Warner, M.D., Taylor, W.R. and Clift, S.E. Finite element biphasic indentation of cartilage: a comparison of experimental indenter and physiological contact geometries. *Proceedings of Institution of Mechanical Engineers - Part H*, 2001a. **215**: p. 487-496.

Warner, M.D., Taylor, W.R. and Clift, S.E. A method for determining contact between a non-porous surface and articular cartilage in a biphasic FE model. In Computer Methods in Biomechanics and Biomedical Engineering – 3. 2001b. Lisbon, Portugal: Gordon and Breach Science Publishers, Amsterdam.

Wayne, J.S., Woo, S.L.Y. and Kwan, M.K. Application of the u-p finite-element method to the study of articular-cartilage. *Journal of Biomechanical Engineering-Transactions of the ASME*, 1991. **113**(4): p. 397-403.

Wayne, J.S. Load partitioning influences the mechanical response of articular cartilage. *Annals of Biomedical Engineering*, 1995. **23**(1): p. 40-47.

Wilson, W., van Donkelaar, C.C., van Rietbergen, B., Ito, K. and Huiskes, R. Stresses in the local collagen network of articular cartilage: a poroviscoelastic fibril-reinforced finite element study. *Journal of Biomechanics*, 2004. **37**: p. 357 - 366.

Wilson, W., van Donkelaar, C.C. and Huyghe, J.M. A comparison between mechano-electrochemical and biphasic swelling theories for soft hydrated tissues. *Journal of Biomechanical Engineering-Transactions of the ASME*, 2005. **127**(1): p. 158-165.

Wu, J.Z., Herzog, W. and Epstein, M. Evaluation of the finite element software ABAQUS for biomechanical modelling of biphasic tissues. *Journal of Biomechanics*, 1998. **31**: p. 165-169.

Wu, J.Z. and Herzog, W. Finite element simulation of location- and time-dependent mechanical behavior of chondrocytes in unconfined compression tests. *Annals of Biomedical Engineering*, 2000. **28**(3): p. 318-330.

Yang, T. A three-dimensional biphasic finite element formulation for hydrated soft tissue. In *Mechanical Engineering*. PhD Thesis. 2003, Rensselaer Polytechnic Institute. p. 181

Appendix A Axisymmetric model of stress relaxation of articular cartilage with a rigid spherical indenter

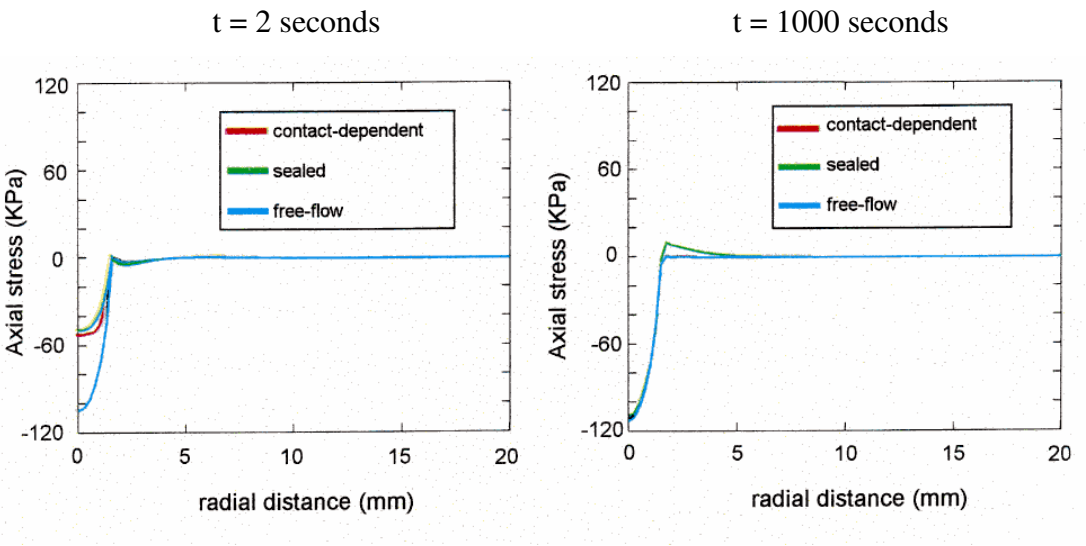

Figure A-1 Axial stress distribution at the cartilage surface at different times (Warner, 2000)

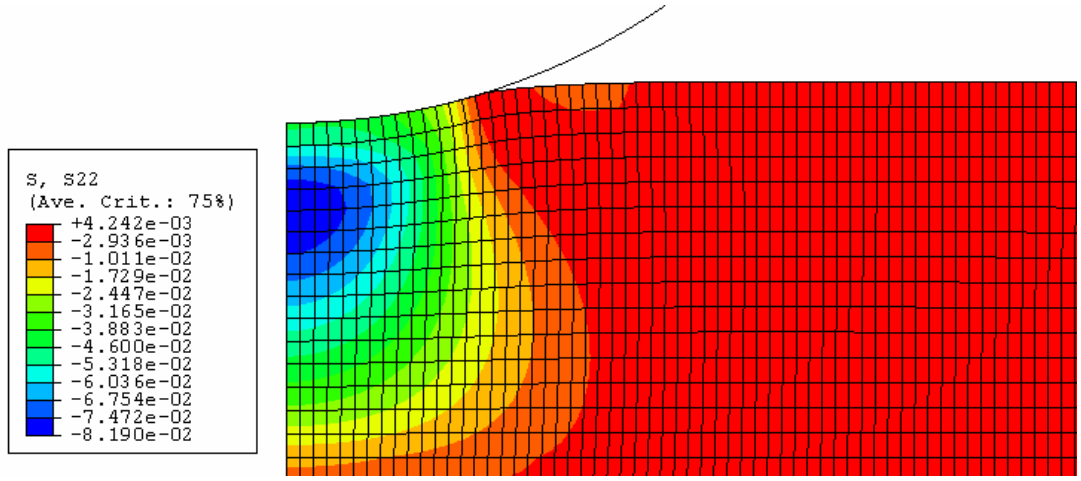

Figure A-2 Axial stress (MPa) contour plot for contact dependent flow after 2 seconds

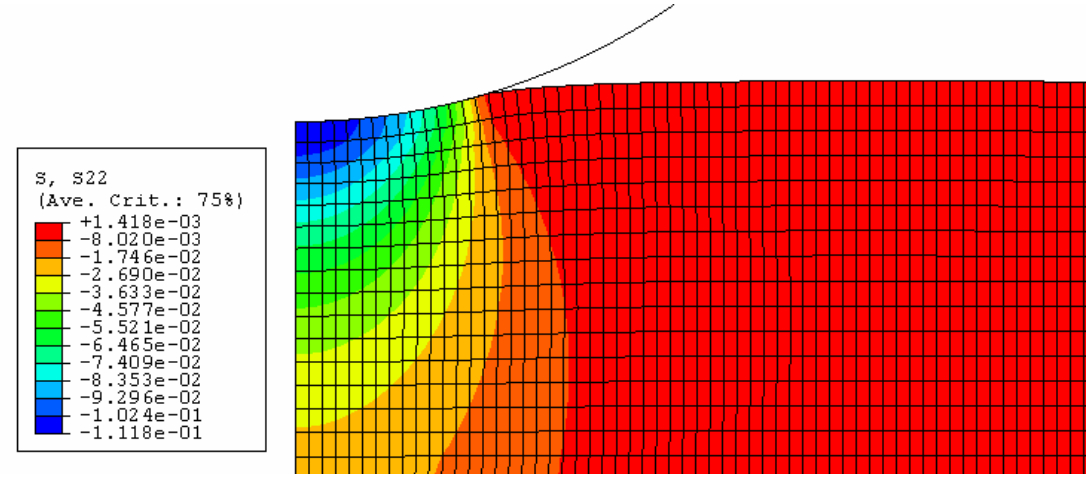

Figure A-3 Axial stress (MPa) contour plot for contact dependent flow after 1000 seconds

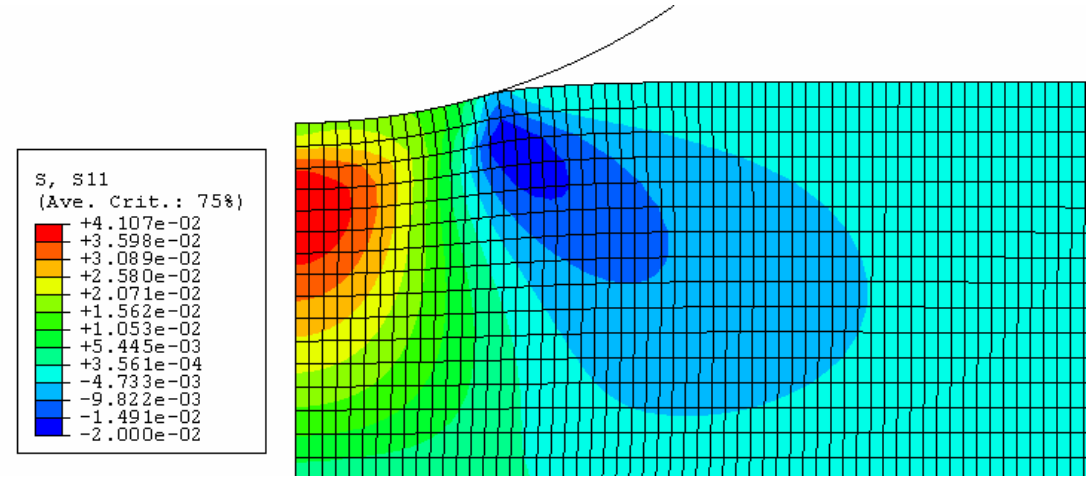

Figure A-4 Radial stress (MPa) contour plot for contact dependent flow after 2 seconds

Appendix B Axisymmetric model of creep deformation of articular cartilage with a rigid spherical indenter

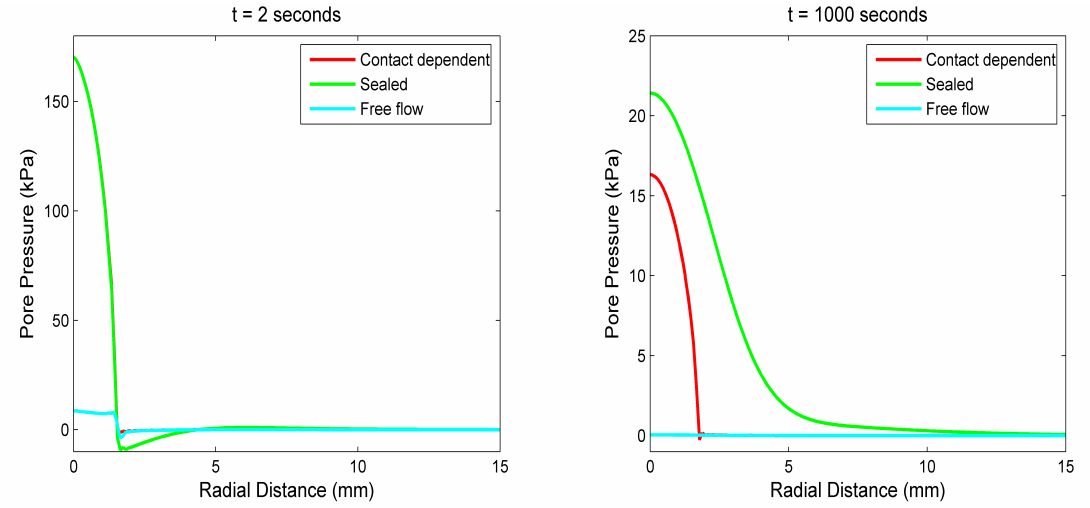

Figure B-1 Pore pressure distribution at the cartilage surface at different times

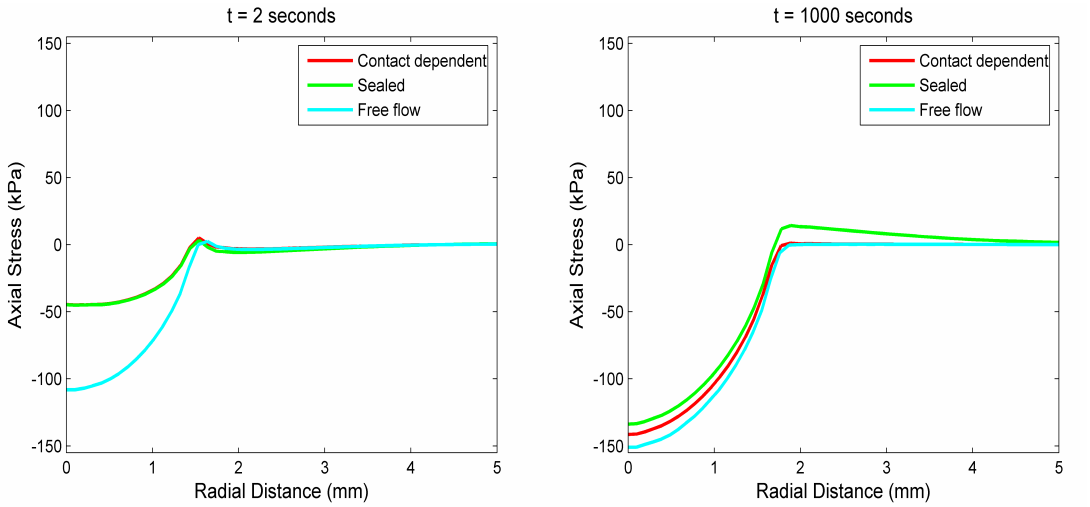

Figure B-2 Axial stress distribution at the cartilage surface at different times

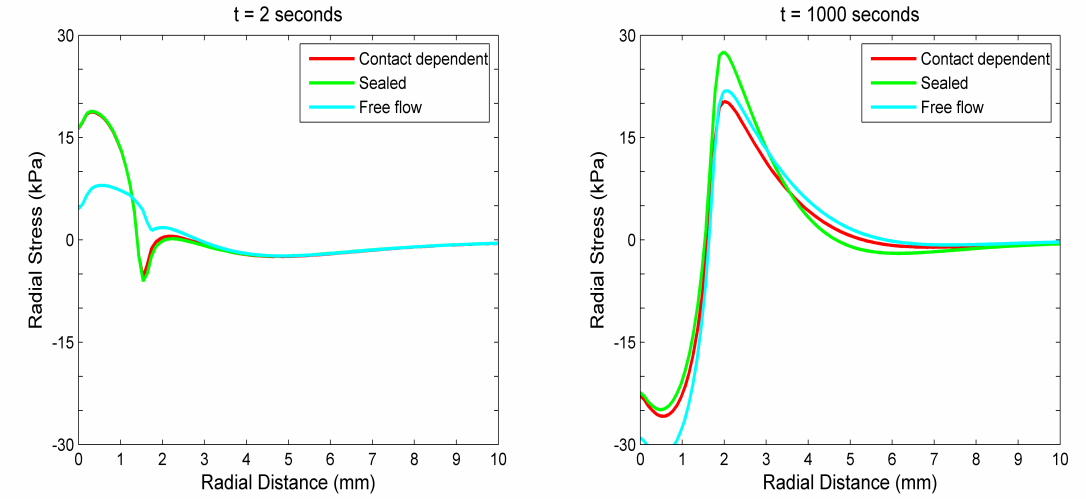

Figure B-3 Radial stress distribution at the cartilage surface at different times

Appendix C Sample Input File

```
**TYPICAL ABAQUS INPUT FILE
*FILE FORMAT, ZERO INCREMENT, ASCII
*Restart, write, FREQUENCY=1
**********************************************************
**Include geometry
*INCLUDE, INPUT=D:\ABAQUS\Thesis\four_node_RIGID_IND.geom
**********************************************************
**Material Definitions
*Solid Section, elset=E_CART, material=MTL_BIPHASIC
*Solid Section, elset=E_IND, material=MTL_STEEL
**********************************************************
** MATERIALS
*Material, name=MTL_BIPHASIC
*Elastic
 0.54, 0.08
*Permeability, specific=1.
 0.004,4.
*Material, name=MTL_STEEL
*Elastic
110000., 0.33
**********************************************************
*INITIAL CONDITIONS, TYPE=RATIO
N_CART, 4.0
**********************************************************
** SURFACES
*Surface, type=ELEMENT, name=S_CART, TRIM=YES
E_TOP, S3
```

```
*Surface, type=ELEMENT, name=S_AXIS, TRIM=YES
E_AXIS, S4
*Surface, type=ELEMENT, name=S_BOT, TRIM=YES
E_BOT, S1
*Rigid Body, ref node=N_IND, analytical surface=S_IND
**********************************************************
** BOUNDARY CONDITIONS
*Boundary
N_BOT, 1, 1
N_BOT, 2, 2
N_AXIS, 1, 1
N_CART_SIDE, 8, 8
N_IND, 1, 1
N_IND, 6, 6
**********************************************************
** INTERACTION PROPERTIES
*Surface Interaction, name=YFRIC
*Friction
 0.02,
** INTERACTIONS
*Contact Pair, interaction= YFRIC, adjust=1.0e-6, extension zone=0.1
S_CART, S_IND
**********************************************************
** STEP: DEFORMATION
*Step, name=DEFORMATION, inc=10000, amplitude=RAMP, nlgeom=YES
*Soils, consolidation, end=PERIOD
0.01, 2.
*Boundary
N_IND, 2, 2, -0.3
```

*SFLOW

S_CART, QNU

*SFLOW

S_AXIS, QD, 0.0

*SFLOW

S_BOT, QD, 0.0

** OUTPUT REQUESTS

** FIELD OUTPUT: F-Output-1

*Output, field, FREQUENCY=1

*Node Output

POR, U, CF

*Element Output

FLUVR, FLVEL, S

*Contact Output

CDISP, CSTRESS

*CONTACT FILE, SLAVE=S_CART, FREQUENCY=1, NSET=N_TOP

CSTRESS

*NODE FILE, FREQUENCY=1, NSET=N_TOP

POR, COORD

*End Step

****

** STEP: CONSOLIDATION

*Step, name=CONSOLIDATION, inc=10000, amplitude=RAMP, nlgeom=YES

*Soils, consolidation, end=PERIOD, utol=0.6, creep=none

0.01, 1000., 1e-15, 10.,

- - - -

Same as used for step DEFORMATION

*End Step

****

Appendix D Sample FORTRAN User Subroutines

Please note that in the following sample program the fixed format is not adhered to and it only shows the pseudo-code. These subroutines can be used for 4-node as well as 8-node element models in two dimensional and axisymmetric analyses. Presently, it allows only 500 surface elements which are more than sufficient for the type of analysis discussed in this thesis. However, it can be easily extended to any number of elements. To use these subroutines, the top cartilage surface has to be named as S_CART, top cartilage surface nodes set has to be named as N_TOP and if second surface is involved the corresponding names should be suffixed by _2. The outputs CSTRESS, POR and COORD for N_TOP and N_TOP_2 have to be written to the result file .fil in the ASCII format and not binary.

```
SUBROUTINE URDFIL(LSTOP,LOVRWRT,KSTEP,KINC,DTIME,TIME)
      INCLUDE 'ABA_PARAM.INC'
      DIMENSION ARRAY(513), JRRAY(NPRECD,513),TIME(2)
      EQUIVALENCE (ARRAY(1),JRRAY(1,1))
C DECLARATIONS
C Structure to hold element data which can be accessed by URDFIL and FLOW
      TYPE ELE_DATA
       SEQUENCE
       DOUBLE PRECISION :: NODE_COORD(9)
       DOUBLE PRECISION :: OPP_NODE_COORD(9)
       DOUBLE PRECISION :: IPT_COORD(9)
       DOUBLE PRECISION :: OPP_IPT_COORD(9)
       DOUBLE PRECISION :: POR(3)
       DOUBLE PRECISION :: OPP_POR(3)
       INTEGER :: ELE_NUM
       INTEGER :: OPP_ELE_NUM
       INTEGER :: NODE_NUM(3)
       INTEGER :: OPP_NODE_NUM(3)
```

```
      INTEGER :: IPT_NUM(3)
      INTEGER :: OPP_IPT_NUM(3)
      INTEGER :: IS_CONT(3)
      INTEGER :: OPP_IS_CONT(3)
    END TYPE ELE_DATA

    TYPE (ELE_DATA) :: K_ELE_DETAILS(500)
    COMMON K_ELE_DETAILS
    PARAMETER (THRESHOLD_CSTRESS=1.0D-5)
************************************************************
C OTHER DECLARATIONS
    INTEGER :: NO_OF_NODES
    INTEGER :: NO_OF_ELEMENTS
    INTEGER :: NO_OF_DIM
    COMMON NO_OF_DIM, NO_OF_NODES, NO_OF_ELEMENTS
************************************************************
C INITIALIZATION
    LSTOP = 0
    LOVRWRT = 1
    LOP = 0
    NO_OF_NODES = 2
    NO_OF_ELEMENTS = 500
    NO_OF_DIM = 2
************************************************************
    DO K1=1,999999
      CALL DBFILE(LOP,ARRAY,JRCD)
      IF (JRCD .NE. 0) GO TO 110
        KEY=JRRAY(1,2)
************************************************************
```

```
      IF(KEY .EQ. 1501) THEN
** KEY 1501 contains surface definitions
**Capture surface name
      ELSE IF(KEY .EQ. 1502) THEN
**KEY 1502 contains surface facet information corresponding to KEY 1501
** Capture Element and Node numbers
      ELSE IF(KEY .EQ. 1911) THEN
**KEY 1911 contains data for Node/Element set
**Capture name for node set N_TOP
      ELSE IF(KEY .EQ. 108 .AND. SURFACE_N_SET .EQ. 'N_TOP') THEN
** KEY 108 contains pore pressure at each node corresponding to KEY 1911
      ELSE IF(KEY .EQ. 107 .AND. SURFACE_N_SET .EQ. 'N_TOP') THEN
** KEY 107 contains co-ordinates of each node
       ELSE IF(KEY .EQ. 1503) THEN
** KEY 1503 contains contact output request definition
**Captures node set name N_TOP
      ELSE IF(KEY .EQ. 1504 .AND. K_NODE_SET .EQ. 'N_TOP') THEN
** KEY 1504 Contains node number in contact surface
      ELSE IF(KEY .EQ. 1511 .AND. K_NODE_SET .EQ. 'N_TOP') THEN
** KEY 1511 contains CSTRESS values
**Decides whether node is in contact or not
 120  CONTINUE
      END DO
 110  CONTINUE
      RETURN
      END
C#################################################################
SUBROUTINE
FLOW(H,SINK,U,KSTEP,KINC,TIME,NOEL,NPT,COORDS,JLTYP, SNAME)
      INCLUDE 'ABA_PARAM.INC'
```

```
      DIMENSION TIME(2), COORDS(3)
      CHARACTER*80 SNAME
C Structure to hold element data which can be accessed by URDFIL and FLOW. Same as in URDFIL
      MIN_DIST = 100.0D0
      DO K25 = 1, NO_OF_ELEMENTS
       DO K26 = 1, NO_OF_NODES
**Find the closest node to this integration point NPT
       END DO
      END DO
      IF(K_ELE_DETAILS(E_INDX)%IS_CONT(N_INDX) .EQ. 0) THEN
**When node is not in contact
       IF(K_ELE_DETAILS(E_INDX)%POR(N_INDX) .GE. 0) THEN
         SINK = 0
         H = 1
C MAKE H = 0; IF FLUID IS NOT TO FLOW INSIDE
       ELSE
         SINK = 0
         H = 1
       END IF
      ELSE IF(K_ELE_DETAILS(E_INDX)%IS_CONT(N_INDX) .EQ. 1) THEN
**When node is in contact
       SINK = 0
       H = 0
      END IF
      RETURN
      END
C###############################################################
```

Appendix E Publications

I) Under review

1] Pawaskar, S.S., Jin, Z. and Fisher, J. Modelling of fluid support inside articular cartilage during sliding. In 33rd Leeds-Lyon Symposium on Tribology. To be published in Proceedings of the Institution of Mechanical Engineers, Part J, Journal of Engineering Tribology. 2006. Leeds, U.K.: Professional Engineering Publishing.

2] Katta, J., Pawaskar, S.S., Jin, Z., Ingham, E. and Fisher, J. Effect of load variation on the friction properties of articular cartilage. In 33rd Leeds-Lyon Symposium on Tribology. To be published in Proceedings of the Institution of Mechanical Engineers, Part J, Journal of Engineering Tribology. 2006. Leeds, U.K.: Professional Engineering Publishing.

II) Planned

1] Pawaskar, S. S. and Jin, Z. Contact mechanics modelling of articular cartilage. Journal of Biomechanics.